Monitoring based condition assessment of offshore wind turbine support structures

Institut für Baustatik und Konstruktion, ETH Zürich

Monitoring Based Condition Assessment of Offshore Wind Turbine Support Structures

Sebastian Thöns

IBK Bericht Nr. 345, Dezember 2012

KEYWORDS: Structural condition assessment, monitoring, offshore wind turbine, measurement uncertainty, cost benefit analysis, structural integrity management

Sebastian Thöns:
Monitoring Based Condition Assessment of Offshore Wind Turbine Support Structures
Bericht IBK Nr. 345, Dezember 2012

Gedruckt auf säurefreiem Papier
Printed in Switzerland

Berichte des IBK beim vdf Hochschulverlag AG an der ETH Zürich

Die Berichte bis Nr. 333 sind unter Angabe der ISBN-Nr. direkt bei:
AVA Verlagsauslieferung AG, Centralweg 16, CH-8910 Affoltern am Albis
Tel. ++41 44 762 42 00, Fax ++41 44 762 42 10, e-mail: avainfo@ava.ch
zu bestellen.

The publications up to no. 333 can be ordered by specifying the ISBN No. direct from:
AVA Verlagsauslieferung AG, Centralweg 16, CH-8910 Affoltern am Albis
Tel. ++41 44 762 42 00, Fax ++41 44 762 42 10, e-mail: avainfo@ava.ch

Berichte des IBK an der ETH Zürich

Die IBK-Berichte ab Nr. 334 werden **nicht mehr verkauft**.
Sie finden die **elektronische Version** auf der e-collection der ETH Bibliothek,
über die Links auf unserer Homepage: www.ibk.ethz.ch

*IBK-reports from no. 334 will **no longer be sold**.*
*You will find the electronic version on the e-collection of the ETH Library with the **links on our homepage:** www.ibk.ethz.ch*

Harikrishna Narasimhan:
Assessment and Determination of Robustness of Structures
Bericht IBK Nr. 337, Mai 2012

Katharina Fischer, Jochen Kohler, Mario Fontana, Michael H. Faber:
Wirtschaftliche Optimierung im vorbeugenden Brandschutz
Bericht IBK Nr. 338, Juli 2012

Gerhard Fink, Jochen Kohler:
Zerstörungsfreie Versuche zur Ermittlung des Elastizitätsmodules von Holzbrettern
Bericht IBK Nr. 339, August 2012

Jacqueline Pauli, Diego Somaini, Markus Knobloch, Mario Fontana:
Experiments on Steel Columns under Fire Conditions
Bericht IBK Nr. 340, Oktober 2012

Daniel Heinzmann:
Stringer-Tafelmodelle für Stahlbeton
Bericht IBK Nr. 341, Oktober 2012

Clare Burns:
Serviceability Analysis of Reinforced Concrete
Based on the Tension Chord Model
Bericht IBK Nr. 342, Oktober 2012

Jacqueline Pauli:
The Behaviour of Steel Columns in Fire
Material – Cross-sectional Capacity – Column Buckling
Bericht IBK Nr. 343, Dezember 2012

Diego Somaini:
Biegeknicken und lokales Beulen von Stahlstützen im Brandfall
Bericht IBK Nr. 344, November 2012

Sebastian Thöns:
Monitoring Based Condition Assessment of Offshore Wind Turbine Support Structures
Bericht IBK Nr. 345, Dezember 2012

MONITORING BASED CONDITION ASSESSMENT OF OFFSHORE WIND TURBINE SUPPORT STRUCTURES

Sebastian Thöns

Institute of Structural Engineering
Swiss Federal Institute of Technology Zurich
December 2012

Introduction

Meeting the challenge of sustainable societal developments necessitates significant progress on several research areas. Among the more important ones, the exploitation of fossil free energy sources plays a central role. Wind energy forms a very valuable renewable energy resource, the relevance of which has been proven and also improved over the last couple of decades. Wind energy is by now a major factor in achieving the desired transition away from fossil fuel based energy. However, large scale wind energy generation necessitates more available space and of course wind - and the next major step in utilization of wind energy has been identified to involve wind energy facilities and infrastructure offshore – at sea.

The thesis starts out by presenting the present general state of planning and developments for offshore wind energy exploitation. One of the challenges in this context is that there have not yet been established a best practice on how to model and assess the life-cycle performance of offshore wind turbine structures. Till now several research and development projects have been undertaken by universities and industry in collaboration aiming to plan and commence the development of offshore wind turbine parks. An important next step is to address the issues relating to the operation of the facilities and hereunder also the health monitoring of wind turbine support structures.

The research presented within the thesis addresses three main aims, namely, to establish the methodical basis for condition assessment and health monitoring, identify and investigate approaches for utilizing monitoring data, to illustrate how monitoring data might be utilized on an example case and finally to support certification authorities in the development of a best practice methodology with regard to modeling and assessing wind turbine support structures.

In achieving the aims the thesis develops a probabilistic framework and model basis for reliability and robustness assessment of wind turbine support structures, models for the assessment of the ultimate and fatigue limit states of the performance of wind turbine structures, a response surface methodology specifically adapted to the needs as encountered in reliability analysis of wind turbine support structures, a modeling and assessment of the effect of measurement uncertainties in structural health monitoring and finally a concept for the utilization of monitoring data as a means for reliability updating.

The results of the presented research may be seen as a major step in identifying and establishing best practices on design and life-cycle management of offshore wind generation facilities. Moreover new approaches for supporting reliability analysis of complex structural systems have been developed and tested. It is believed that the presented work will be not only of interest but also of significant benefit for both academia and industry.

I wish you enjoyable reading,

Michael Havbro Faber

December 2012

Abstract

A central societal need in developed countries is the energy production with a low environmental impact. Thus ambitious energy programs have been initiated aiming at the establishment of renewable energies as a main contributor to the energy mix in the next decade. Like no other renewable energy, the offshore wind energy possesses a high potential and constitutes the main contributor to this aim.

The development of large scale wind parks is one of the major challenges in the offshore industry today while the first wind parks of significant size and in considerable water depths are being built. In preparation for the next step, this thesis aims to contribute to the efficient and cost effective operation of wind parks. It specifically addresses the support of the inspection and maintenance activities of offshore wind turbines by the development of methods for the assessment and monitoring of support structures.

The essential finding of this thesis is that the operation efficiency of wind turbine structures can be significantly enlarged by monitoring based assessment procedures. It is found that a substantial expected life-cycle benefit for the operation can be achieved by the conceptual integration of structural monitoring techniques in the structural reliability theory. The integration should be bidirectional in the sense that the generic design decisions for structural monitoring systems are based on a structural reliability assessment and that simultaneously a possible reduction of the uncertainty associated with the condition is utilized for the structural reliability assessment and thus for the inspection and maintenance planning.

The thesis covers the issues of

(I) the integration of monitoring data in the framework for structural reliability assessment of the Joint Committee on Structural Safety (JCSS),

(II) the issue of the consistent determination of the measurement uncertainties utilizing all available information of the measurement process,

(III) the issue of the application of monitoring techniques for structural integrity management and

(IV) the establishment of a full probabilistic performance model basis for the support structure of an offshore wind turbine.

To cover these issues the thesis comprises (1) the development of probabilistic structural, loading and limit state models, (2) a response surface algorithm for a multiple component reliability analysis, (3) a reliability analysis of an offshore wind turbine support structure applying the model basis, (4) a framework for the determination of measurement uncertainties utilizing process and observation data and (5) concepts for utilizing monitoring data in a structural reliability analysis as well as for the risk based inspection planning.

The starting point of this thesis is the development of the model basis containing the models for the structural performance of a reference case, namely a support structure of an offshore wind turbine. The model basis comprises the structural, loading and probabilistic characterization of the ultimate, fatigue and the serviceability limit states and is derived considering the constitutive physical equations. The introduced models for the structural performance and loads account for design, production and execution information. A sensitivity study is performed on the basis of a non-linear coefficient of

correlation. The process of establishing and analyzing these models contributes to an enhanced understanding of the performance of the structure and is documented in detail.

The reliability analysis of an offshore wind turbine support structure builds upon the developed model basis. In order to facilitate the reliability analysis with such complex multiple component models, an adaptive response surface algorithm is developed. This algorithm utilizes clustered experimental designs in combination with an efficient augmentation scheme for these designs. The results of the reliability analyses comprise the system reliabilities and the probabilities of failure for the components in the individual limit states. With these results critical components are identified. A comparison with the target reliabilities specified in DIN EN 1990 (2002) shows that the target reliabilities are met.

A novel contribution, as mentioned above, constitutes a new approach for the determination of measurement uncertainties in the context of the structural reliability theory. This approach builds upon two types of measurement uncertainties (as defined in the ISO/IEC Guide 98-3 (2008a)), namely the uncertainty based on a statistical analysis of observations and the uncertainty derived from a process equation describing physically the measurement process. Both types of measurement uncertainties are utilized for the derivation of a posterior measurement uncertainty by Bayesian updating. This facilitates the quantification of a measurement uncertainty using all available data of the measurement process. The measurement uncertainty models derived are analyzed through a sensitivity study and are discussed in detail resulting in an identification of the most relevant sources of measurement uncertainties.

For the utilization of monitoring data in a structural reliability analysis the approach for the determination of measurement uncertainties data is applied. Monitoring data can be interpreted in two ways, namely as probabilistic loading model information and as probabilistic resistance model information, i.e. proof loading. For both ways the influence of the measurement uncertainties on the structural reliability is shown and how the specific modeling of monitoring data in a reliability analysis can result in a reduction of uncertainties and as a consequence in an increase of the reliability. The proof loading concept is developed further to account for probabilistic proof loading information, i.e. information subjected to measurement uncertainties. In conjunction with an alternative proof loading concept utilizing Bayesian updating techniques, a criterion to facilitate a consistent choice of the appropriate proof loading method is developed.

The developed approaches and the findings are applied in a life-cycle cost-benefit analysis comprising the expected costs of failure, of inspection, of repair and of the monitoring system as well as its operation. Here, concepts for the design decision support of monitoring systems are introduced by formulating the life-cycle cost-benefit analysis as an optimization problem. On this basis, it can be determined which components should be monitored to achieve a life cycle benefit. Furthermore, an approach for the reduction of monitoring period is introduced. The most significant result of the cost-benefit analysis is that a substantial expected life-cycle benefit is achievable by the application of the developed concepts.

Zusammenfassung

Eine zentrale gesellschaftliche Notwendigkeit der Industrieländer ist die umweltfreundliche Energieproduktion. Hierfür wurden ambitionierte Programme mit dem Ziel entwickelt, die erneuerbaren Energien als einen wesentlichen Bestandteil des zukünftigen Energiemixes zu etablieren. Wie keine andere erneuerbare Energie besitzt die Offshore-Windenergie ein hohes Potential und kann dadurch den größten Teil zu diesem Ziel beitragen.

Die Entwicklung von groß angelegten Windparks ist derzeitig die Herausforderung der Windenergieindustrie. Momentan werden die ersten kommerziellen Windparks signifikanter Größe in einer Wassertiefe von 30 m bis 40 m errichtet. Zur wissenschaftlichen Vorbereitung des nächsten Schrittes hat diese Dissertation einen effizienten und kosteneffektiven Betrieb von Offshore-Windparks zum Ziel. Im Speziellen wird die Unterstützung des Betriebs von Offshore-Windenergieanlagen durch die Entwicklung einer Inspektions- und Wartungsplanung für die Gründungsstrukturen, basierend auf Bewertungs- und Überwachungsverfahren, behandelt.

Das grundlegende Ergebnis dieser Dissertation ist, dass die Kosteneffizienz des Betriebs durch die Anwendung von überwachungsbasierten Zustandsbewertungsverfahren signifikant gesteigert werden kann. Die Steigerung der Kosteneffizienz des Betriebs bedeutet dabei eine substantielle Senkung der erwarteten Lebenszykluskosten, welche durch die konzeptionelle Integration von Überwachungsverfahren und der Zuverlässigkeitstheorie erreicht werden kann. Die konzeptionelle Integration sollte dabei bidirektional erfolgen, d. h. dass die generischen Entscheidungen für die Auslegung eines Überwachungssystems auf der Grundlage der Tragwerkszuverlässigkeitstheorie erfolgen und dass gleichzeitig eine mögliche Reduktion der Unsicherheiten des Zustandes der Struktur für die Berechnung der Tragwerkszuverlässigkeit und somit für die Inspektions- und die Wartungsplanung eingesetzt wird.

In dieser Dissertation werden die folgenden Schwerpunkte behandelt:

(I) Die konzeptionelle Integration von Überwachungsdaten in das Rahmenwerk für die Berechnung der Tragwerkszuverlässigkeit des Joint Comittee on Structural Safety (JCSS),

(II) Die konsistente Bestimmung der Messunsicherheiten unter Verwendung aller verfügbaren Informationen des Messprozesses,

(III) Die Verwendung von Überwachungsdaten für das Management der Tragwerksintegrität und

(IV) Die Entwicklung einer vollständig probabilistischen Modellgrundlage für die Gründungsstruktur einer Offshore-Windenergieanlage.

Um diese Schwerpunkte abzudecken, umfasst die vorliegende Dissertation (1) die Entwicklung von probabilistischen strukturmechanischen Modellen, Lastmodellen und Grenzzustandsmodellen, (2) die Entwicklung eines Antwortflächenverfahren für die Zuverlässigkeitsanalyse mit komplexen Modellen (4) eine Zuverlässigkeitsanalyse der Gründungsstruktur einer Offshore-Windenergieanlage, (3) einen Ansatz für die Bestimmung von Messunsicherheiten unter Verwendung aller Informationen des Messprozesses und (4) Konzepte für die Verwendung von Überwachungsdaten in der Zuverlässigkeitsanalyse sowie für die Risikobasierte Inspektionsplanung.

Am Anfang der Dissertation steht die Entwicklung der Modellgrundlage für das Strukturverhalten des Referenzbeispiels, der Gründungsstruktur einer Offshore-Windenergieanlage. Die Modellgrundlage wurde ausgehend von den grundlegenden physikalischen Gleichungen abgeleitet und umfasst probabilistische strukturmechanische

Modelle und probabilistische Lastmodelle für die Grenzzustände der Tragfähigkeit, der Ermüdung und der Gebrauchstauglichkeit. Bei der Entwicklung der Modellgrundlage wurden Entwurfs-, Produktions- und Ausführungsinformationen berücksichtigt. Der Prozess der Entwicklung und der Analyse der Modellgrundlage trägt zu einem erweiterten Verständnis des Strukturverhaltens, einschließlich der Identifikation der sensitiven Modellparameter durch eine Sensitivitätsanalyse, bei und wurde detailliert dokumentiert.

Die Zuverlässigkeitsanalyse der Gründungsstruktur baut auf der entwickelten Modellgrundlage auf. Um die Zuverlässigkeitsanalyse mit dieser komplexen Modellgrundlage zu ermöglichen, wurde ein adaptives Antwortflächenverfahren entwickelt. Dieses Verfahren verwendet gruppierte, experimentelle Stichprobenentwürfe und ein effizientes Erweiterungsverfahren dieser Stichprobenentwürfe. Die Ergebnisse der Zuverlässigkeitsanalyse sind die Systemzuverlässigkeiten und die Zuverlässigkeiten der Komponenten. Ein Vergleich mit den Zielzuverlässigkeiten nach DIN EN 1990 (2002) zeigt, dass diese eingehalten werden. Weiterhin wurden die kritischen Komponenten der Struktur identifiziert.

Ein wesentliches Ergebnis dieser Dissertation, wie oben erwähnt, stellt der neue Ansatz zur Bestimmung der Messunsicherheiten unter Berücksichtigung Tragwerkszuverlässigkeitstheorie dar. Dieser Ansatz baut auf zwei Arten von Messunsicherheiten nach ISO/IEC Guide 98-3 (2008a) auf, dass heißt auf der Messunsicherheit modelliert durch eine Prozessgleichung und auf der Messunsicherheit bestimmt durch eine statistische Beschreibung der Beobachtungen des Messprozesses. Beide Arten der Messunsicherheit werden für die Berechnung der A-posteriori Messunsicherheit durch Bayes'sche Aktualisierung verwendet. Damit kann die Messunsicherheit auf der Grundlage aller zur Verfügung stehenden Informationen abgeleitet werden. Die Modelle für die Berechnung der Messunsicherheiten wurden mit einer Sensitivitätsstudie analysiert und diskutiert. Im Ergebnis konnten die Parameter identifiziert werden, welche am meisten zur Messunsicherheit beitragen.

Für die Verwendung von Überwachungsdaten in der Zuverlässigkeitsanalyse wird der Ansatz für die Bestimmung der Messunsicherheiten angewendet. Überwachungsdaten können dabei auf zwei Arten interpretiert werden. Sie können dem Lastmodell zugeordnet werden oder als ein Belastungstest interpretiert werden, d.h. dem Widerstandsmodell zugeordnet werden. Für beide Varianten wird der Einfluss der Messunsicherheit auf die Tragwerkszuverlässigkeit gezeigt und es wird diskutiert, wie die Verwendung von Überwachungsdaten zu einer Erhöhung der Zuverlässigkeit führen kann. Das Trunkierungskonzept für die Integration von Belastungstestergebnissen in die Zuverlässigkeitsanalyse wurde in Hinblick auf die Integration von probabilistischen Belastungstestergebnissen, d. h. von Belastungstestergebnissen behaftet mit Messunsicherheiten, weiterentwickelt. Im Zusammenhang mit einem alternativen Konzept, auf der Grundlage der Bayes'schen Aktualisierung, wurde ein Kriterium für eine konsistente Anwendung des jeweils zutreffenden Ansatzes entwickelt.

Die entwickelten Ansätze und Ergebnisse werden für eine Lebenszykluskostenanalyse angewendet. Diese schließt erwartete Kosten infolge Versagen, Inspektionen, Reparatur und Überwachung ein. Weiterhin werden Konzepte zur Entscheidungsunterstützung für den Entwurf eines Überwachungssystems, durch die Formulierung der Lebenszykluskostenanalyse als ein Optimierungsproblem, eingeführt. Auf dieser Grundlage kann entschieden werden, welche und wie viele Komponenten überwacht werden sollten, um einen Vorteil für die Lebenszykluskosten zu erreichen. Das wichtigste Ergebnis dieses Kapitels ist, dass ein substantieller erwarteter Lebenszykluskostenvorteil durch die Anwendung der entwickelten Verfahren erreicht werden kann.

TABLE OF CONTENTS

1 Introduction

One of the present challenges in the field of renewable energies constitutes the development of large scale offshore wind parks. As this thesis started in 2007, research projects on the design of offshore wind turbines were finished or in their final stages (e.g. Hendriks and Zaaijer (2004) and Zielke and Haake (2007)) and several building permissions for offshore wind parks in the North Sea and the Baltic Sea were granted by the German Federal Maritime and Hydrographic Agency. Despite these facts, the start of the commissioning of offshore wind parks in considerable water depths up to 40 m was substantially delayed. A further amendment of the German law for renewable energies in combination with a higher electricity feed in tariff was necessary to attract investors and to regulate the responsibilities for the grid connection of the offshore wind parks (Amendment of the German Law for Renewable Energies (EEG) in 2008). These developments lead to the construction of the first German offshore wind park Alpha Ventus (Hildebrandt (2010)). By the time this was achieved, the world financial crisis caused delays for the commissioning of commercial wind parks. However, by the time of completion of this thesis, the construction of the first German commercial wind park "BARD Offshore I" has started in water depths up to 40m.

In preparation for the next step, the operation of offshore wind parks, the project for the development of an "Integral Monitoring and Assessment System for Offshore Wind Energy Converters (IMO-WIND)" was initiated early by the Division of "Buildings and Structures" of the BAM Federal Institute for Materials Research and Testing. Based on this research project it was agreed on a cooperating with the "Chair of Risk and Safety" of the ETH Zurich in the research field of operation support for offshore wind turbines which constitutes the aim of this thesis. The challenge here is to build upon the experience and concepts of the offshore industry and to further account for actual methodological and technology developments as well as the specific requirement of the offshore wind industry. As after three years the project IMO-WIND was concluded, the research continued within the EU Seventh Framework project "Integrated European Risk Reduction System (IRIS)".

This situation, namely the conceptual research challenges in combination with the industry-driven research projects and the start of a new industry constitute the most influencing factors contributing to this thesis.

1.1 Aim of the thesis

This thesis aims at the development of methods for the assessment and the monitoring of structures for offshore wind turbines to support the operation and maintenance activities. To systematically achieve this aim, the thesis is divided in two main parts, namely the methodological and conceptual issues as well as the applied research issues. Both parts are then further substructured as described in the following.

The methodological and conceptual aims are the development of a framework which facilitates the condition assessment by utilizing all available information comprising the design, the production and the construction process as well as monitoring data. This constitutes a challenging task because such methodologies do not exist in this holistic approach and furthermore the field of wind turbines engineering is a rather new

discipline. Another aspect is the consideration of a new type of support structure, namely a tripod structure, as this necessitates the development of a completely new model basis.

The second issue associated with conceptual research work is to investigate the utilization of measurement data, i.e. monitoring data, for the structural reliability analysis. This has to be consistent with the approach for the determination of the structural reliability and furthermore should represent a general framework. This can be a highly complex issue as it is associated with sensor and measurement technologies and thus constitutes a research field in itself. However, existing approaches in the field of measurement uncertainties are the starting point here.

The methodologies developed for the model based condition assessment and monitoring based condition assessment are to be applied to a reference case which represents a support structure of the offshore wind turbine prototype Multibrid M5000. This is of importance to fulfill the industry-driven project aims but represents simultaneously a challenge because the developed conceptual approaches have to be applied not only to a generic example but to a complex reference case to show their value for the application.

To support the function of BAM Federal Institute for Materials Research and Testing as a part of the certification authority for offshore wind parks, a model basis is required with specific investigations in regard to the design process. Since in general the practical experiences with offshore wind turbines are very limited, the analysis of relevant failure modes is an important issue to enhance the understanding of the support structure. The most sensitive parameters and components for all limit states should be identified in order to ensure an efficient certification process.

1.2 Scope

This thesis covers the issues of integration of monitoring data in the framework for the structural reliability assessment of the Joint Committee on Structural Safety (JCSS), the issue of the consistent determination of the measurement uncertainties utilizing all available information of the measurement process and the application of monitoring techniques for the structural integrity management. It contains

- A reliability analysis of an offshore wind turbine support structure applying a developed independent model basis,
- A response surface algorithm for a multiple component reliability analysis,
- A framework for the determination of measurement uncertainties utilizing a process equation and observation data and
- Concepts for utilizing monitoring data in reliability analysis and for the risk based inspection planning.

The most basic assumption of this thesis is the Bayesian definition of probability as this the underlying assumption of the structural reliability theory (e.g. Faber (2008a)). This definition of probability is then applied to the field of measurement uncertainties, which is historically driven by meteorological researchers. The framework for the determination of measurement uncertainties is thus built completely on the Bayesian

definition which is advocated in the scientific community (e.g. Bich (2008)) but the potentials of this approach are not fully used in the view of the author.

The methodological core of this thesis is based on the structural performance assessment by the methods of structural reliability and their application in the field of offshore wind turbines. This necessitates loading and structural models which are developed in the framework of the established non-linear Finite Element Method. These models are developed for one support structure of a prototype of an offshore wind turbine based on the information available for the derivation of the models.

In the further course of this thesis the support structure associated with multiple components, comprising the steel structure from the pile guides to the top of the tower, constitutes the reference case. Based on the component reliabilities, procedures for the management of the structural integrity are developed. The most important findings are then applied to the reference case for a life-cycle cost-benefit analysis.

The models implemented in the model basis are established on a physical basis and thus go beyond engineering models as they are limited in the way they cover system effects and may incorporate substantial conservativeness. The limit state models also go beyond the current engineering approaches and at the same time take basis in approaches contained in the current Eurocode generation.

1.3 Relevance

Renewable energies, especially the wind energy, have been in the societal focus in the last decades as a part of environmental sustainability. This can be seen as a consequence of the Callendar publication (Callendar (1938)) which constitutes the most influential research work for the identification of the green house effect. The consecutive discussion in research and the societal discourse in combination with a rapid economical development in the second half of the 20^{th} century lead to a societal awareness of the human impact on the ecological system. From the society as a whole comprising research, politics and industry, the focus towards renewable energies for energy production has emerged mainly in the last two decades as energy production is one central societal necessity in the developed countries.

The political situation today is that the further expansion of renewable energies is an important part of European and national (e.g. German) energy policies. The major aim on European level is here to achieve a contribution of renewable energies in the EU's overall energy mix of 20% by 2020 (e.g. European Commision (2007a) and European Commision (2007b)). The European Strategic Energy Technology Plan (SET-Plan) contains as one focus the improvement of the competitiveness of the wind energy production including harnessing the offshore wind energy resources (European Union (2010)). The main focus of the German energy concept is on establishing renewable energies as a major component of future energy production. Here the emphasis lies on the expansion of the offshore wind industry to achieve 25 GW installed power in 2030 (Bundesministerium für Wirtschaft und Technologie (BMWi) (2010)).

The current situation in the wind energy industry is that a substantial amount of wind turbines have been installed and are operated onshore. This amounts to 74.1 GW installed onshore wind power in Europe (European Wind Energy Association (EWEA)

(2009a)). The situation offshore is that the first wind parks in significant water depths (up to 40 m) are currently in the installation process and a variety of projects are under development (Pestke (2010)). Near-shore and in shallower waters there are currently 2.1 GW wind power installed (European Wind Energy Association (EWEA) (2009a)). The focus of the offshore wind industry moves from developing the turbines towards the operation of wind parks and hence to methods and technologies to support the inspection and maintenance activities.

The methods of structural reliability theory comprising the methodological basis for this research work have become an important research field driven by the work of the Joint Committee on Structural Safety (JCSS) and its associated researchers. One major achievement is that the basis of design and the safety concept (DIN EN 1990 (2002)) of the current Eurocode generation is based on these methods of structural reliability. Building upon the methods of structural reliability theory, the next step towards risk assessment is taken by the JCSS (see e.g. Faber (2008b)) and this is the topic of actual major research projects within the 7th Framework Program of the European Union such as IRIS (e.g. VCE (2009)) and iNTeg-Risk (e.g. Jovanovic, Renn et al. (2010)). The European Risk Reduction System (IRIS) project constitutes the current project framework for this thesis.

In addition, research institutions are founded and/or reoriented towards renewable energies with the focus of offshore wind energy all over Europe such as e.g. the Fraunhofer Institute for Wind Energy and Energy System Technology (IWES), the GIGAWIND research group (e.g. with the project GIGAWIND Alpha Ventus, funded by the German Federal Ministry for the Environment, Nature Conservation and Nuclear Safety), the Energy Research Centre of the Netherlands (ECN) and the National Laboratory for Sustainable Energy in Denmark (Risø DTU).

1.4 State of the scientific and technological knowledge

The application of monitoring data for the condition assessment is a very new research topic in various engineering fields e.g. in aircraft engineering (Enright, Hudak et al. (2006)). The first approaches in civil engineering can be found in Frangopol, Strauss et al. (2008) and Liu, Frangopol et al. (2010). However, these frameworks seem to have limited consistency with the established structural reliability analysis frameworks especially in regard to the consideration of the representative uncertainties.

The relevant research fields and technologies associated with the area of condition assessment and monitoring procedures are discussed here in regard to their historical development and the state of research. This includes the wide field of structural reliability analysis in connection with risk analysis and assessment procedures. A section on the monitoring and inspection technologies completes this overview.

1.4.1 Reliability analysis

One of the earliest works considering structural reliability is the work of Mayer (1926). It contained the basic thought that the safety of structures is a matter of the applied statistics and probabilistics. For the first time partial safety factors were mentioned, which is the standard concept for code based design in its current generation. However, the concept itself was not formulated comprehensively in mathematical terms. Several

works followed, such as e.g. Freudenthal (1947), and it lasted until 1954 when the basics of the concept of structural reliability theory were formulated by Freudenthal (1954). Here, not only the mathematical and statistical basis was developed, but it was distinguished between the probability of unserviceability and the probability of failure of structures. Freudenthal showed later the geometric properties of the simple reliability index as his calculations were based on fully probabilistic models (Freudenthal (1956)). However, these models were very difficult to apply at that time.

The development of the reliability theory slowly progressed until this concept was based on a Bayesian interpretation of probability by Raiffa and Schlaifer (2000) in 1961. A milestone of the work of Raiffa and Schlaifer is that the reliability theory was directly linked to decision support.

An early and widely used concept to estimate the structural reliability was the second order moment concept defined in Cornell (1969) - see e.g. Ditlevsen (1979b). This concept only requires the first two moments of the random variables to calculate the reliability of structures and hence does not involve the complete distribution functions. The next step was taken with a geometric interpretation of the reliability index (Hasofer and Lind (1974)) to circumvent the invariance problem of the second order moment concept which was described by Ditlevsen (1973). However, the concept of the geometrical reliability index cannot distinguish certain reliability problems which have a constant reliability index but different probabilistic properties, as it is the case when the limit state function has the same tangent at the design point but different shapes. Consistent with the definition of the geometric reliability index, the concept of the First Oder Reliability Method (FORM) was formulated. Consecutively, a more general interpretation defined the reliability index as being associated with the probability of survival and thus as the integral of the joint probability density function of the random variables in the safe set. As an alternative improvement to the First Oder Reliability Method (FORM), the Second Order Reliability Method accounting for a curvature of the limit state function was introduced.

The definition of the reliability as an integral facilitates the application of the Monte Carlo Method as this can be estimated by a series of stochastic experiments. The probability of failure for structures is usually very small which requires a high number of simulations and restricts the complexity of the models used. To circumvent this, several techniques have been developed to modify the sampling density for an efficient estimation of the probability of failure, as suggested first by Shinozuka (1983). These techniques which include e.g. an updating method as well as directional, adaptive and spherical sampling methods, are summarized with the term importance sampling (Engelund and Rackwitz (1993)). Various techniques are implemented in software programs, like STRUREL and COMREL (Gollwitzer, Kirchgäßner et al. (2006)).

The response surface methodology has been developed in chemical engineering to optimize chemical processes. Here, the analyst is confronted with highly complex experiments which restrict significantly the sample size of the experiments. The paper of Box and Wilson (1951) is seen as the origin of this method. With the development of the Finite Element Method this approach was adapted to randomized Finite Element models (e. g. Haldar and Mahadevan (2000), Bucher (2009b)).

A milestone in the response surface methodology is the paper of Bucher and Bourgund (1990) where the information of the design point is utilized for the definition of the response surface. This contributes to the improvement of the response surface accuracy in the most relevant region around the design point.

Since the first publication of the book "Response Surface Methodology " in 1971 this book belongs to the standard literature on this topic as it was regularly revised and is currently available as the 2002 edition (Myers and Montgomery (2002)). It covers a large variety of experimental designs and methods applying response surfaces. Some of these methodologies are implemented in the Dynardo software packages. Other methods which are not as sophisticated are implemented in ANSYS (Reh, Beley et al. (2006)).

A state of the art overview of response methodology in the area of structural mechanics is given in the paper of Bucher and Most (2008) where an adaptive sampling method in combination with a least squares regression analysis is described. Moreover, neural networks are applied to similar problems. The main thought for both methods is that "it is essential to achieve high quality of approximation primarily in the region of the random variable space which contributes most significantly to the probability of failure" (Bucher and Most (2008)).

A recently developed concept is the Asymptotic Sampling by e.g. Naess, Leira et al. (2009), Nishijima, Qin et al. (2010) and Bucher (2009a). This concept relies on reformulating the reliability problem to depend on a parameter and exploiting the regularity of the tail probability as a function of this parameter which then allows for the application of Monte Carlo method and the significant reduction of the computational effort. It is communicated within the scientific community for solving high dimensional reliability problems in terms of random variables and in terms of the considered component numbers.

Another methodology for the determination of the probabilistic properties is the description of random processes. Here, outcrossing rates of a random process are determined which can then be used for the determination of probabilities of failure. This methodology was first described by Bolotin in 1959 (Bolotin (1981)) and in a more complete way by Shinozuka (1964). Further methods, also including mechanical transfer functions for derivation of the statistical properties of the response are contained in Madsen, Krenk et al. (1986).

As the structural reliability theory covers the reliability of components, methods for the reliability calculation for structural systems consisting of a set of components were developed. Here the main focus is the identification of the system characteristics and the dependencies between the probabilities of failure. The early approaches were based on developing boundaries and then to develop as narrow boundaries as possible (e.g. Cornell (1967), Ditlevsen (1979a), Ditlevsen and Bjerager (1986)). As these approaches very practical, they are commonly used in research (Ditlevsen and Madsen (2005)). Recently methods for accounting for the dependencies directly have been developed (e.g. Straub and Der Kiureghian (2008)).

1.4.2 Assessment of existing structures

The assessment of existing structures has become a societal focus in the last decades with a significant increase of the number of ageing structures constituting important

transport and production infrastructures for the society. For instance the ASCE Report Card for Americas Infrastructure estimates that investments of about 10% of the gross domestic product in the next five years are needed to restore deteriorated infrastructure.

The main difference of the assessment of an existing structure to the design of new structures is the amount of information which is and which can be made available. In principle, the assessment covers all methods which give information about the condition of the structure. This information includes data of the design, production and construction process and all procedures and methodologies to gather information about a structure such as inspections, testing, monitoring as well as methodologies to interpret these information applying physical and probabilistic models.

From the beginning the condition assessment was associated with probabilistic and reliability theory (e.g. Yao (1979)). As described in Yao (1979) the involved research fields such as structural damage assessment and system identification are associated with the structural reliability but a closed form solution integrating these research fields did not exist. Yao and Natke (1994) published a paper where the system identification is linked to structural reliability.

The early damage assessment procedures were aiming at a qualitative representation of the damage. A milestone in this field is the publication of Blockley (1978) as he first associated the possible damage of a structure with the structural design process as a decision formulation. However, his study was based on fuzzy sets – a method which is rarely applied today.

The most sophisticated framework for the assessment of existing structures has been formulated by the Committee on Structural Safety (JCSS). This framework described in Faber (2000) and documented in JCSS (2001) builds mainly upon the basic ideas found earlier, as described, in the literature and reflects the substantial development of these methods in the last decades. Furthermore it takes basis in the decision theory and contains a theoretical framework and an outline of typical assessment decision situations.

One of the most fundamental assumptions underlying the JCSS framework (JCSS (2001)) is that it builds upon the Bayesian definition of probability. This facilitates to apply the Bayesian decision theory and furthermore account for new information in a consistent way by Bayesian updating of the whole assessment process. One important aspect of such a framework are target reliabilities which are described in part three of JCSS (2001). These are calculated utilizing a cost-benefit analysis and accounting for human safety.

The framework for the assessment of existing structures is supported by the Probabilistic Model Code (JCSS (2006)) which gives guidance for deriving the probabilistic models needed for the structural reliability analysis. As the structural reliabilities represent an element for a risk analysis, such a framework has been developed recently (Faber (2008b)).

The ISO 13822 (2001), issued by the International Organization of Standardization, constitutes another general framework for the assessment of existing structures. This comprehensive framework is more practically oriented as it is linked to design codes

and enables beside a structural reliability based assessment also a deterministic or semi probabilistic assessment taking basis in design codes. This practical orientation is supported by formal sections which cover the data collection process of an existing structure and the documentation process. As Bayesian updating is described herein, this standard clearly builds upon the Bayesian definition of probability in conjunction with ISO 2394 (1998) which serves as the basis of ISO 13822 (2001). The framework references also the target reliability levels of ISO 2394 (1998).

Based on the mentioned ISO framework, a guideline for the assessment of existing structures was developed within the EU funded research project SAMCO (Rücker, Hille et al. (2005) and Rücker, Hille et al. (2006)). The major step which has been taken here is to classify the condition assessment routines into 6 levels. This enables a differentiation first between a qualitative assessment and a quantitative assessment (level 0 vs. the other levels), and between a measurement and threshold based assessment and an assessment which is supported by models (level 1 vs. levels 2 to 5). A level 2 assessment is then performed based on the design of the structure, i.e. based on the models used herein, and a visual inspection of the condition of the structure. As a level 3 assessment incorporates site specific tests, measurements and more sophisticated calculation procedures and models, it is based on semi-probabilistic methods. A level 4 assessment then allows for the modification of partial safety factors. The most sophisticated method for the assessment is then a fully probabilistic assessment – a level 5 assessment based on the framework of ISO 2394 (1998) and ISO 13822 (2001).

The SAMCO guideline (Rücker, Hille et al. (2005)) combines various methods used by scientists and engineers and with the introduction of a classification it gives a clear arrangement and affiliation of these methods. It shows a structure for refining the assessment process and clarifies the choice of methods for the practical assessment.

As mentioned at the beginning, the development of assessment procedures was initiated by the needs of securing a safe operation of societal important infrastructures such as offshore structures. This is the focus of this thesis and the procedures of relevant standards are described in the next paragraphs.

Standards for the assessment of offshore structures include the ISO 19902 (2007) and the API (2000). The assessment process specified in ISO 19902 (2007)) aims at the demonstration of the “fit for purpose” taking basis in assessment initiators which are in detail described and include e.g. damage or deterioration of a primary structural component or changes from the original design. The assessment process is closely related to the design process with additional specification of assessment criteria. Generally, two different types of assessment namely the ultimate limit state assessment and the design level assessment, comprising all limit states namely the ultimate, the fatigue and the serviceability limit state, are distinguished. Furthermore this standard explicitly allows for a structural reliability analysis (SRA) without any further references. A decision analysis framework is not included.

The latest research results regarding the assessment of offshore structures can be found in Ersdal (2005). Here methods, specific procedures and example calculations for practical purposes aiming at a life extension of existing offshore platforms are analyzed. One major conclusion of this thesis is that a risk analysis should be included in the

assessment process. It contains detailed work on indicators and different methodologies for the calculation of the indicators on the example of an offshore jacket structure.

1.4.2.1 Monitoring and inspection technologies and methodologies

One of the earliest technologies for measuring responses of mechanical systems constitutes the strain gage technology. In its current form the development is attributed to Arthur Ruge and Edwards Simmons in 1938 who worked simultaneously on it (Stein (2006)). However, the principle was first described by William Thomson (later known as Lord Kelvin, 1824-1907) as the research issue at that time in physics was how magnetic and electric quantities could be measured by means of mechanical quantities (Schneider (1991)). Surprisingly, and despite the later dated invention, one of the first application is reported in the early twenties of 20th century associated with reinforced concrete bars by Slater, Hagener et al. (1923).

Strain gages were first used in the airplane industry and then consecutively for the determination of material properties in the scientific community (MacGregor (1944)) but also for large engineering projects. An interesting example can be found in 1968 when again strain gages were applied on reinforcing bars in the construction phase of a containment structure of a nuclear power plant as reported in Bekowich (1968). A further area was the development of new types of sensor such as acceleration sensors.

In regard to offshore structures the first comprehensive report on inspection, testing and monitoring technologies and methodologies for offshore applications for operation was published Frank Busby (1979). As the development proceeded, new technologies emerged in research and crack detection became a main focus. The latest comprehensive study in this area is from 2000 where various technologies crack detection were evaluated within an European Union funded project (Visser Consultancy Limited (2000)).

Based on the measurement technologies several methodological approaches which can be distinguished in inspection and monitoring have been developed. Inspections usually provide condition information at a certain point in time for the structure as a whole or for certain parts of the structure. Monitoring provides with permanent installed sensors continuous local information.

Today a variety of technologies for the monitoring of structures is available. This includes the classical and established technologies such as strain gages (e.g. (Keil (1995), Hoffmann (1987))), acceleration sensors and inclination sensors. New technologies include radar, the utilization of the global positioning system, laser vibrometer and acoustic emission sensors. To distinguish these technologies from mechanical testing, i.e. destructive testing, the abbreviation NDT for non destructive testing is established for referring to these technologies.

Clearly, measurements are subjected to uncertainties and measurement errors. A milestone in the determination of the measurement uncertainty is the Guide for Uncertainty of Measurements (GUM) first released in 1995. Originally developed for a consistent determination of the measurement uncertainties in metrology (Bich (2008)) it has found it is way also to other research fields and has currently the status of an ISO

Guide (ISO (2008a)). Furthermore, the field of measurement uncertainties has become a separate research field (e.g. Sommer, Kühn et al. (2009)).

The integration of measurement data in the structural reliability analysis is relatively young research topic. Tang proposed in 1973 to use the information of the measurement system, i.e. the reliability of the measurement system, for updating of inspection results (Tang (1973)). Later the risk based inspection planning was developed (by Madsen, Skjong et al. (1987)) as the inspection outcomes were used to update the structural reliability and the risks. The latest research in this field was conducted to develop generic approaches (see Faber, Engelund et al. (2000), Straub (2004)).

1.5 Outline

This paper thesis consists of six chapters. The thesis starts with a paper where the basic approach and procedure is presented followed by two papers describing the model basis. It follows one paper with the results of the reliability analysis and the adaptive response surface algorithm succeeded by a paper which introduces a framework for the determination of measurement uncertainties and its integration in a structural reliability analysis. The thesis concludes with a chapter which elaborates the application of the developed methods for the management of the structural integrity. The conclusions and an outlook as well as a curriculum vitae of the author close this thesis.

Consecutive to the introduction, chapter two provides an overview of the research ideas and approaches with emphasis on a framework for the risk based assessment and monitoring of the performance of offshore wind energy converters in operation. As a starting point, best practices from related engineering fields specifically addressing typically applied procedures for the design of offshore wind turbines, general codes and guidelines for the assessment of offshore structures and finally some requirements to the inservice monitoring of offshore wind turbines in operation as prescribed from the side of a certification society. In terms of structural analysis the proposed framework builds upon an overall dynamic analysis model of the wind energy converter which is typically established already in the design phase. The structural reliability is analyzed utilizing a stochastic Finite Element representation of the structure in conjunction with response surface technologies. The structural system characteristics, the systems reliability and the risks are assessed which through the loading and deterioration processes may lead to structural damages, overall structural collapse and loss of operation and thereby result in economical losses. The risk assessment framework facilitates that the reliability and the robustness of the wind energy converter system as such can be quantified. This in turn facilitates that efficient monitoring schemes can be identified which in combination with optimized thresholds for structural response characteristics can be utilized to reduce operation risks.

The third and the fourth chapter establish the model basis regarding the ultimate, the serviceability and the fatigue limit state consisting of probabilistic structural and loading models of a prototype Multibrid M5000 support structure, the reference case. The model basis is derived on the basis of analyzing several aspects of the developed models and of the results of a sensitivity study in conjunction with the developed probabilistic models. The starting point for the derivation is the consideration of the constitutive physical equations and the methodology of solving these which then in combination

with the limit state requirements leads to the specific constitutive relations for the individual limit states. As a result finite element models based on shell and solid elements incorporating a structural and a loading model are introduced and described in detail. Applying these models, the ultimate capacity of the support structure and the tripod structure are determined with a geometrically and materially non-linear finite element analysis. The observed failure mechanisms are the basis for the definition of the ultimate limit state responses. Furthermore, analyses of the influence on the hot spot stresses by applying a contact formulation for the pile guide brace connection and the application of a finite element formulation using solid elements are included. For the serviceability limit state, the comparison of the natural frequencies of a discrete rotor model with a continuous rotor model is documented. A probabilistic model accounting for the uncertainties involved is derived on the basis of literature review and measurement data from a prototype Multibrid M5000 support structure. With the developed structural and loading models, a sensitivity analyses in regard to the responses relevant for the limit states are performed to enhance the understanding and to refine the developed models.

The reliability analysis documented in the fifth chapter builds upon structural, loading, limit state and uncertainty models comprising design, production and construction data. The complexity of the individual models dictates an efficient solution scheme for the reliability analysis. Such an algorithm is developed consisting of an adaptive response surface algorithm and an importance sampling Monte-Carlo algorithm. The response surface algorithm is based on predetermined experimental designs and facilitates the adjustment of design parameters for an optimized prediction variance in the design point region. Approaches for the consideration of multiple design points and the augmentation of the design for reduction of the prediction variance are described.

Further, in the fifth chapter a limit state model is developed for the specific purpose of an evaluation of the support structure structural reliability. It consists of models for the individual limit states, namely the fatigue, the ultimate and the serviceability limit state going beyond the current engineering approaches and taking at the same time basis in approaches contained in the current Eurocode generation. The results constitute the reliabilities of the individual components of the support structure of the reference case are documented and compared to the target reliabilities specified in DIN EN 1990 (2002).

Chapter six introduces an approach for structural reliability analysis utilizing monitoring data and the associated measurement uncertainties. A new approach for the determination of measurement uncertainties building upon the framework of the Guide for Uncertainties in Measurements (GUM) is presented. The approach introduced in this paper utilizes two types of measurement uncertainties for the derivation of a posterior measurement uncertainty by Bayesian updating. This facilitates the quantification of the measurement uncertainty using all information of the measurement process. The measurement uncertainty models derived in this paper are analyzed with a sensitivity study and are discussed in detail resulting in an identification of the most relevant sources of measurement uncertainty. Furthermore all types of measurement uncertainties are utilized the for a generic fatigue reliability analysis applying the limit state models developed in the previous chapters.

The purpose of the seventh chapter is to illustrate the application of the developed methods for the management of the structural integrity and in the broader perspective of the decision theory. The description of methods for utilizing monitoring data in a reliability analysis comprises two concepts for the ultimate limit state reliability analysis and a discussion regarding the serviceability limit state. The approaches for the utilization of monitoring data in a reliability analysis are applied in a life-cycle cost-benefit analysis comprising the expected costs of failure, of inspection, of repair and of the monitoring system as well as its operation. Here, concepts for the design decision support of monitoring systems are introduced by formulating the cost-benefit as an optimization problem. On this basis, it can be determined which components and hot spots as well as how many components should be monitored. Furthermore, an approach for the reduction of monitoring period is introduced.

2 Assessment and monitoring of reliability and robustness of offshore wind energy converters (Paper I)

S. Thöns

BAM Federal Institute for Materials Research and Testing, Berlin, Germany and

Swiss Federal Institute of Technology, Zurich, Switzerland

M. H. Faber

Institute of Structural Engineering, ETH Zurich, Zurich, Switzerland

W. Rücker

BAM Federal Institute for Materials Research and Testing, Berlin, Germany

R. Rohrmann

BAM Federal Institute for Materials Research and Testing, Berlin, Germany

Proceedings of ESREL 2008 and 17th SRA-Europe Conference. 22.-25.09.2008, Valencia, Spain.

Abstract

The present paper provides an overview of existing approaches for design and assessment of offshore structures and on this basis proposes a framework for the risk based assessment and monitoring of the performance of offshore wind energy converters in operation. In recognition of the fact that there are presently no established best practices for the assessment and monitoring of offshore wind energy converters the first part of the paper provides an overview of best practices from related engineering fields specifically addressing typically applied procedures for the design of offshore wind energy converters, general codes and guidelines for the assessment of offshore structures and finally some requirements to the inservice monitoring of offshore wind energy converters in operation as prescribed from the side of a certification society. Based on the reviewed best practices a risk based assessment and monitoring framework for offshore wind energy converters is proposed. In terms of structural analysis the proposed framework builds upon an overall dynamic analysis model of the wind energy converter which is typically established already in the design phase for wind energy converters in the megawatt class. The structural reliability is analyzed utilizing a stochastic finite-element representation of the structure in conjunction with modern response surface technologies. The structural system characteristics, the systems reliability and the risks are assessed through Bayesian probabilistic network representations of the scenarios which through the loading and deterioration processes may lead to structural damages, overall structural collapse and loss of operation and thereby result in economical losses. The risk assessment framework facilitates that the robustness of the wind energy converter system as such can be quantified. This in turn facilitates that efficient monitoring schemes can be identified which in combination with optimized thresholds for structural response characteristics can be utilized to reduce in operation risks. The framework is illustrated through an example considering a prototype of the Multibrid 5MW offshore wind energy converter. The numerical results from the example indicate that the structure has a high level of structural reliability and that the overall risks are low.

2.1 Introduction

With the realization of large scale wind farms the research interest has shifted from design and construction challenges towards operation. Maintenance, inspection and repair planning has become the focus of research. With reduced accessibility due to the offshore environment, assessment in combination with monitoring is a potential approach as pursued in the IMO-WIND project.

The IMO-WIND project initiated by the department “Buildings and Structures” of the Federal Institute for Materials Research and Testing pursues the development of an integral monitoring and assessment system for offshore wind energy converters (OWECs). This system is aiming to provide online condition assessment and hence support decision making for inspection and maintenance planning.

Offshore structures are subject to deterioration mechanisms and a generally hostile loading environment; an adequate structural performance must thus be ensured taking into account the joint effect of deterioration and extreme load events. In the last decades substantial advances in maintenance and inspection planning of offshore structures have

been achieved (Faber, Straub et al. (2001), Moan (2005)). The focus here was on fatigue deterioration. Further developments of these approaches have been made with the focus of practicability (Straub (2004), Faber, Sørensen et al. (2005)).

The methods of structural reliability are well established and applied in various fields. Most significantly the safety concepts of structural design codes take basis in structural reliability. Other applications are the assessment of existing structures (Rücker, Hille et al. (2005), JCSS (2001)) and reliability based design (e. g. Sørensen and Tarp-Johansen (2005)).

Generally standards, assessment codes and guidelines are mostly restricted to member design. Design or assessment requirements to system characteristics such as robustness are stated only in a general way, usually by the requirement that the damages should not be disproportional to the causes of the damage. Holistic frameworks for detailing such requirements have recently developed and are still an issue of research (Faber, Maes et al. (2007)).

Wind energy converters represent a rather special type of structure in the sense that pure structural characteristics interact with mechanical and electronic systems. The loading on the structure and thus also the load effects in the structure depend not only on the environmental load conditions but moreover on the controlling of the turbine. In assessing the performance of such structures it is even more important to include system effects, however, not only by considering the structural system but instead by including in the assessment all scenarios of damages and failures of control systems, mechanical components and structural components which might lead to consequences. To meet these challenges the design and assessment as well as the strategies for condition monitoring should take basis in a holistic and integral framework. Taking basis in existing best practices for design and assessment of offshore structures together with more recent developments in structural risk and structural reliability theory the present paper proposes such a framework and illustrates its application on an example considering a Multibrid tripod prototype structure.

2.2 Design of offshore wind energy converters

The modeling of the structural response of OWECs is subject to substantial uncertainties due to the uncertainties associated with the wind and the wave loading and their interaction. Therefore the design process considers these uncertainties using semi-probabilistic approaches. The present state of the art approach in Europe to load effect calculations of multi-megawatt OWECs takes basis in an overall dynamic analysis (DIN EN 61400-3 (2009), GL Wind IV - Part 2 (2005), DNV-OS-J101 (2004)). For design situations like e.g. power production, start up and emergency shut down and their corresponding load cases time series of usually 600 seconds are computed and statistically analyzed to yield an ultimate design envelope and a damage equivalent stress resultant for fatigue.

The overall dynamic analysis contains a model of wind and wave loads, a model for aerodynamics, a model for structure-dynamics, a foundation model as well as a model of the operation unit (e.g. Bossanyi (2006), Gasch and Twele (2007)). The wind model contains a three dimensional wind field modeling the height distribution of the wind

speed and the corresponding turbulence. The uncertainties are represented through a site specific stochastic model, usually in terms of Weibull distributed random variables with parameters including a dependency of height. The wave loads are represented by a Jonswap or Pierson-Moskowitz spectrum. The aerodynamics are assessed on the basis of blade elementum theory including dynamics of the wake and a representation of dynamic stall. The model for the operation unit covers the control of the blade pitch angle, for variable speed turbines, the rotor speed and the behavior for operational maneuvers like starts and stops.

Due to the complexity and resulting numerical efforts associated with this overall dynamic analysis the models for structure and foundation dynamics are restricted to beam and spring elements formulations.

For the design of special support structures additional analysis might be required. In case of the considered tripod a beam model represents only a rough model because of the length to diameter ratio of the components. Here shell or solid finite element analyses are used to calculate the structural response.

2.3 Assessment of offshore structures

Existing code provisions for the assessment of offshore facilities include design and assessment codes (ISO/FDIS 19902 (2006) or API RP 2A-WSD (2000)) together with guidelines (Rücker, Hille et al. (2006)) and more general principles and procedures e.g. JCSS (2001).

The assessment process specified in (ISO/FDIS 19902 (2006)) aims at the demonstration of the "fit for purpose" taking basis in an assessment initiator such as damage or deterioration of a primary structural component or changes from the original design. The assessment process is closely related to the design process with additional specification of assessment criteria.

After collecting information about acceptance criteria, the condition of and the loading on the structure a screening assessment based on the design and exposure documentation is performed. In case it cannot be demonstrated that the structure is fit for purpose a resistance assessment using either an ultimate strength analyses or a complete design level analysis has to be performed. The ultimate strength analysis includes only the ultimate limit state assessment whereas the design level analysis includes all limit states namely the ultimate, the fatigue and the serviceability limit state. For an ultimate strength analysis the assessment criteria is formulated through the Reserve Strength Ratio *RSR* (Equation (2.1)) and in case of damaged structures, the Residual Influence Factor *RIF* (Equation (2.2)). The ultimate load capacity is denoted by *F*. For both assessment criteria results of non-destructive testing procedures can be used instead of code provisions for e.g. dimensions and material strengths.

$$RSR = F_{collapse} / F \tag{2.1}$$

$$RIF = F_{collapse,damage} / F_{collapse} \tag{2.2}$$

The guideline for assessment of existing structures (Rücker, Hille et al. (2006)) contains a classification of the assessment procedures in 6 levels. With each level the methods

and the used data are becoming more sophisticated. A level 5 assessment consists of probabilistic procedures, monitoring and material test data.

2.4 Monitoring and assessment of wind energy converters

For onshore WECs periodic examinations are required which usually take basis in visual inspections of relevant components specified in a user manual (e.g. DIBt (2004)). Similar requirements are stated for offshore wind turbines in GL Wind IV - Part 2 (2005) and DNV-OS-J101 (2004). Actually no guidelines exist for the assessment in case of damage or deterioration of a primary structural component or changes from the original design (see also ISO/FDIS 19902 (2006)).

For OWECs certified by GL Wind IV - Part 2 (2005) a condition monitoring system is obligatory. A corresponding guideline for the certification of condition monitoring systems for OWECs has been published (GL Wind IV - Teil 4 (2007)). Here monitoring requirements are specified for the complete OWEC including the main gear, main bearing, the generator, the nacelle and the tower. Vibrations and operation parameters such as e.g. the wind speed, the wind direction and the temperature of machinery parts are to be monitored and to be compared with threshold values delivered by the manufacturer. A dual stage alarm is required consisting of a pre-alarm and a main alarm.

For the tower structure vibration monitoring in the frequency domain between 0.1 Hz up to at least 100 Hz in wind and lateral direction is required in combination with monitoring of broad band characteristic values, amplitude spectrum and respective frequency related characteristic values.

2.5 Assessment and monitoring framework

The proposed assessment framework for the OWEC structures is based on both a component and overall structural reliability assessment together with a quantification of the robustness index following Faber, Maes et al. (2007). Additionally sensor signals are compared ensuring an adequate structural behavior through predetermined thresholds (Figure 2-1).

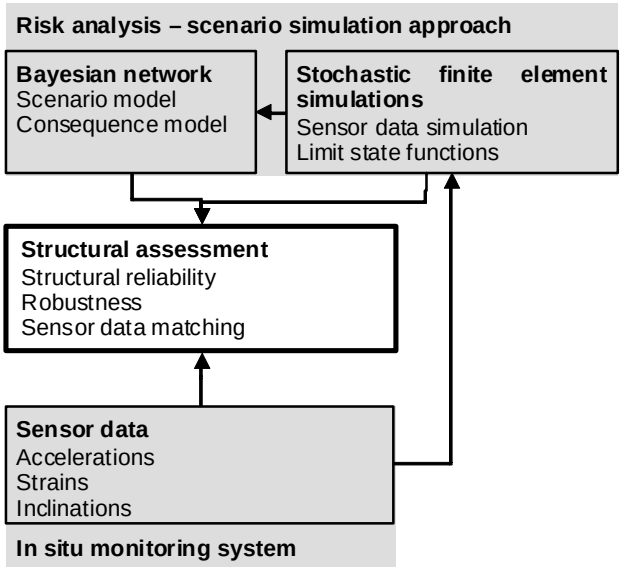

Figure 2-1: Assessment and monitoring framework

The structural reliability and the sensor signals are determined using one model representing the detailed structural behavior and the associated uncertainties. This model is formulated as a stochastic finite element model of the overall structure containing the foundation, the tripod and the tower of the OWEC.

The Bayesian network contains the scenario and consequence model for the equation of the robustness. The probabilities are evaluated using structural reliability theory or Bayesian probabilities.

The framework is based on a preceding overall dynamic analysis. Hence a loading envelope consisting of the statistical evaluation of all considered (design) scenarios is available. In case of the ultimate limit state this consists of tables containing the minimum and maximum values of the stress resultants in the corresponding components (DIBt (2004)). For the fatigue limit state a damage equivalent constant stress range is derived. However, the assessment process can be based on either the design loading or a specifically assessed loading through location relevant measurements.

Because of different requirements concerning the level of overall structural modeling detail and detailing in the modeling of limit states, the structural reliability analyses are subdivided such that the ultimate, the fatigue and the serviceability limit states are assessed individually. The failure mechanisms for the corresponding limit states are modeled through stochastic finite element models directly or through corresponding response surfaces.

The probability of failure at a systems level P_F is based on the assessment of the probability of failure for all n individual component failure modes $P(F_i)$. At component level the structure of the OWEC is regarded a series system and hence simple bounds of the structural systems probability of failure dependent on full correlation or no correlation can be assessed as:

$$\max_{i=1}^{n}\left\{P(F_i)\right\} \le P_F \le 1-\prod_{n}^{i=1}(1-P(F_i)) \tag{2.3}$$

For fully correlated failure modes the system probability of failure becomes the maximum single probability of failure.

The application of Ditlevsen bounds (Ditlevsen (1979a)) usually leads to more narrow bounds. These bounds are equated on the basis of all individual failure mode probabilities and all the pairwise mode intersection failure probabilities:

$$P(F_1)+\sum_{i=2}^{n}\max\left\{P(F_i)-\sum_{j=1}^{i-1}P(F_i\cap F_j),0\right\} \le P_F \tag{2.4}$$

$$\sum_{i=1}^{n}P(F_i)-\sum_{i=2}^{n}\underbrace{\max}_{j<i}P(F_i\cap F_j) \ge P(F) \tag{2.5}$$

Dependencies and system effects can additionally be modeled with Bayesian networks.

Modeling the fatigue and serviceability limit state requires additional considerations and in general a more detailed approach than at the component level. Here failures do not necessarily lead to component failure. The overall probability of failure is therefore assessed using Bayesian networks allowing individual mechanism modeling.

Further, the structural reliability analysis provides valuable information in regard to the distribution of reliability between components and failure modes and thus supports the design of a monitoring system.

Beside the structural reliability, the robustness index I_D (Faber, Maes et al. (2007)) is used as an assessment criterion. The robustness index is defined as the ratio of direct risks R_D to sum of direct and indirect risks R_{ID}:

$$I_D = \frac{R_D}{R_{ID}+R_D} \tag{2.6}$$

The direct risk is assessed as a summation over the probability of the different relevant damage states $\mathbf{C}_l$, $p\left(\mathbf{C}_l \mid EX_k\right)$ conditional on the relevant exposures EX_k multiplied with the associated direct consequences $c_D(\mathbf{C}_l)$:

$$R_D = \sum_{k=1}^{n_{EXP}}\sum_{l=1}^{n_{CSTA}} c_D(\mathbf{C}_l)\times p\left(\mathbf{C}_l \mid EX_k\right)p(EX_k) \tag{2.7}$$

In Equation (2.7) n_{EXP} is the number of different exposures n_{CSTA} is the number of different damage states.

The indirect risk is calculated as a product between the probability of the systems state S_m, $p\left(S_m \mid \mathbf{C}_l, EX_k\right)$ and the corresponding consequences $c_{ID}(S_m, c_D(\mathbf{C}_l))$. It is summed up over the number of exposures, the number of damage states and the number of system states associated with indirect consequences n_{SSTA}:

$$R_{ID} = \sum_{k=1}^{n_{EXP}}\sum_{l=1}^{n_{CSTA}}\sum_{m=1}^{n_{SSTA}} c_{ID}(S_m, c_D(\mathbf{C}_l))\times p\left(S_m \mid \mathbf{C}_l, EX_k\right) p(\mathbf{C}_l \mid EX_k)\, p(EX_k) \tag{2.8}$$

A Bayesian network for robustness analyses requires the identification of all exposure events and their interrelations together with all constituent failure events and direct as well as indirect (follow-up) consequences (see Faber, Maes et al. (2007)).

As an example for the index of robustness one could think of the collapse of the Ronan Point building in 1968 (e.g. Pearson and Delatte (2005)). The partial collapse of this building was caused by the collapse of one bearing wall due a gas explosion. Considering this collapse the building possesses small direct consequences c_D (collapse of a bearing wall) compared to the indirect consequences c_{ID} (the collapse of one entire corner of the 22 story building). The structural design of the building caused the probability of the system collapse given the specific damage state and exposure $p(S_m \mid \mathbf{C}_l, EX_k)$ to be high. This high probability together with the ratio of the consequences causes a low index of robustness near zero.

2.5.1 Monitoring

To ensure an appropriate performance of the structural system the assessment is related to monitoring with multiple sensors. Since a structural model as well as an uncertainty model exists measureable entities can be simulated based on a loading envelope. Once such statistical determined measureable entities have been established a monitoring system can be fed with thresholds. When the design loading is utilized as basis for the loading envelope it can be monitored whether the structure behaves as specified in the certification.

Strains and inclinations can directly be simulated with a static finite element model. For the case of acceleration sensors such data can be simulated by time step analysis. A modal analysis can provide natural frequencies which in turn can be compared with Fourier-transformed time series from acceleration sensors.

2.6 Application of the framework

In the subsequent the proposed framework is applied on a prototype offshore WEC (Figure 2-2). This prototype was equipped within the IMO-WIND project with 235 sensors. 135 strain, acceleration and inclination sensors were applied on the structure (Rohrmann, Rücker et al. (2007)).

Based on this prototype structure the model framework and corresponding analysis results considering the ultimate limit state are outlined in the following sections. The design of this offshore WEC is based on DIBt (1993) and DIBt (2004).

2.6.1 Structural model and loading

The focus is to develop an overall finite element model based on shell elements with a high level of detailing incorporating the nonlinearities of the foundation.

A sensitive detail concerning the modeling of the structure is the pileguide-foundation connection. The onshore prototype WEC is connected to the soil through a reinforced concrete foundation with a pile group. This is contrary to the typically applied offshore foundation which consists of three individual piles. Here the nonlinearities due to the concrete within the pile guide are taken into account in order to increase the precision of the stress calculation; a contact formulation including friction effects has been applied

(Figure 2-2). The applied material model idealizes the material performance through linear elastic and ideal plastic behavior. The pile groups are represented through springs.

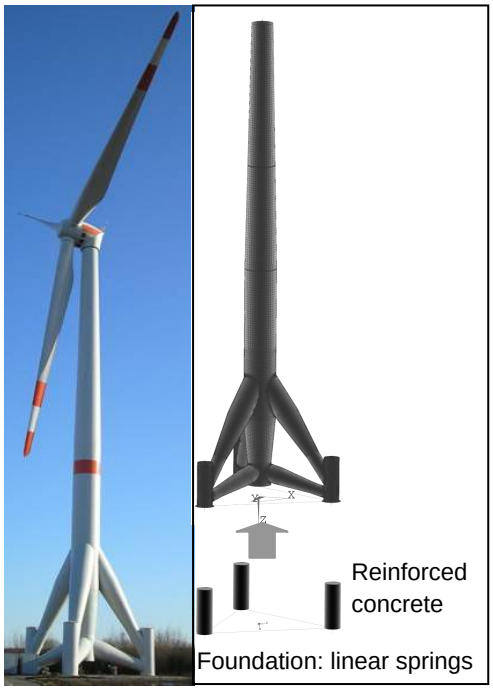

Figure 2-2: Multibrid M5000 OWEC prototype (left); finite-element representation of the structure with exploded view of the foundation model (right)

The loading is determined through the design envelope, i.e. a table containing the minimum and maximum forces and moments, of the nacelle loading for the ultimate limit state. It consists of a load case representing the design envelope and the corresponding wind loads on the structure. A respective load vector for the nacelle loading has been applied at the top of the tower. The gust response factor for the wind load on the tower was used.

The model is analyzed with a nonlinear static analysis using a sparse direct solver (ANSYS (2006)). With the respective stress state the eigenvalue problem is solved using a Block-Lanczos-solver with a Sturm-sequence check. The contact status here remains constant to assure the required linearity for solving the eigenvalue problem.

2.6.2 Limit state functions

The limit state functions represent the generic failure mechanisms of the structure for the ultimate limit state. The considered limit state functions are yielding, shell buckling and overall stability.

The failure mode yielding is directly accounted for in the finite element model and includes section yielding as well as punching shear at the tube connections. The corresponding limit state function g_y containing the component capacity C dependent on the yield stress f_y and the component force A may be written as:

$$g_y = C(f_y) - A \tag{2.9}$$

The failure mode shell buckling is accounted for based on DIN EN 1993-1-6 (2007). It contains rules for the application of numerically based shell buckling loads. Two formats with different numerical expenses are given ranging from linear analyses to geometrically nonlinear with nonlinear material including the effect of imperfections. For this study the plastic reference capacity and the ideal buckling resistance are computed with a nonlinear finite element analysis using the approach based on a nonlinear finite element and an eigenvalue analysis (MNA / LBA see DIN EN 1993-1-6 (2007)).

The respective limit state function for component buckling contains the plastic reference resistance R_{Pl} and the buckling reduction factor χ_{ov}:

$$g_B = \chi_{ov} R_{Pl} - 1 \tag{2.10}$$

The plastic reference resistance is defined by the ratio of the yield strength f_y to a membrane equivalent stress σ_{EQ}:

$$R_{Pl} = \frac{f_y}{\sigma_{EQ}} \tag{2.11}$$

The value of the membrane equivalent stress σ_{EQ} is determined by a nonlinear finite element analysis. The buckling reduction factor χ_{ov} is determined through the slenderness ratios $\bar{\lambda}_{ov}$ (related overall slenderness), $\bar{\lambda}_0$ (fully plastic slenderness) and the $\bar{\lambda}_p$ (partly plastic slenderness):

$$\chi_{ov} = 1 \text{ if } \bar{\lambda}_{ov} \le \bar{\lambda}_0 \tag{2.12}$$

$$\chi_{ov} = 1 - \beta \left(\frac{\bar{\lambda}_{ov} - \bar{\lambda}_0}{\bar{\lambda}_p - \bar{\lambda}_0} \right)^{\eta} \text{ if } \bar{\lambda}_0 < \bar{\lambda}_{ov} < \bar{\lambda}_p \tag{2.13}$$

$$\chi_{ov} = \frac{\alpha}{\bar{\lambda}_{ov}^2} \text{ if } \bar{\lambda}_p \le \bar{\lambda}_{ov} \tag{2.14}$$

where η is the exponent for the buckling curve, α is the reduction factor for imperfections and β is the factor for the plastic region. The related slenderness ratio for the overall shell is assessed from the plastic reference resistance and the ideal buckling load R_{cr} determined by an eigenvalue analysis:

$$\bar{\lambda}_{ov} = \sqrt{R_{pl} / R_{cr}} \tag{2.15}$$

Overall stability is accounted for with the limit state function g_{os} containing the loading factor f which is also determined by the eigenvalue analysis:

$$g_{OS} = f - 1 \tag{2.16}$$

2.6.3 Uncertainties

Generic uncertainties for WECs range from structural system variables over load variables to model inherent uncertainties (e.g. Sørensen and Tarp-Johansen (2005)). As references for adjusting the statistical model of the uncertainties the probabilistic model

code JCSS (2006) in combination with the design documents (DIBt (2004)) and tests have been used.

The material parameters Young's modulus and yield strength are adjusted JCSS (2006).

The statistical model for the geometrical misalignment is taken from JCSS (2006). Adjustments are made such that the 95% quantile meets the specified value for misalignments in DIBt (2004).

During the application of sensors at the structure of the prototype 100 thickness measurements are made. With these measurement the probabilistic model of the JCSS (2006) is verified and adjusted.

Table 1: Uncertainties in stochastic finite element simulations

	Distr.	Mean Value	Stand. Dev.	Refer.
Misalignment (rad)	N	0.0	0.0048	JCSS (2006); DIBt (2004)
Thickness-deviation (mm)	N	1.2	0.7	JCSS (2006); Tests
Youngs modulus (N/mm²)	LN	210000	6300	JCSS (2006)
Yield strength (N/mm²)	LN	370	24.23	JCSS (2006)
Model Uncertainty	LN	1.0	0.15	JCSS (2006)
Wind load factor	WB	0.4891	0.2256	DIBt (2004)

N: Normal distribution; LN: Lognormal distribution; WB: Weibull distribution

A model uncertainty for the nacelle loading is introduced to represent the uncertainties associated with the preceding overall dynamic analysis. According to JCSS (2006)a lognormal distribution was assumed. The coefficient of variation was adjusted to 0.15 to account for the presumably higher uncertainties of this established but not yet extensively used design procedure.

The Weibull-distribution of the wind load factor was adjusted using the specified scale factor of 2.3 (DIBt (2004)) to the 2% quantile according to the specified recurrence period of 50 years.

2.6.4 Analysis of structural reliability

The finite element model is parameterized to account for the specified uncertainties. Due to the complexity of the model a simulation approach using response surfaces approach is utilized for the calculation of the structural reliability.

The response surfaces are applied to represent system responses rather than individual component limit states. This contributes to the precision due to avoidance of approximating discontinuous limit state functions (e.g. shell buckling) with continuous response surfaces.

A fractionated central composite design was used for the design of experiments. This design belongs to the class of so-called factorized designs (Myers and Montgomery (2002)) consisting of 2^{k-f} points of a k-dimensional hypercube, a centre point and $2k$ axis

points. Especially for higher numbers of random variables the number of runs provided by this design diverges substantially from the number of the coefficients of the response surface. In order to keep the numerical expenses affordable by keeping most of the precision a fractionated central composite design considering one half fraction is thus used (f=1). The location of the points is adjusted so that the relevant part of the event space is covered.

A fully quadratic response surface is applied. The coefficients a_i, b_{ij} and c are determined using linear forward-stepwise regression (ANSYS (2006)).

$$\bar{g}(\mathbf{X}) = c + \sum_{i=1}^{r} a_i X_i + \sum_{i=1}^{r} \sum_{j=1}^{r} b_{ij} X_i X_j \tag{2.17}$$

The system responses, i.e. R_{cr} and σ_{EQ}, are represented by the analyzed response surfaces and the reliability is assessed using the limit state functions with a latin-hypercube Monte-Carlo simulation scheme.

The results in regard to the probability of failure for selected sections of the structural system are given in (Figure 2-3). The probabilities of failure are generally very low compared to the target reliabilities for the ultimate limit state of 1.00×10^{-5} (JCSS (2006)). The dominating failure mode is shell buckling. The graphical representation gives an overview in regard to the structural reliability of the sections 7 to 11 belonging to the lowest tower segment (Figure 2-3).

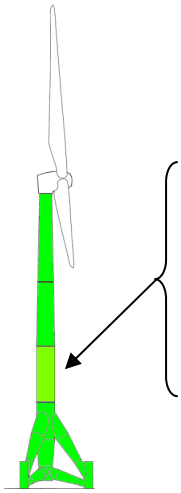

Component	Yielding	Buckling
…	…	..
Section 7	$< 10^{-6}$	$< 10^{-6}$
Section 8	$< 10^{-6}$	2.35×10^{-6}
Section 9	$< 10^{-6}$	3.75×10^{-6}
Section 10	$< 10^{-6}$	2.40×10^{-6}
Section 11	$< 10^{-6}$	$< 10^{-6}$
…	…	…

Figure 2-3: Probability of failure for selected limit state functions and overall representation of structural reliability

With consideration of all components and failure modes the system reliability is calculated for the ultimate limit state. The tower is considered as a non-redundant system. At component level the tripod is also assumed to have no redundancy. In case of failure of a part of the brace the capacity of the tripod is significantly reduced and is therefore considered as being equal to zero. Due to the ultimate limit state loading and the material properties the limit states are correlated. As a consequence the system reliability is modeled approximately through a series system with fully correlated failure

modes. The resulting probability of failure is equal to 3.75x10-6 yielding also a high reliability of the overall structure.

2.6.5 Monitoring data

The thresholds values for 45 strain gauges at the main structural components are simulated. For the simulation the described structural model and the uncertainty modeling specified in the foregoing is utilized. The strains are calculated at the exact position of the strain gauges at the structure in the finite element model using linear interpolation between the nodes (ANSYS (2006)). Fully quadratic response surfaces are determined based on the results. Using the response surfaces with Latin Monte-Carlo simulations non-parametric cumulative distribution function for the strains at the sensor positions were derived.

Three levels of thresholds are suggested. Threshold “A” takes basis in the deterministic model with the design loading under consideration of all limit states. The procedure of determining this threshold follows the design and represents in this context a characteristic value. Therefore the threshold “A” is directly linked to the design or certification process. When measured strains are less than this threshold the probability of failure of the design state is not exceeded.

Based on the probabilistic model i.e. under additional consideration of the uncertainties a fractile value can be derived based on a non-parametric distribution function. This leads to the threshold “B”. Below this threshold the component does not exceed the probability of failure as designed under consideration of the uncertainties.

The third threshold is derived generating a strain distribution for the limit state function value being smaller than zero. A fractile value of this strain distribution is defined as threshold “C”. Reaches a measured strain this threshold the probability of failure is nearly one.

In the region between threshold “B” and “C” the probability of failure is higher than in the certification. Actions to reduce the component strain and for determining the reason of the deviations would be required.

Further thresholds in terms of probabilities of failure determined by acceptance criteria are possible. The comparison with measured values is not yet representative for ultimate limit state since the measurements are taken just since 10 months within the project corporation.

2.6.6 Robustness index for ultimate limit state

A preliminary robustness index evaluation of an OWEC including all limit states and failure rates of the nacelle components indicates a very high robustness. The following detailed robustness consideration here represents only one possible limit state namely the ultimate limit state. Usually buildings, especially infrastructure buildings, have in this case a low robustness associated with high consequences ranging from property loss to the loss human lives.

To assess the robustness in quantitative terms necessitates the modeling of the indirect or follow-up consequences i.e. the consequences associated for each failure mechanism. Representative for the ultimate limit state the failure of segment 3 is modeled here.

In case of local section yielding it is assumed that the section retains most of the ultimate limit strength i.e. the ultimate strain is not exceeded in large regions.

The failure mechanism shell buckling on the other hand is associated with a rapid loss of strength after reaching the ultimate load. For an OWEC structure this means that such a failure with a very high probability is associated with further collapse and total loss of the functionality.

Because of the nature of these failure mechanisms the probability of the state "Collapse" of the node "Tower collapse" is assumed to 1 in case of buckling and 0.2 in case of yielding (Figure 2-4). With the tower collapse and the associated nacelle and rotor collapse there is certain probability that the tripod gets damaged or collapses through falling objects. This would also result in an overall collapse. Assuming the collapse mechanisms depicted in Figure 2-4 a probability of overall collapse in case of tower failure of 0.2 is assumed.

These collapse mechanisms are modeled with a Bayesian network (Figure 2-4) under further consideration of the consequences in monetary units resulting in the direct and indirect risks.

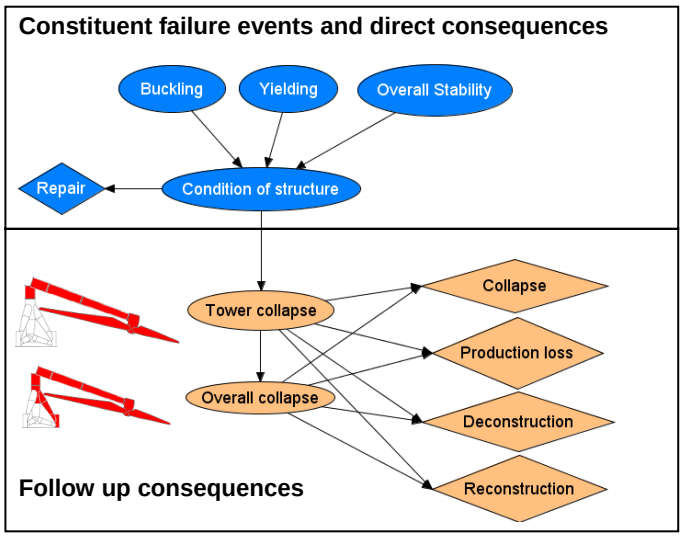

Figure 2-4: Bayesian network representation of ultimate limit state

The robustness index is found to be low due to the fact that probability of the high indirect consequences (tower and overall collapse) is in the same order of magnitude as the probability of the rather moderate direct consequences. However, the consequences and thus the associated risks are limited and are only related to economic loss of a single OWEC.

2.7 Conclusion and Outlook

A framework for the assessment and condition monitoring of OWECs integrating structural reliability, the robustness index and predetermined thresholds has been proposed and partially applied for the assessment of an OWEC prototype.

The assessment indicators structural reliability and robustness represent the design status of the considered OWEC prototype. Furthermore, sensitive components have been identified by comparing the structural reliabilities of the components.

The structural reliability i.e. the probability of failure is very low despite the rather high uncertainties associated with especially the loading.

The analysis of consequences shows very limited indirect consequences. The robustness index for the ultimate limit state is low as would be expected for other infrastructure buildings.

This proposed framework should be further verified and extended to the assessment of the serviceability and fatigue limit states.

3 Ultimate limit state model basis for assessment of offshore wind energy converters (Paper II)

S. Thöns

BAM Federal Institute for Materials Research and Testing, Berlin, Germany and

Swiss Federal Institute of Technology, Zurich, Switzerland

M. H. Faber

Institute of Structural Engineering, ETH Zurich, Zurich, Switzerland

W. Rücker

BAM Federal Institute for Materials Research and Testing, Berlin, Germany

Journal of Offshore Mechanics and Arctic Engineering (JOMAE), August 2012, Volume 134, Issue 3, 031904 (9 pages)

http://dx.doi.org/10.1115/1.4004513

Abstract

This paper establishes the model basis regarding the ultimate limit state consisting of structural, loading and probabilistic models of the support structure of offshore wind energy converters together with a sensitivity study. The model basis is part of a risk based assessment and monitoring framework and will be applied for establishing the "as designed and constructed" reliability as prior information for the assessment and as a basis for designing a monitoring system. The model basis is derived considering the constitutive physical equations and the methodology of solving these which then in combination with the ultimate limit state requirements leads to the specific constitutive relations. As a result finite element models based on shell elements incorporating a structural and a loading model are introduced and described in detail. Applying these models the ultimate capacity of the support structure and the tripod structure are determined with a geometrically and materially non-linear finite element analysis. The observed failure mechanisms are the basis for the definition of the ultimate limit state responses. A probabilistic model accounting for the uncertainties involved is derived on the basis of literature review and measurement data from a prototype Multibrid M5000 support structure. In combination with the developed structural and loading models, sensitivity analyses in regard to the responses are performed to enhance the understanding and to refine the developed models. To this end, as the developed models necessitate substantial numerical efforts for the probabilistic response analysis predetermined designs of numerical experiments are applied for the calculation of the sensitivities using the Spearman rank correlation coefficient. With this quantification of the sensitivity of the random variables on the responses including non-linearity the refinement of the model is performed on a quantitative basis.

3.1 Introduction

The assessment of offshore wind energy converter (OWEC) structures plays an important role for their integrity management during their entire life-cycle. Efficient strategies for structural response and condition monitoring utilizing appropriate probabilistic assessment models enhance life-cycle optimal decision making in regard to inspection and maintenance activities which for offshore structures are associated with significant costs.

To develop models appropriate for the assessment of the wind energy converter support structure necessitates that extensive information is available; drawings which document the built structure, engineering models, certification documents, information about the construction, production data for the support structure and site specific environmental measurements. The integration of this information is an important task in the assessment and involves the application of stochastic models and procedures. Furthermore, it is typical that engineering models as utilized for design purposes are not directly useful for assessment purposes. This is due to the extensive use of conservative empirical models in design engineering. For this reason refinements or reformulation of engineering models are required. These are met by the proposed assessment and monitoring framework as described in Thöns, Faber et al. (2008).

Initially the assessment and monitoring framework integrating this model basis is summarized. The model basis for the assessment of the wind energy converter

substructure is then introduced beginning with a general constitutive physical model leading to the specific finite element representation of the constitutive equations.

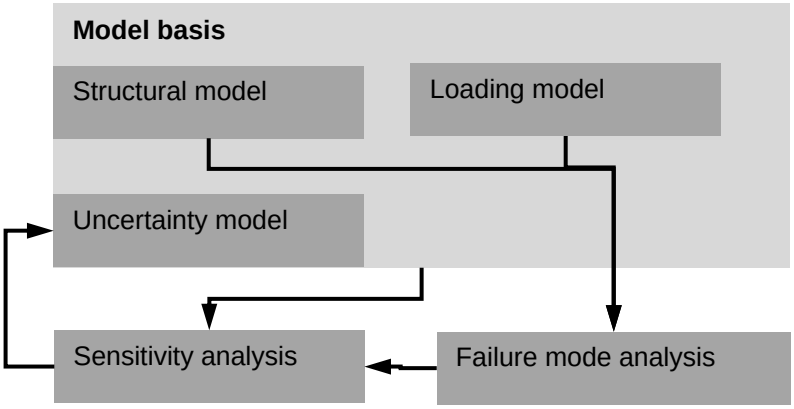

Figure 3-1: Paper organization containing the model basis and analyses for model development.

Subsequently the failure modes of the tripod structure and the overall support structure in the ultimate limit state are analyzed by a geometrically and materially non-linear analysis with the developed structural and loading models. With this the responses for the sensitivity analysis are determined. The uncertainty models of the structural and loading model parameters are introduced in the following section. The methodology and the results of a sensitivity study are documented in the third section followed by the conclusions containing an improved uncertainty model. This paper organization and the relations between the models and the methods are depicted in Figure 3-1.

3.2 Monitoring and assessment framework

The proposed assessment framework for the offshore wind energy converter structures (Thöns, Faber et al. (2008)) integrates risk analysis with system monitoring data. The structural assessment is based on components and overall structural systems reliability analysis together with the risk based robustness index following Faber, Maes et al. (2007). Sensor signals are compared with criteria for ensuring an adequate structural behavior through predetermined thresholds of limit state specific indicators (Figure 3-2).

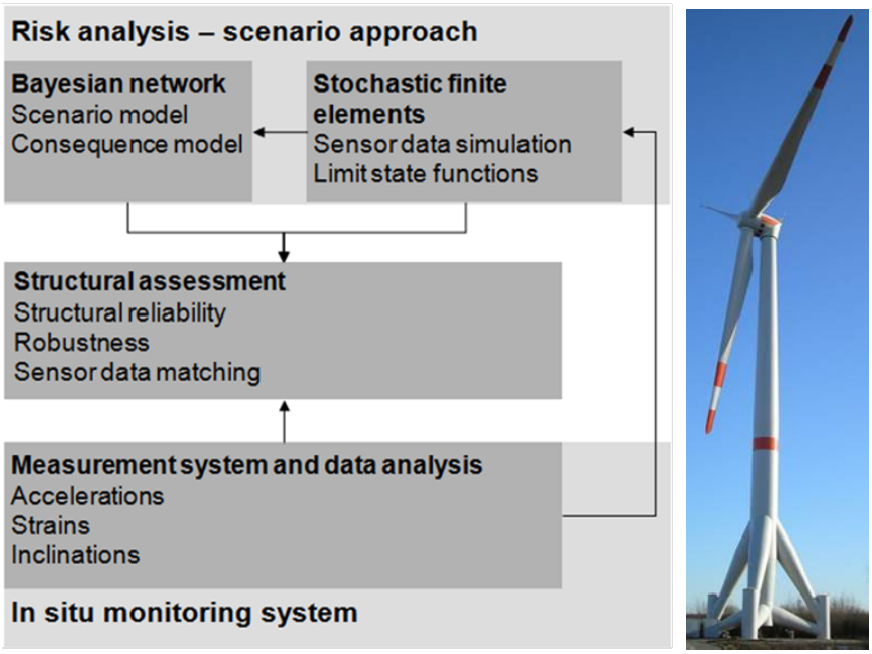

Figure 3-2: Assessment and monitoring framework with an offshore Multibrid M5000 prototype installed onshore.

The prior structural reliability (meaning "as designed and constructed") and the sensor signals are calculated applying the model basis to be introduced in the subsequent sections consisting of structural, loading and stochastic models. The structural performance is monitored, the probabilistic characteristics are updated based on measurements and compared with predetermined thresholds. The prior robustness is also initially quantified based on the prior probabilistic models and the Bayesian network containing the scenario model and the consequence model, see Thöns, Faber et al. (2008). The robustness is monitored and updated using monitoring data in a similar way as the reliability. This framework is finally developed and tested on a Multibrid M5000 prototype structure which is installed onshore in Bremerhaven equipped with a monitoring system consisting of strain, acceleration and inclination sensors.

3.3 Model basis

The ultimate limit state model basis for the support structure is derived based on the constitutive physical models of the overall wind energy converter including interaction with all environmental media as well as the grid connection (Figure 3-3). The complexity of this system, however, necessitates the application of different modeling detail levels; first an overall rather simple dynamic model is established facilitating time domain calculations on the basis of which the input for more refined (structural) models is generated. The refined models to be introduced here are formulated with due consideration of common modeling aspects regarding the ultimate limit state.

3.3.1 Constitutive physical model for offshore wind energy converters

An OWEC consists of a control unit, a rotor, an electro-mechanical conversion system and a support structure. There are major and minor interactions within this system and to the environment characterizing the complexity. The support structure is influenced by

the rotor, the aerodynamic loading, the hydrodynamic loading and the soil behavior (Figure 3-3).

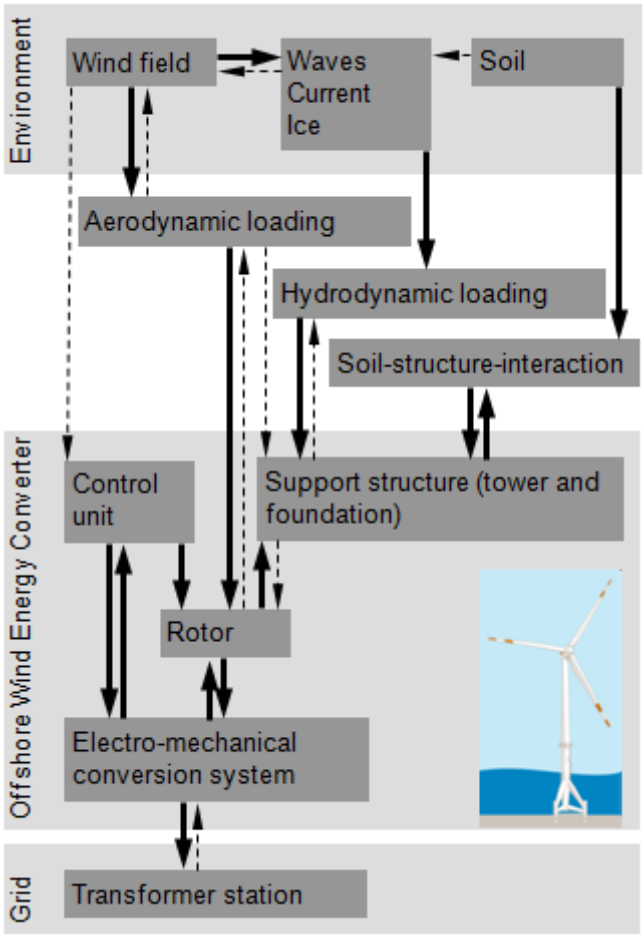

Figure 3-3: Interactions (thick line: major interaction; dashed line minor interaction) within the offshore wind energy converter and between the offshore wind energy converter and the environment (Kühn (2001)).

A constitutive physical model of the offshore wind energy converter can be written based on a discrete dynamic equation with mass matrices $\mathbf{M}$, the damping matrices $\mathbf{D}$, the stiffness matrices $\mathbf{K}$, the degree of freedom vectors $\mathbf{x}$ and the loading vectors $\mathbf{f}$ distinguishing between the wind turbine (index WT: nacelle, hub and rotor) as well as the support structure (index SS: tower, e.g. tripod and foundation). The matrices and the force vectors (Equation (3.1)) are sub-divided into the aerodynamic fraction (index a) and the hydrodynamic fraction (index h). The hydrodynamic mass matrix and loading vector is only relevant for the support structure.

The wind turbine relevant parts of the matrices in Equation (3.1) are time variant. Furthermore various dependencies are introduced due to nonlinearities. The strongest nonlinearities are caused by aerodynamics due to flow separation. Geometrical nonlinearities are introduced due to substantial deflections of both the structure and the blades. In addition hydrodynamic effects caused by large waves cause nonlinearities.

The hydrodynamic drag coefficient and the soil dynamics are assumed to be linear in accordance with Kühn (2001).

$$\left[\mathbf{M}^{WT+SS}+\mathbf{M}_h^{SS}\right]\ddot{\mathbf{x}}+\left[\mathbf{D}^{WT+SS}+\mathbf{D}_a^{WT+SS}\right]\dot{\mathbf{x}}+\left[\mathbf{K}^{WT+SS}+\mathbf{K}_a^{WT+SS}\right]\mathbf{x}=\mathbf{f}_a^{WT+SS}+\mathbf{f}_h^{SS} \qquad (3.1)$$

In general the non-linear, dynamic constitutive relation given in Equation (3.1) can be solved in the time domain, i.e. by the generation of time series from wind and wave spectra applying time step integration followed by a Rainflow counting of stress ranges for fatigue. Another option is to formulate and conduct the analysis in the frequency domain, i.e. applying the environmental spectra directly in combination with a linear spectral analysis and subsequently calculating the stress range distribution from the spectral moments. The time domain approach is usually used for the design of offshore wind energy converters as it is validated against measurements and overcomes difficulties of the frequency domain approach such as the time dependency of the mass, damping and stiffness matrix and the wide band characteristics of the aerodynamic loading (Kühn (2001)).

The complexity and the high computational requirements of the overall dynamic simulation in the time domain limit especially the structural models to simple beam and spring models. However, the loading for the individual sections of the support structure can be calculated using the generated force vectors. The representation of the limit states of relevance for the support structure requires more refined models in order to appropriately represent the response of this shell type structure.

For the ultimate limit states of the support structure normally calculations of stresses and buckling factors for extreme loading conditions are required. These analysis results are established by the application of the finite element method. The application of less computationally involving approaches such as analytical limit state design imply coarser engineering models and do not facilitate for the consistent modeling of overall system properties and interactions. With the concept outlined using finite element method representations the analyses of the ultimate limit state is performed. The constitutive physical relations utilized for the analysis of the ultimate limit state are given in Equation (3.2) and Equation (3.3) reduced to a steady state problem and a generalized eigenvalue problem. Equation (3.3) contains the matrix of the mode shapes $\mathbf{\Phi}$, the diagonal matrix of the eigenvalues $\mathbf{\Lambda}$ and the geometrical stiffness matrix $\mathbf{S}^{SS}$. Perhaps nonlinearities like geometric nonlinearities cause dependencies and contact formulations additional terms in Equation (3.2) containing the boundary functions to be imposed.

$$\mathbf{K}^{SS}\mathbf{x}=\mathbf{f}^{SS} \qquad (3.2)$$

$$\mathbf{K}^{SS}\mathbf{\Phi}=\mathbf{S}^{SS}\mathbf{\Phi}\mathbf{\Lambda} \qquad (3.3)$$

3.3.2 Deterministic models

3.3.2.1 Structural model

The support structure of the wind energy converter consists of the tower divided in segments by ring flanges, the tripod consisting of upper braces, lower braces, the pile

guide as well as the foundation, which in contrast to the case where the structure would be installed offshore consists of circular reinforced concrete slabs attached to a pile group (Figure 3-4a). The stresses in the tower sections may be calculated using beam theory, but the stress calculation of the tripod requires at least a shell model due to the diameter to length ratio of the components involved. As a consequence all components are represented in the finite element modeling by means of shell elements.

The finite element models developed incorporate iso-parametric displacement based shell elements (SHELL 181: ANSYS (2006)) combining plate and membrane theory with linear interpolation functions. At geometrical discontinuities, especially at the tube connections within the tripod the mesh was refined until the resulting stresses became independent of the mesh.

The ring flanges in the tower are modeled with their thickness by shell elements representing a constraint for the tower segments. The ring flanges are assumed rigidly connected due to the pre-stress of the bolts.

The support structure is connected to the foundation through the pile guides (Figure 3-4a). The pile guides contain reinforced concrete and shear connectors which are welded to the inside of the pile guide. Through the shear connectors and through friction this system (pile guide / reinforced concrete) acts mechanically as one solid section. For the case that a tension force is applied to the outer steel section of the pile guide (due to the braces) the pile guide and the reinforced concrete do not act as one section since the tension forces between steel and concrete are not transmitted. In this case the local behavior is different from the global behavior. This mechanical phenomenon can only be modeled by a contact finite element formulation. The same argumentation applies to a grout connection, which is utilized for the offshore installation of this support structure.

The inside of the pile guide and the outside of the reinforced concrete is meshed with contact elements (CONTA173/174 and TARGE170). The initial contact conditions are adjusted such that the contact forces are independent of the meshes of the pile guide and the reinforced concrete. A friction coefficient of 0.8 which incorporates the friction coefficient between concrete and steel (0.2 – 0.4) and the influence of the shear connectors is applied. The reinforced concrete is connected to the spring elements which represent the foundation stiffness determined by a separate model (Figure 3-4a).

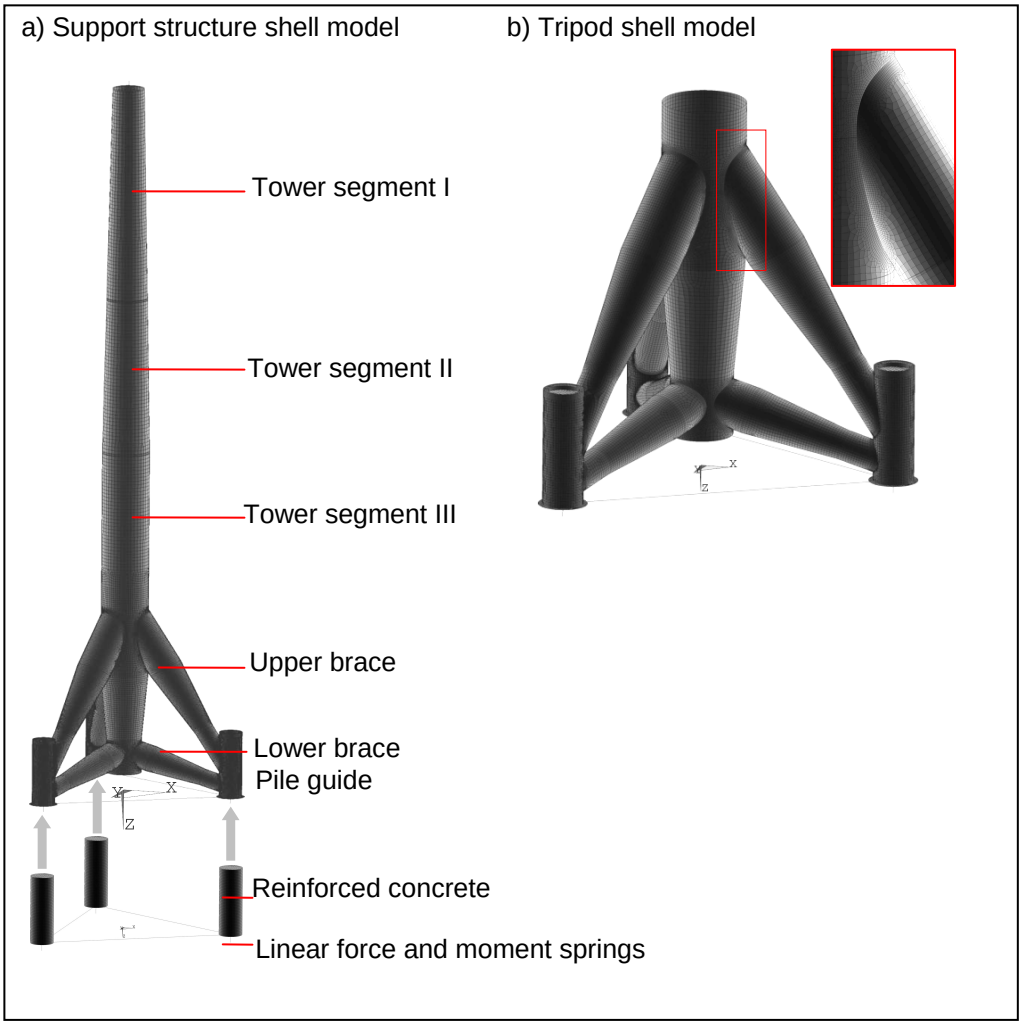

Figure 3-4: Ultimate limit state model basis consisting of the support structure model (a) and a tripod model (b)

3.3.2.2 Loading model

The loading model consists of the loading vectors at the top of the support structure calculated by the time domain analysis and the distributed wind loading on the support structure. The loading vectors for the ultimate limit state have the format of a matrix where all load cases leading to a maximum or minimum of an element of the vector are listed. Within this matrix a representative load case is selected resulting in the highest horizontal force and therefore causing the highest overturning moment.

The wind loading on the structure is small in comparison to the resulting forces of the wind loading on the rotor and nacelle even in the ultimate limit state (in regard to the base overturning moment the magnitude is about 5%). However, the wind loading is modeled for the ultimate limit state considering the gust response factor according to (Schaumann, Böker et al. (2007)).

For the wind loading the outer surface of the structure is meshed with surface effect elements (SURF154) for applying pressure loading. Since the stresses induced by the circumferential wind pressure distribution are very small due to the dominating rotor

and nacelle loading this effect is not included in the model. The circumferential distribution of the wind pressure is uniform corresponding to the projected area. The height distribution is subdivided in certain regions in accordance with the height distribution function contained in DIBt (2004) (Figure 3-5).

The force vectors are applied to nodes where the degrees of freedom are coupled with the nodal degrees of freedom of the shell section. This ensures the coupling of the nodes of the shell section and hence results in a rigid region which is a good approximation for sections where a stiff ring flange is located like at the top of the tower (Figure 3-4a). At the top of the tripod (Figure 3-4b) this introduces a modeling imprecision but plays a minor role since the relevant sections are located at a sufficient distance from the rigid sections.

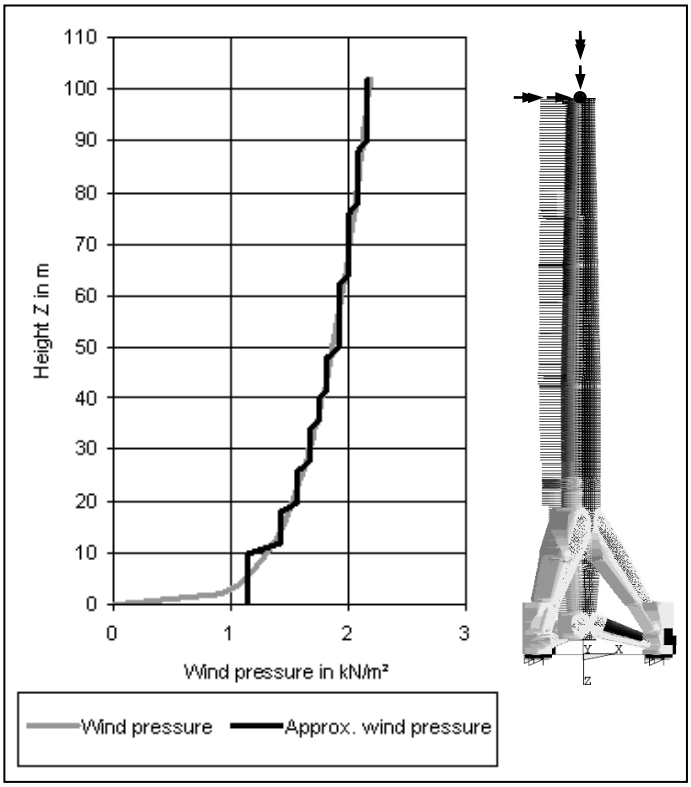

Figure 3-5: Height varying wind pressure distribution and nacelle loading vector at the top of the support structure.

3.3.3 Ultimate loading capacities of the tripod and the overall support structure

For the determination of the mechanisms leading to the ultimate loading capacity a geometrically and materially nonlinear analysis (GMNA, DIN EN 1993-1-6 (2007)) for the tripod and for the overall support structure are conducted. Global imperfections (misalignments) are introduced according to DIBt (2004). A von Mises yield criterion without hardening (linear elastic, ideal plastic material model) is assumed. No strain limit is fixed. Geometric nonlinearities are applied leading to a third order theory analysis, i.e. equilibrium in deformed state including nonlinear geometry. The loading is applied on the top of the tripod (Figure 3-4b) using nodal degree of freedom coupling.

With the exception of the dead load the loading is increased until the stiffness matrix becomes singular which then causes a termination of the calculation. The factor between the design loading and the actual loading is defined as the loading factor.

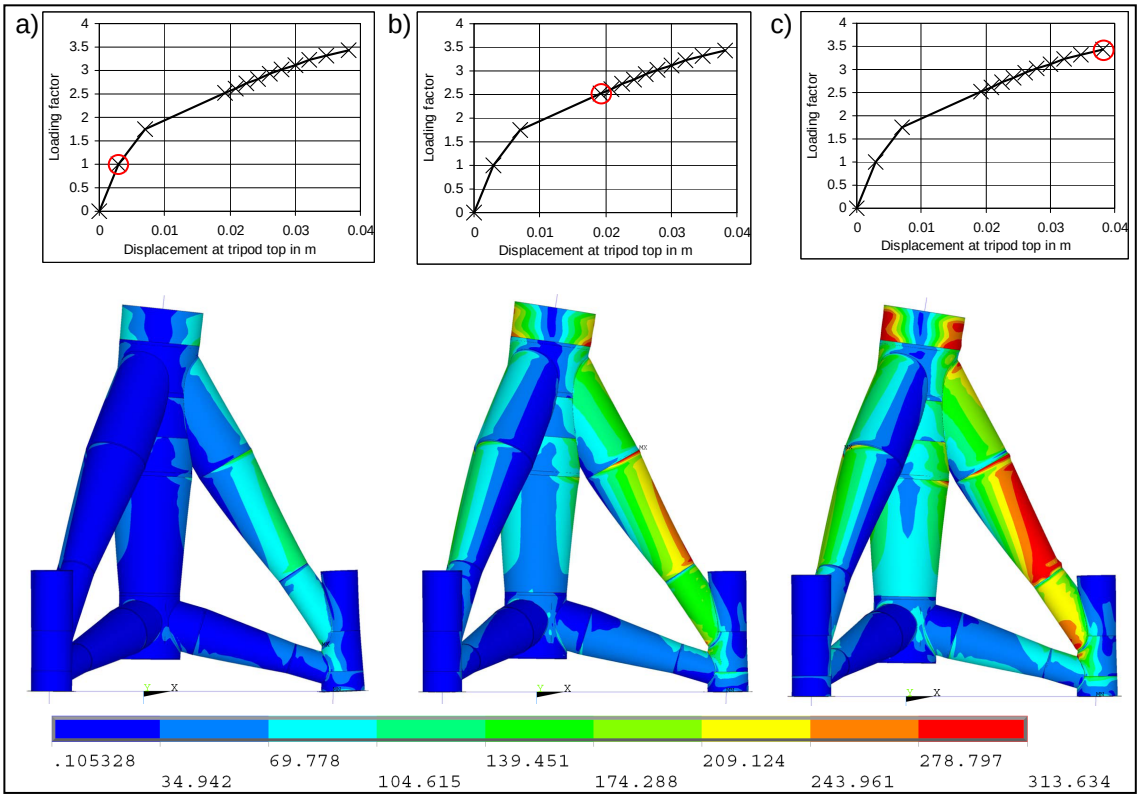

Figure 3-6: Von Mises equivalent stress (Figures a) to c)) for three points of the load deflection curve, (ANSYS printout).

The loading deflection curve of the tripod shows a ductile behavior (Figure 3-6 and Figure 3-7). The first plastic strains develop at the connection between the lower brace and the pile guide followed by plastic strains in the upper brace at the upper connection between the cylindrical part and the conical part (Figure 3-7a). Furthermore the stress on the top-side of the conical part of the upper brace increases significantly at this load step (Figure 3-6b). The plastic strains cause a redistribution of stresses and a further increase of the capacity of the tripod. As a consequence further plastic strains develop at the lower connection between the cylindrical part and the conical part and at the connection of the tower with the upper brace (Figure 3-7b). The ultimate loading is not reached at locations where the plastic strains develop first, but in the conical section close to the lower cylindrical part of the upper brace (Figure 3-7c). At this location a substantial part of the section is plasticized (Figure 3-7c) and the stresses in the upper area of the upper brace conical section are at or very close to the yield stress (Figure 3-6c). Looking at the deformation an outward deformation in the form of one half ring develops in the plasticized region (Figure 3-7c) indicating that the ideal buckling strength might also be reached. The ultimate loading capacity is reached when 3.42 times the design loading (see Section 3.3.2.2) is applied.

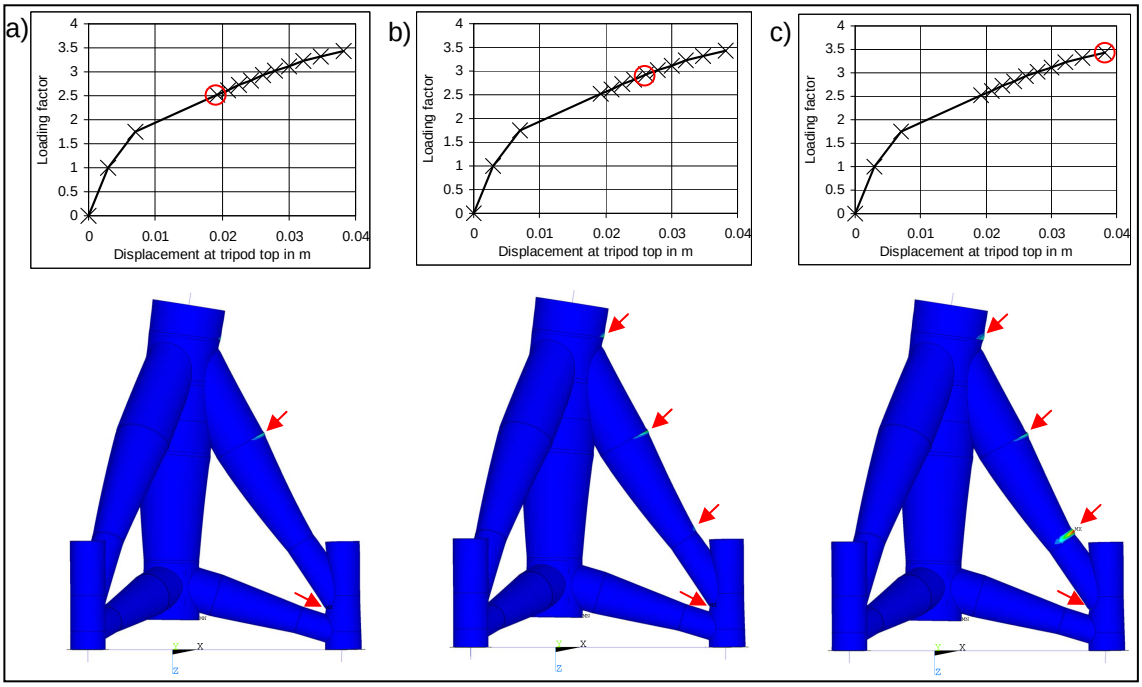

Figure 3-7: Equivalent plastic strains (Figures a) to c)) for three points of the load deflection curve, (ANSYS printout).

The load deflection curve of the overall support structure (Figure 3-8) is linear until the loading reaches 1.6 times the design loading (see Section 3.3.2.2). However, in a small region in the lowest tower segment III the first plastic strains start to develop at a loading factor of 1.4 (Figure 3-8b). With further load increase the yield stress is reached in further sections of this segment. The ultimate loading capacity is reached with further concentration of the plastic strains in this section but without complete plastification (Figure 3-8 c bottom). It is observed that in the region of plastic strains a few short wave half ring buckles develop which is typical for flexural shell buckling. In combination with the significant length of the structure this leads due to the loss of stiffness and due to the movement of the neutral axis to a phenomenon known as interaction buckling, i.e. the combination of global (Euler flexural) and local (shell buckling) buckling. The behavior for the overall support structure is therefore not very ductile leading to a capacity of 1.65 in respect to the design loading.

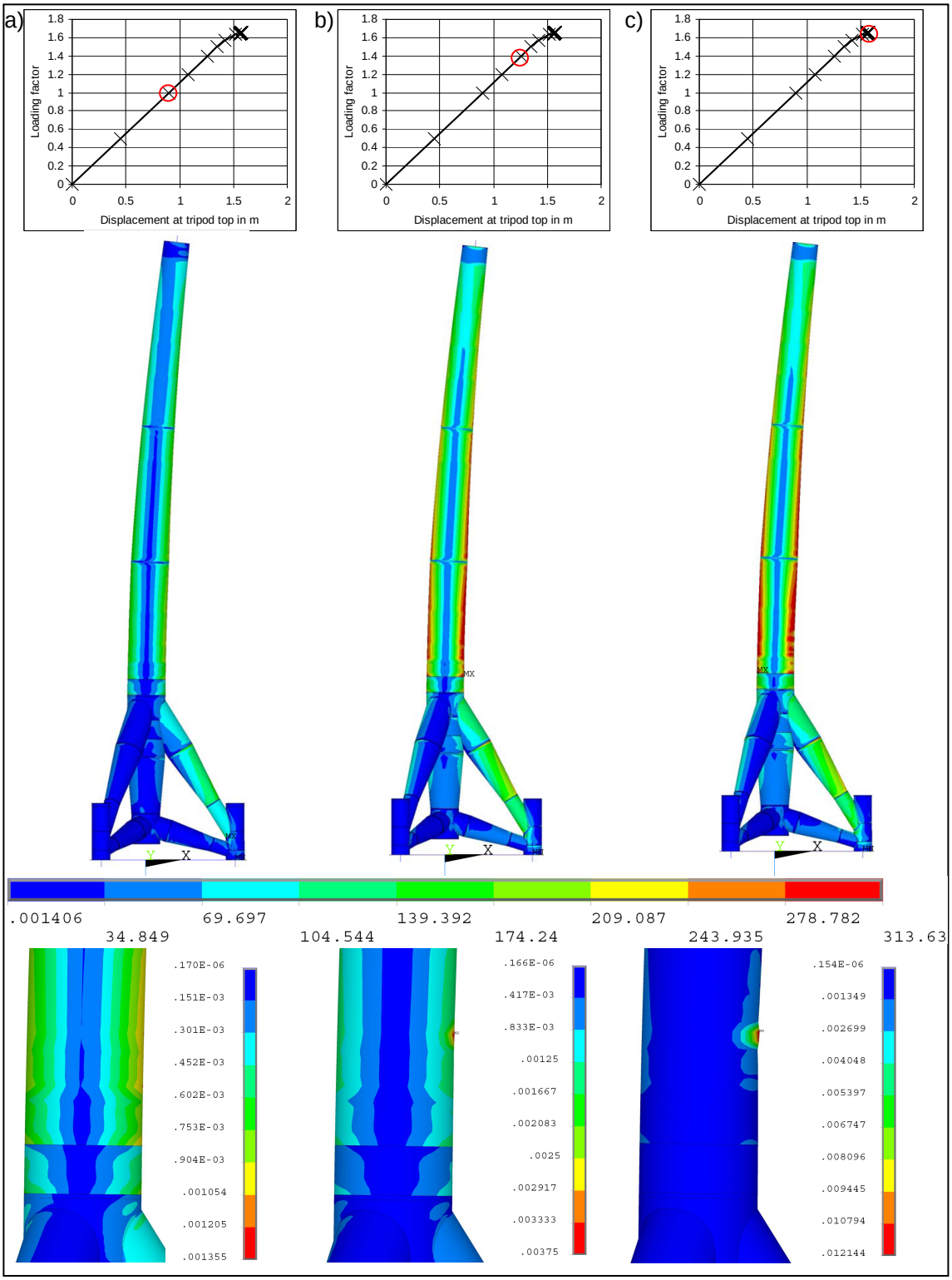

Figure 3-8: Von Mises equivalent stress (top) and equivalent strains (bottom) for three points of the load deflection curve.

For both analyses it should be kept in mind that the failure mechanism of shell buckling is only represented in the modeling with the ideal buckling capacity because local imperfections are not incorporated in the structural model. For the overall support

structure the ideal shell buckling capacity (which here is considered as the initiating cause for interaction buckling) determines the loading capacity. The buckling capacity with consideration of local imperfection is then lower but the failure mechanism is clearly identified.

The mechanism determining the ultimate capacity of the tripod is on the first sight yielding for the case without consideration of local imperfections, i.e. by a GMNA analysis. However, the observed half ring buckle indicates that the buckling and yielding does not necessarily occur strictly separated and secondly that the ideal buckling capacity might also be reached. The buckling capacity applying a geometrically and materially nonlinear analysis with local imperfections (GMNIA) will then be lower than the ideal buckling capacity and hence lower than the yielding capacity. Therefore it is in the further assumed that shell buckling is the mechanism leading to the ultimate capacity below the factor of 3.42 as assessed when local imperfection effects are included.

3.3.4 Probabilistic parameters model

To support the assessment and service-life health monitoring and management a risk and reliability based approach is utilized. Thus all relevant uncertainties influencing the performance of the OWEC need to be modeled probabilistically. Probabilistic modeling of OWEC structures necessitates the consideration of the global structural system variables over load variables to model uncertainties (e.g. Sørensen and Tarp-Johansen (2005)). In the present modeling basis the probabilistic modeling is adapted to the probabilistic model code (PMC) of the Joint Committee on Structural Safety JCSS (2006) in combination with design documents (e.g. DIBt (2004)) and experimental investigations. For the structural and loading models the probabilistic models given in Table 3-1 are applied incorporating the foundation stiffness factor, the steel section thickness deviation, the modulus of elasticity, the global misalignment of the support structure, the yield stress, the model uncertainty of the preceding dynamic analysis and the wind load factor.

The probabilistic model of the foundation stiffness factor is established applying a prior indication of the coefficient of variation of the foundation stiffness according to JCSS (2006), Part 3.07 Soil Properties. A full correlation of the foundation stiffness factor f_g for all three legs is assumed and the springs representing the foundation soil interaction are parameterized with this model.

The statistical model for the structural steel section thickness deviation is derived utilizing on site measurement data. On the Multibrid M5000 prototype structure (Figure 2-1) 100 thickness measurements are made using an ultrasonic thickness measuring device (Panametrics 360L Plus) with a probe size of about 1 cm^2. The measurements were taken within nine different sections. These data indicate that the deviations from nominal material thicknesses depend on the absolute values of the thicknesses. Further the measurement data contain local spatial variations due to the small probe size.

The probabilistic model of the thickness deviation according to JCSS (2006), Part 3.02: Structural Steel, utilizes a normal distribution with a mean between -1 mm and 1mm with standard deviation less than 1 mm with no spatial variation. The thickness deviation f_t is added to the nominal thickness of the sections. As a starting point the

parameters of this statistical model are evaluated applying the maximum likelihood method and using all measurement data. This leads to a slightly higher mean value of 1.2 mm and a standard deviation of 0.7 mm.

The probabilistic model of the modulus of elasticity E is established according to JCSS (2006), Part 3.02: Structural Steel fully correlated over the entire structure implying no spatial variation. The misalignment α of the support structure represents misalignments due to construction and due to solar radiation. The angle of misalignment which is specified in the design guideline (DIBt (2004)) is taken as the 95% fractile value for evaluating the standard deviation of the Normal distribution assuming a mean value equal to zero.

Table 3-1: Probabilistic models for the structural and loading models

Parameter	Distr.	Mean	Standard deviation	Reference
Foundation stiffness factor f_g	LN	1.0	0.6	JCSS (2006)
Thickness-deviation f_t (mm)	N	1.2	0.7	JCSS (2006), Meas. on prototype
Modulus of elasticity E (N/mm²)	LN	210000	6300	JCSS (2006)
Misalignment α (rad)	N	0.0	0.0048	JCSS (2006); DIBt (2004)
Yield stress f_y (N/mm²)	LN	$f_{y,sp} - K$	$0.07\left(f_{y,sp} - K\right)$	JCSS (2006)
Model uncertainty $f_{M\,\mathrm{od}}$	LN	1.0	0.1	JCSS (2006)
Wind load factor f_w	WB	0.4891	0.2256	DIBt (2004)

N: Normal distribution; LN: Lognormal distribution; WB: Weibull distribution

The variability of the yield stress f_y is of further interest and has been modeled according to JCSS (2006), Part 3.02: Structural Steel with the constant K and with the yield strength $f_{y,sp}$ specified in DIN EN 10025 (2005b) assuming full correlation for all components.

The loading vector at the top of the tower and the wind pressure (see Figure 3-5) in the ultimate limit state is multiplied with the random variable f_w, the wind load factor, representing the long-term wind load distribution. The probabilistic model is derived from the following consideration. The wind load for the load case considered (derived from the min/max matrix – see Section 4.2.2) is based on the 5 sec. mean value of the wind speed corresponding to a 50 year return period with a reference period of one year. Assuming a Weibull-distribution for the wind load, the wind load factor f_w is introduced. The parameters are derived using the site specific scale factor of 2.3 (OWT

(2009)) and calculating the shape parameter assuming that the given loading represents the 98% fractile value of this distribution.

The random variable $f_{M\,\mathrm{od}}$ represents the model uncertainty associated with the structural and loading models of the preceding overall dynamic analysis (see Section 3.3.1) which determines the loading. This uncertainty includes random effects that are neglected in the models and simplifications in the mathematical relations. The factor $f_{M\,\mathrm{od}}$ is determined using the probabilistic model code (JCSS (2006), Part 3.09 Model Uncertainties) and is applied to the loading vectors.

3.4 Sensitivity analysis

Using the structural, loading and uncertainty models introduced in the previous sections the sensitivity of the random variables in regard to the relevant responses is determined by the coefficient of correlation quantifying the degree of functional dependency. The responses and a solution strategy in the view of applying this concept for later reliability calculations are defined in the next section. Measures of correlation taking into account also non-linear dependencies are introduced in the subsequent section. The results are documented and summarized in the last section.

3.4.1 Definition of responses and solution strategy

The responses are defined for the ultimate limit state having in mind that this sensitivity study will be followed by a reliability calculation. For this purpose the solution strategy is developed for the specific failure mechanisms hence facilitating the definition of relevant responses.

The failure mechanisms for the ultimate limit state are yielding and stability which comprises of global and local instability. In contrast to Section 3.3.3 where a GMNA analysis is performed, here a combination of a linear buckling analysis (LBA) and a material non-linear analysis (MNA) is applied (DIN EN 1993-1-6 (2007)). This concept facilitates the calculation of both stability failure mechanisms including the effect of local imperfections and of the yielding failure mechanism avoiding a computational demanding iterative approach to assess the ultimate loading capacity. Hence this concept will be used for reliability calculations. The responses σ_{EQ} being the equivalent membrane stress (Equation (3.4)) with the membrane forces n_θ and n_x), the ideal buckling resistance factor r_{Rcr} and the ratio of the bending induced stress to the overall stress σ_M / σ are introduced. These responses are calculated for each section of the support structure (see Figure 3-4a).

$$\sigma_{EQ} = \frac{1}{t}\sqrt{n_x^2 - n_x \cdot n_\theta + n_\theta^2 + n_{x\theta}^2} \tag{3.4}$$

When solving the steady state equation (Equation (4.2)) for the support structure model (Figure 3-4), incorporating a relatively large number of nodes, higher order shell elements and non-linearity due to the contact formulation, an iterative approach using a Newton-Rapson line search is applied (ANSYS (2006)). The convergence criteria incorporate a force, a moment and a degree of freedom criteria. For all criteria the Euclidian vector norm is checked at each load step with an allowance of 5% in regard to a model based reference value. The individual iterations are solved with an iterative

solver namely the preconditioned conjugate gradient solver. The ideal buckling capacities of the support structure (Equation (3.3)) are calculated applying a Block-Lanczos algorithm with a Sturm sequence check (ANSYS (2006)).

3.4.2 Measures of correlation and design of experiments

The linear coefficient of correlation r_{xy} is defined as the ratio of the covariance s_{xy} to the product of the standard variations s_x and s_y of realizations of the considered random variables x and y (see Equation (3.5)). To account for non-linear dependencies between the response characteristics and the realization of the random parameters the Spearman rank correlation coefficient ρ_{xy} is introduced (Equation (3.6)). In principle the Spearman rank correlation is equivalent to the linear coefficient of correlation but the realizations of variables are converted into ranks before the correlation coefficients are calculated. This mathematical operation converts values of a function in a number according to a rank in an ordered row and effectively means that any biunique function dependency between the random variables x and y (e.g. parameters and responses) is linearized. Therefore any biunique dependency between the random variables x and y leads to Spearman rank coefficient equal to one.

$$r_{xy} = \frac{s_{xy}}{s_x s_y} = \frac{1}{n} \frac{\sum_{i=1}^{n} \left(x_i - \overline{x}\right)\left(y_i - \overline{y}\right)}{s_x s_y} \tag{3.5}$$

$$\rho_{xy} = \frac{\sum_{i=1}^{n} \left(rg\left(x_i\right) - \overline{rg}_x\right)\left(rg\left(y_i\right) - \overline{rg}_y\right)}{\sqrt{\sum_{i=1}^{n} \left(rg\left(x_i\right) - \overline{rg}_x\right)^2} \sqrt{\sum_{i=1}^{n} \left(rg\left(y_i\right) - \overline{rg}_y\right)^2}} \tag{3.6}$$

Restricted by the complexity and numerical efforts associated with the finite element calculations predetermined designs of experiments for the random variables are used namely a Central Composite Designs consisting of 2^{k-f} points of a k-dimensional hypercube, one centre point and $2k$ axis points. Fractional designs with a resolution V are applied, which facilitates the modeling of non-linear responses.

Another important aspect is the choice of the central point of the experimental design. This point should be chosen near the design point, i.e. near the point of the limit sate surface which is the closest to the origin in the standardized normally distributed space. For the sensitivity analysis conducted here a guess of the design point is used by classifying the random variables into resistance and load variables. The centre point is selected as $x_{C_i} = \mu_{X_i} \mp 3s_{X_i}$ (with the mean μ_{X_i}) for load variables with the plus and resistance variables with the minus and a range for both of $x_{C_i} \mp s_{X_i}$. Because of the application of non-symmetrical probability distribution functions in the probabilistic modeling the probabilities determined with a standard normal distribution are used.

3.4.3 Results

With the mentioned methodology the Spearman rank correlations are assessed using a central composite design of experiments. The symmetrical Spearman rank correlation matrix for the ultimate limit state is shown in Figure 3-9 containing the correlations for

7 random variables (f_g, f_t, E, α, f_y, f_w and f_{Mod}) and for 7 responses namely the equivalent membrane stresses σ_{EQ}, the stress ratios σ_M / σ and the ideal buckling resistance factor r_{Rcr} for the sections 8 to 10 of tower segment III (see Figure 3-4a). These sections have been chosen because they are assumed to be relevant for later reliability calculation due to their high stresses.

	f_g	f_t	E	f_y	α	f_{Mod}	f_w	$\sigma_{EQ,S9}$	$\sigma_{EQ,S10}$	$\sigma_{EQ,S11}$	$\frac{\sigma_{M,S9}}{\sigma_{S9}}$	$\frac{\sigma_{M,S10}}{\sigma_{S10}}$	$\frac{\sigma_{M,S11}}{\sigma_{S11}}$	r_{Rcr}
f_g	1.00	0.03	0.03	0.03	0.03	0.04	0.03	-0.07	-0.07	-0.07	0.10	0.12	0.14	0.04
f_t	0.03	1.00	0.03	0.03	0.03	0.04	0.03	-0.16	-0.16	-0.16	-0.11	-0.09	-0.08	0.19
E	0.03	0.03	1.00	0.03	0.03	0.04	0.03	0.03	0.03	0.03	-0.04	-0.03	-0.03	0.10
f_y	0.03	0.03	0.03	1.00	0.03	0.04	0.03	0.03	-0.03	0.03	-0.06	-0.07	-0.05	0.00
α	0.03	0.03	0.03	0.03	1.00	0.04	0.03	-0.01	-0.01	-0.01	0.01	0.01	0.01	0.01
f_{Mod}	0.04	0.04	0.04	0.04	0.04	1.00	0.00	0.35	0.35	0.35	0.35	0.35	0.35	-0.36
f_w	0.03	0.03	0.03	0.03	0.03	0.00	1.00	0.88	0.88	0.88	0.88	0.88	0.88	-0.86
$\sigma_{EQ,S9}$	-0.07	-0.16	0.03	0.03	-0.01	0.35	0.88	1.00	1.00	1.00	0.97	0.96	0.96	-0.98
$\sigma_{EQ,S10}$	-0.07	-0.16	0.03	-0.03	-0.01	0.35	0.88	1.00	1.00	1.00	0.98	0.97	0.97	-0.99
$\sigma_{EQ,S11}$	-0.07	-0.16	0.03	0.03	-0.01	0.35	0.88	1.00	1.00	1.00	0.97	0.96	0.96	-0.98
$\frac{\sigma_{M,S9}}{\sigma_{S9}}$	0.10	-0.11	-0.04	-0.06	0.01	0.35	0.88	0.97	0.98	0.97	1.00	1.00	1.00	-0.98
$\frac{\sigma_{M,S10}}{\sigma_{S10}}$	0.12	-0.09	-0.03	-0.07	0.01	0.35	0.88	0.96	0.97	0.96	1.00	1.00	1.00	-0.97
$\frac{\sigma_{M,S11}}{\sigma_{S11}}$	0.14	-0.08	-0.03	-0.05	0.01	0.35	0.88	0.96	0.97	0.96	1.00	1.00	1.00	-0.97
r_{Rcr}	0.04	0.19	0.10	0.00	0.01	-0.36	-0.86	-0.98	-0.99	-0.98	-0.98	-0.97	-0.97	1.00

Figure 3-9: Spearman rank correlation matrix for ultimate limit state random variables and responses.

The most important results are the correlations between the random variables and the responses. In regard to the responses the wind load factor f_w shows a high correlation of 0.88 to the stresses and stress ratios as well as a high negative correlation of -0.86 to the ideal buckling capacity. From the Spearman rank coefficient of correlation any biunique functional dependency can be identified having in mind that the Central Composite design of experiments delivers samples with variations of all random variables. The latter fact implies that a high Spearman rank coefficient of correlation is only achieved when the variation of the response due to the variations of the considered random variable is large compared to the variation caused by the other random

variables. Hence it is concluded that the responses have a biunique functional dependency on the wind load factor and that the variation of the responses caused by the wind load factor is large in comparison to the response variations caused by the other random variables.

Further influence on the responses shows the model uncertainty $f_{M\,\mathrm{od}}$ applied to the loading with a correlation of 0.35 and -0.36 respectively to all responses which is explained with the loading stress dependency. A minor influence on the responses shows the ground stiffness f_g which is explained with the fact that the considered sections are located in the tower structure and the stresses there are less dependent on the ground stiffness but rather depend on the stiffness independent equilibrium. The thickness deviation f_t is in general also of minor influence showing the highest influence on the ideal buckling resistance factor with a correlation of 0.19. A further but also minor influence on the ideal buckling resistance factor shows the modulus of elasticity E which has practically no influence on any other response. A nearly zero correlation to the responses are equated for the yield stress f_y and the misalignment α. The yield stress has a minor influence because the yielding occurs only to a very small extend. All responses are fully positively or negatively correlated showing the relation between stresses, stress ratios and their inversely related ideal buckling resistance factor.

3.5 Conclusions

The ultimate limit state model basis of offshore wind energy converters is introduced and an analysis of the ultimate limit state capacity as well as a sensitivity study of the random variables utilized to represent the associated uncertainties are conducted and documented. This part of the model basis will be applied for calculating the reliability in the ultimate limit state for the support structure as prior information for the continuous assessment with monitoring systems.

The reliability analysis requires full understanding of the deterministic and probabilistic models applied as well as the mechanics involved. To that end the ultimate limit state capacity of the support structure has been analyzed leading to the definition of the failure mechanisms. Further the sensitivity study has been conducted identifying on the basis of the Spearman rank correlation coefficient functional dependencies between the random variables representing the uncertainties and the responses as a part of the limit state functions. These functional dependencies between the random variables and the responses are defined by structural mechanics. The degree of these dependencies is identified with the Spearman rank coefficient of correlation considering by definition any biunique functional dependency. It is important that the experimental designs involved are chosen so that a non-linear functional dependency can be identified. For the applied fractional Central Composite design this is the case.

Given the coefficient of correlation between random variables and responses it can then be concluded which parameters, i.e. random variables, are important and which parameters are more important than others. Parameters having a low coefficient of correlation implying a low degree of functional dependency can be neglected. This leads to the refined probabilistic model summarized in Table 2 regarding the structural and loading model of the support structure. The relevant random variables having a

functional dependency on the responses of the ultimate limit state namely the stresses and the ideal buckling strength are the foundation stiffness factor, the thickness deviation, the model uncertainty, the modulus of elasticity and the wind load factor. Within the limit state functions which are not defined in this paper further random variables like e.g. the yield strength will be used.

Table 3-2: Optimized probabilistic model

Random Variables	Distribution	Mean	Standard deviation
Foundation stiffness factor f_g	LN	1.0	0.6
Thickness-deviation f_t (mm)	N	1.2	0.7
Modulus of elasticity E (N/mm²)	LN	210000	6300
Loading Model Uncertainty $f_{M\,\mathrm{od}}$	LN	1.0	0.1
Wind load factor f_w	WB	0.4891	0.2256

N: Normal distribution; LN: Lognormal distribution; WB: Weibull distribution

The deterministic models involved describing the mechanical behavior of the support structure are applied to analyze the ultimate limit state capacity providing understanding of the failure mechanisms involved. From a geometrically and materially non-linear analysis including a contact formulation for the pile guide foundation it is concluded that the ultimate loading capacity for the support structure and the tripod structure is determined by the buckling capacity. More specifically for the overall support structure interactive column/shell buckling and for the tripod pure shell buckling are concluded to be the capacity limiting failure modes. The tripods load deflection behavior is more ductile due to its statically indeterminacy with a significant higher capacity in comparison to the overall support structure.

With this refined ultimate limit state model basis established, the identification of the relevant random variables and the failure mechanisms identified reliability calculations can be set up which are the next step within the introduced assessment framework. However the model basis for the fatigue and the serviceability limit state has to be developed considering the individual limit state aspects and performing a sensitivity study. Further analysis of the influence of the contact formulation is needed since this is important for the calculation of the fatigue stresses.

4 Fatigue and serviceability limit state model basis for assessment of offshore wind energy converters (Paper III)

S. Thöns

BAM Federal Institute for Materials Research and Testing, Berlin, Germany and

Swiss Federal Institute of Technology, Zurich, Switzerland

M. H. Faber

Institute of Structural Engineering, ETH Zurich, Zurich, Switzerland

W. Rücker

BAM Federal Institute for Materials Research and Testing, Berlin, Germany

Journal of Offshore Mechanics and Arctic Engineering (JOMAE), August 2012, Volume 134, Issue 3, 031905 (10 pages)

http://dx.doi.org/10.1115/1.4004514.

Fatigue and serviceability limit state model basis for assessment of offshore wind energy converters (Paper III)

Abstract

This paper develops the models for the structural performance the loading and probabilistic characterization for the fatigue and the serviceability limit states for the support structure of offshore wind energy converters. These models and a sensitivity study are part of a risk based assessment and monitoring framework and will be applied for establishing the "as designed and constructed" reliability as prior information for the assessment and the design of monitoring systems. The constitutive physical equations are introduced in combination with the fatigue and serviceability limit state requirements as the starting point for the development of the structural performance and loading models. With these models introduced in detail several modeling aspects for both limit states are analyzed. This includes analyses of the influence on the hot spot stresses by applying a contact formulation for the pile guide brace connection and the application of a finite element formulation using solid elements. Further, the comparison of the natural frequencies of a discrete rotor model with a continuous rotor model is documented. To account for uncertainties associated with the structural and loading models a probabilistic model is derived on the basis of literature review and measurement data from a prototype Multibrid M5000 support structure. The sensitivity study is based on the calculation of a non-linear coefficient of correlation in conjunction with predetermined designs of experiments. This is conducted by a systematic analysis of the influence of the random variables on limit state responses and hence on the structural reliability. Integrating the analyses and sensitivity studies of the fatigue and serviceability limit state models developed in this paper as well as the ultimate limit state models in Thöns, Faber et al. (2009b) the model basis for the assessment is completed. The process of establishing and analyzing such a model basis contributes to a detailed understanding of the deterministic and probabilistic characteristics of the structure and provides valuable insights in regard to the significance of available data.

4.1 Introduction

The assessment of offshore wind energy converter (OWEC) structures plays an important role for their integrity management during their entire life-cycle. Efficient strategies for structural response and condition monitoring utilizing appropriate probabilistic assessment models enhance life-cycle optimal decision making in regard to inspection and maintenance activities which for offshore structures are associated with significant costs.

The proposed assessment framework for the offshore wind energy converter structures (Thöns, Faber et al. (2008)) integrates risk analysis with system monitoring data. The structural assessment is based on components and overall structural systems reliability analysis together with the risk based robustness index following Faber, Maes et al. (2007). Sensor signals are compared with criteria for ensuring an adequate structural behavior through predetermined thresholds of limit state specific indicators.

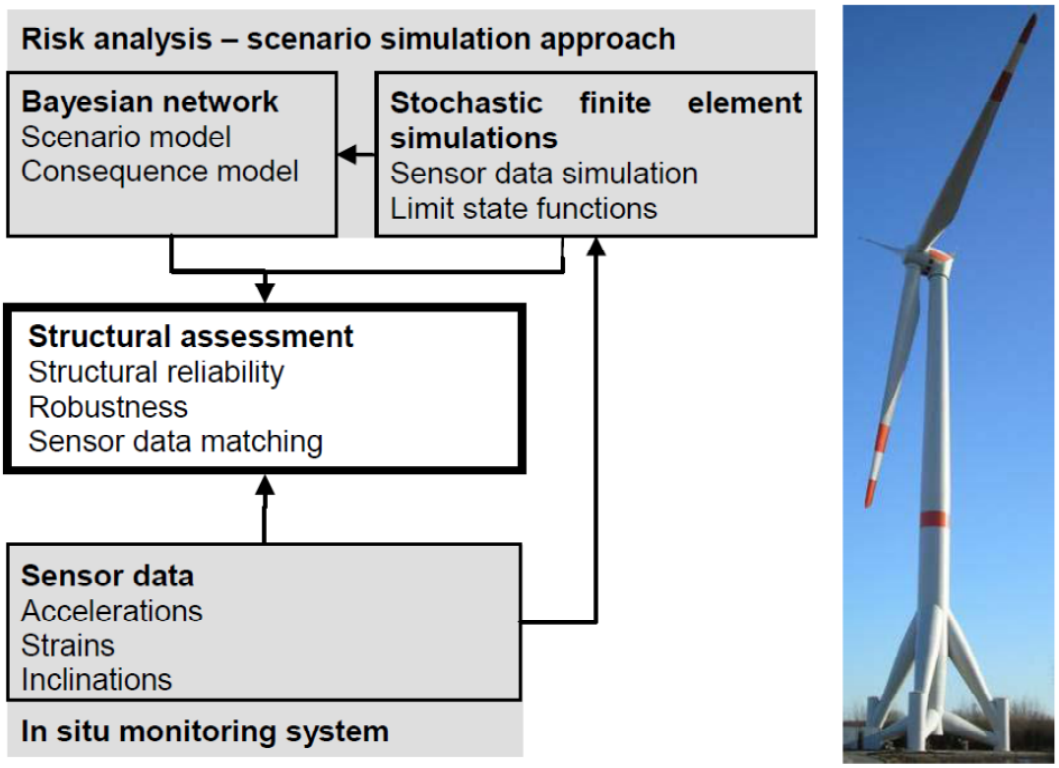

Figure 4-1: Assessment and monitoring framework with an offshore Multibrid M5000 prototype installed onshore.

The prior structural reliability (meaning "as designed and constructed") and the sensor signals are calculated applying the model basis to be introduced in the subsequent sections consisting of structural, loading and stochastic models. The structural performance is monitored and the probabilistic characteristics of the structural responses are updated based on measurements and compared with predetermined thresholds. The prior robustness is also initially quantified based on the prior probabilistic models and the Bayesian network containing the scenario model and the consequence model, see Thöns, Faber et al. (2008). The robustness is monitored and updated using monitoring data in a similar way as the reliability. This framework is finally developed and tested on a Multibrid M5000 prototype structure which is installed onshore in Bremerhaven equipped with a monitoring system consisting of strain, acceleration and inclination sensors.

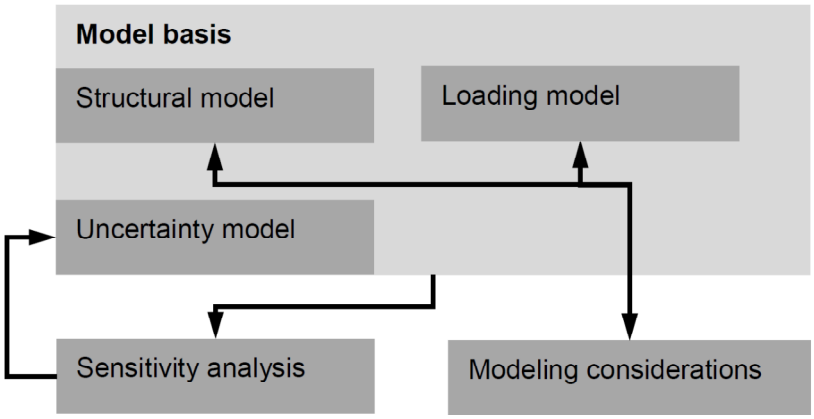

Figure 4-2: Paper organization containing the model basis and analyses for model development.

The paper organization and the relations between the models and the methods are visualized in Figure 4-2. The model basis for the assessment of the wind energy converter substructure is introduced summarizing a general constitutive physical model leading to the specific finite element representation. Subsequently certain aspects are analyzed concerning the modeling of the structure in regard to the fatigue and the serviceability limit states. The probabilistic models of the input parameters are introduced in the last section. The methodology and the results of a sensitivity study are documented in the third section followed by a discussion and the conclusions with the focus on deriving an improved uncertainty model.

4.2 Model basis

The model basis for the support structure is derived based on the constitutive physical models of the overall wind energy converter including interaction with all environmental media (wind, waves, soil) as well as the grid connection (for more details: Thöns, Faber et al. (2009b)). The complexity of this system, however, necessitates the application of different modeling detail levels; first an overall rather simple dynamic model is established facilitating time domain calculations on the basis of which the input for more refined (structural) models is generated. The refined models to be developed here are formulated with due consideration of common modeling aspects regarding the fatigue and the serviceability limit states.

A constitutive physical model of the offshore wind energy converter can be written based on a discrete dynamic equation with mass matrices $\mathbf{M}$, the damping matrices $\mathbf{D}$, the stiffness matrices $\mathbf{K}$, the degree of freedom vectors $\mathbf{x}$ and the loading vectors $\mathbf{f}$ distinguishing between the wind turbine (index WT; nacelle, hub and rotor) as well as the support structure (index SS: foundation, tripod and tower). The matrices and the force vectors are sub-divided into the aerodynamic fraction (index a) and the hydrodynamic fraction (index h). The hydrodynamic mass matrix and loading vector is only relevant for the support structure.

The wind turbine relevant parts of the matrices in Equation (4.1) are time variant. Furthermore various dependencies are introduced due to nonlinearities. The strongest nonlinearities are caused by aerodynamics due to flow separation. Geometrical nonlinearities are introduced due to substantial deflections of both the structure and the

blades. In addition hydrodynamic effects caused by large waves cause nonlinearities. The hydrodynamic drag coefficient and the soil behavior are assumed to be linear in accordance with Kühn (2001).

$$\left[\mathbf{M}^{WT+SS}+\mathbf{M}_h^{SS}\right]\ddot{\mathbf{x}}+\left[\mathbf{D}^{WT+SS}+\mathbf{D}_a^{WT+SS}\right]\dot{\mathbf{x}}+\left[\mathbf{K}^{WT+SS}+\mathbf{K}_a^{WT+SS}\right]\mathbf{x}=\mathbf{f}_a^{WT+SS}+\mathbf{f}_h^{SS} \qquad (4.1)$$

For the individual limit states of the support structure normally calculations of extreme stresses (for the ultimate limit state), stress variations at stress concentration points (hot spots for the fatigue limit state) and a modal analysis (for the dynamic analysis in the serviceability limit state) are required. These analysis results are established by the application of the finite element method. The constitutive physical relation utilized for the analysis of the fatigue limit state is given in Equation (4.2). In this equation dependencies are caused by nonlinearities like e.g. geometric nonlinearities. Furthermore additional terms are necessary when a contact problem has to be solved e.g. by the augmented Lagrange method.

$$\mathbf{K}^{SS}\mathbf{x}=\mathbf{f}^{SS} \qquad (4.2)$$

Within the serviceability limit state usually recommendations to deformations and accelerations are specified. For support structures of wind energy converters the serviceability is related to energy production and hence specific requirements are defined by the manufacturer. Here the dynamic characteristics have significant importance because of permanent excitations due to continuously moving parts like the rotor. Deformations and accelerations are of minor importance as they are not limited by the manufacturer. Therefore a modal analysis is performed to determine the natural frequencies of the support structure to ensure that there is no resonance of the support structure with excitations such as the rotor revolutions and the blade passing frequency. The latter is caused by changing the aero-dynamical conditions when a rotor blade passes the tower.

The constitutive relation utilized for the modal analysis, i.e. the general eigenvalue problem with the eigenvector matrix $\mathbf{\Phi}$ and the diagonal eigenvalue matrix $\mathbf{\Lambda}$, is given in Equation (4.3). In case damping effects are accounted for, this relation transforms to the quadratic eigenvalue problem with complex eigenvalues (index i; Equation (4.4)):

$$\mathbf{K}^{SS}\mathbf{\Phi}=\mathbf{M}^{SS}\mathbf{\Phi}\mathbf{\Lambda} \qquad (4.3)$$

$$\mathbf{K}^{SS}\mathbf{\Phi}+\mathbf{D}^{SS}\mathbf{\Phi}\bar{\mathbf{\Lambda}}=\mathbf{M}^{SS}\mathbf{\Phi}\bar{\mathbf{\Lambda}}\bar{\mathbf{\Lambda}} \text{ with } \bar{\mathbf{\Lambda}}=\mathbf{\Lambda}\pm i\mathbf{\Lambda}_i \qquad (4.4)$$

4.2.1 Structural model

The support structure of the wind energy converter consists of the tower divided in segments by ring flanges, the tripod consisting of upper braces, lower braces, the pile guide as well as the foundation (Figure 4-3), which in contrast to the case where the structure would be installed offshore consists of circular reinforced concrete slabs attached to a pile group. For the serviceability limit state, i.e. the modal analysis a coarser mesh is used, because here the global stiffness for the important first natural frequencies plays a major role.

The edgewise and flapwise stiffness of the rotor blades is ensured by four carbon fiber reinforced polymer chords combined with an outer shell. These materials possess, due to the fibers, an orthotropic material behavior. The cross-section is varying and twisted

along the rotor axis. These properties of the rotor blade geometry are modeled with two node finite beam elements (BEAM 4 ANSYS (2006)) of equal length. The moments of inertia about the cross section axes as well as the torsional inertia are calculated for the individual sections and assigned to these elements with six degrees of freedom at each node. Both the modulus of elasticity and the shear modulus are considered. Warping effects are not accounted for.

The hub and the connection of the hub to the rotor blades are assumed to have infinite stiffness and are modeled utilizing constraint equations (ANSYS (2006)). In reality the hub has a finite stiffness but considering the low stiffness of the rotor, it can be modeled with good approximation with infinite stiffness. The same applies to the connection where the prestress of the bolts prevents any deformation. Both the nacelle and rotor coordinates are parameterized to enable the calculation of different nacelle and rotor angles. No structural or aerodynamic damping is applied to the rotor blades.

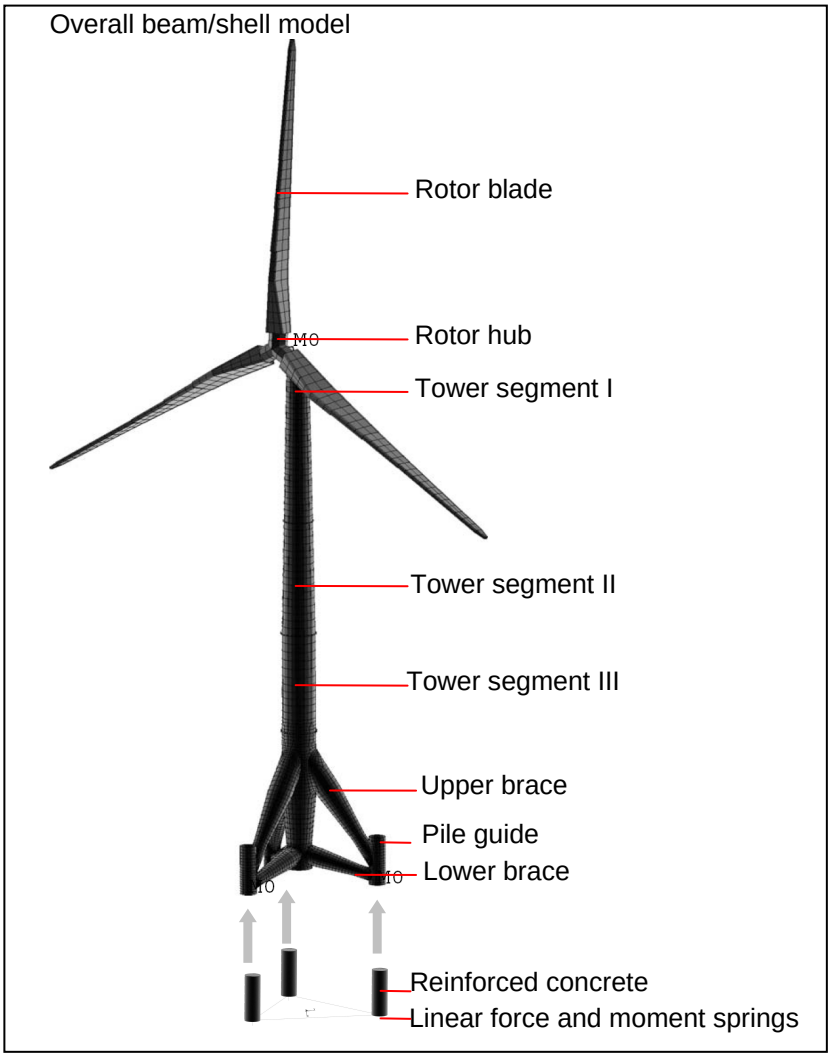

Figure 4-3: Overall beam/shell model of the serviceability model basis

The stress calculation for the fatigue limit state of the tripod requires at least a shell model due to the diameter to length ratio of the components involved (Figure 4-4a).

Additionally a solid element model of the tripod sub structure is developed (Figure 4-4b). The finite element models developed incorporate iso-parametric displacement based shell elements (SHELL 181/281 ANSYS (2006)) combining plate and membrane theory with linear (for the serviceability limit state) or quadratic interpolation functions (for the fatigue limit state). At geometrical discontinuities, especially at the tube connections within the tripod the mesh was refined until the resulting stresses became independent of the mesh. For the solid model iso-parametric displacement based elements with 20 nodes containing quadratic interpolation functions namely SOLID186 (ANSYS (2006)) were used. For all tubular sections at least two layers of elements in thickness direction are applied. The mesh was refined at all section changes and tube connections. The maximum element size at the tubular connections in the local x-directions of the components (see Figure 4-5) is half the thickness. For illustration the mesh at the connection between the tower and the upper brace is visualized in Figure 4-4c with elements whose size was shrunken by 30%. Since the chosen solid elements are not insensitive to angular distortions caused by the missing terms in the interpolation functions the volumes are defined with regular meshing without curved edge distortions (for details see Bathe (1996)). Both the higher order interpolation functions and the fine mesh facilitate precise calculation of the stresses in regions with high stress gradients like at the tube connections. This applies for the both the shell element model and the solid element model.

The support structure is connected to the foundation through the pile guides (Figure 4-3). The pile guides contain reinforced concrete and shear connectors which are welded to the inside of the pile guide. Through the shear connectors and through friction this system (pile guide / reinforced concrete) acts mechanically as one solid section. For the case that a tension force is applied to the outer steel section of the pile guide (due to the braces) the pile guide and the reinforced concrete do not act as one section since the tension forces between steel and concrete are not transmitted. In this case the local behavior is different from the global behavior. This mechanical phenomenon can only be modeled by a contact finite element formulation. The same argumentation applies to a grouted connection, which is utilized for the offshore installation of this support structure.

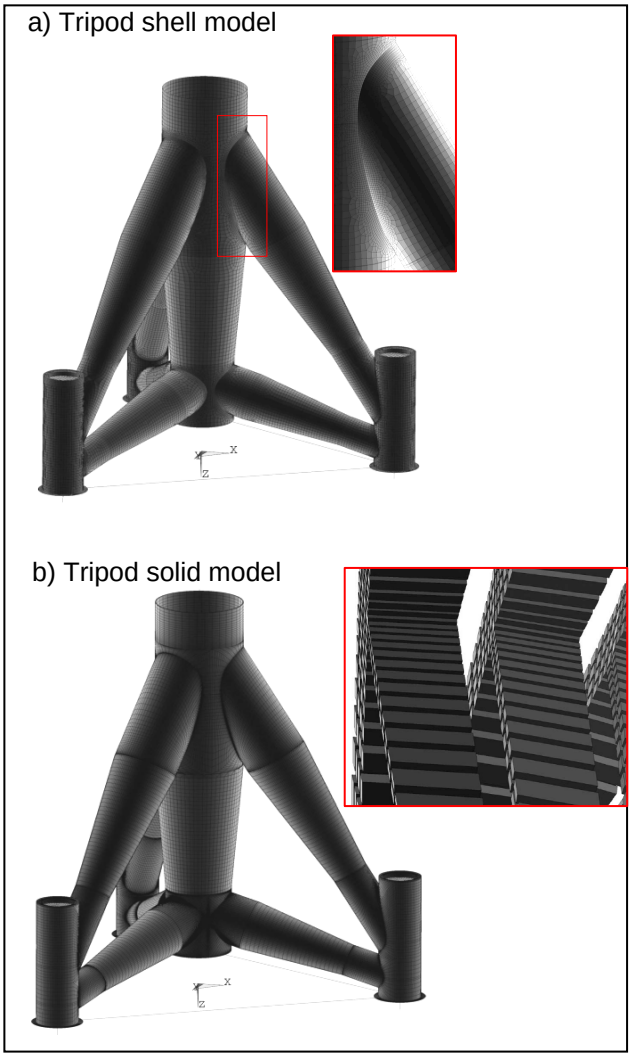

Figure 4-4: Fatigue model basis consisting of a tripod shell model (a) and a tripod solid model (b)

The inside of the pile guide and the outside of the reinforced concrete is meshed with contact elements (CONTA173/174 and TARGE170). The initial contact conditions are adjusted such that the contact forces are independent of the meshes of the pile guide and the reinforced concrete. A friction coefficient of 0.8 which incorporates the friction coefficient between concrete and steel (0.2-0.4 see Goris and Schneider (2006)) and the influence of the shear connectors is applied. The reinforced concrete is connected to the spring elements which represent the foundation stiffness determined by a separate model (Figure 4-3). For the modal analysis model the contact is always closed. Further, specific modeling aspects for the individual limit states are discussed in the following sections.

4.2.2 Loading and mass model

The loading model for the fatigue limit state is determined by the time domain analysis. For the fatigue limit state the loading vector consists of time series representing the fatigue loading scenarios. They include normal power production operating conditions as well as start and stop operations. The loading scenario corresponding to normal power production consists of load cases which are usually calculated utilizing 600 sec.

time series for wind speeds classes incremented by 2 m/s beginning with 4 m/s and ending at the cut-out wind speed at 25 m/s (OWT (2009)). For higher wind velocities the operation is shut down. The number of stress cycles for each wind speed class is weighted according to a long term wind speed density function. Additionally a certain number of start and stop maneuvers for cut in and cut out wind speeds are considered. The wind loading on the structural components is negligible (see Thöns, Faber et al. (2009b)).

The force vectors are applied to nodes representing the degrees of freedom of the shell section. This results in a rigid region which is a good approximation for section at the load application where a stiff ring flange is located like at the top of the tower (e.g. Figure 4-4a). At the top of the tripod (e.g. Figure 4-4b) this introduces a modeling imprecision but plays a minor role since the relevant sections are located at a sufficient distance from the rigid sections.

The mass distribution of the nacelle (containing the gear unit, the generator and the converter) and the hub is modeled with single mass elements (Figure 4-3) whereas the rotor blades are modeled by continuous masses. The masses of the tower, the tripod and foundation are modeled according to the density of the material applying additional masses to account for not explicitly modeled components like installations inside the tower and the foundation plates. The material damping ratio is assumed equal to 5% according to Kühn (2001).

4.2.3 Modeling considerations

The models introduced in the previous sections are applied for the fatigue and the serviceability limit states in order to analyze certain aspects and modeling assumptions deterministically. For the fatigue limit state the influence of the contact formulation for the foundation and of using a solid model instead of a shell model are analyzed. For the serviceability limit state the results obtained from the overall model (Figure 4-3) are compared to the results obtained from a discrete rotor model.

4.2.3.1 Modeling aspects for hot-spot stress evaluation in fatigue limit state

Two modeling aspects are introduced and discussed in the following section, namely the influence of including or neglecting the contact formulation on the hot-spot stresses in the pile guide connection and a comparison of hot spot stresses determined by a shell model and a solid model. A damage equivalent load vector at the top of the tripod structure is applied for these analyses. This load vector represents a conservative approximation since it is theoretical determined only for one component of the load vector (see Equation (4.7)).

As outlined in the general modeling considerations (Section 4.2.1) the interaction between the steel section of the pile guide with reinforced concrete filling incorporates a local behavior (no transmission of tensile stresses between pile guide and reinforced concrete) and a global behavior (acting as one section for e.g. bending loading conditions). This implies that the local behavior is clearly non-linear, but the global behavior (acting as one section) only incorporates only small nonlinearities. However, when introducing a contact formulation for the modeling of this behavior the computational effort increases significantly.

The comparison of the stresses in the pile guide when neglecting the reinforced concrete core and coupling the foundation springs to the pile guide with inclusion of the reinforced concrete and the contact shows differences in the stresses along the tube connection line between the upper brace and the pile guide. The peak stresses are calculated for both modeling assumptions at the lowest point of the connection. At this point the local y-coordinate equals zero and the coordinate s along the connection line equals 1.93 m with the starting point as indicated (Figure 4-5). For the "no contact" model a normalized value of the hot spot stress of 1.0 is calculated in comparison to a peak hot spot stress of 0.89 for the "contact" model. Going further from the centre a local maximum is observed on both sides which is caused by a thickness change in the pile guide. The stresses for the "contact" model are approximately symmetrically. The stresses for the "no contact" model contain slightly more asymmetry. This reflects the different global behavior of the models including only the pile guide or including the pile guide, the reinforced concrete and a contact formulation. However, the results produced by the "no contact" model are conservative.

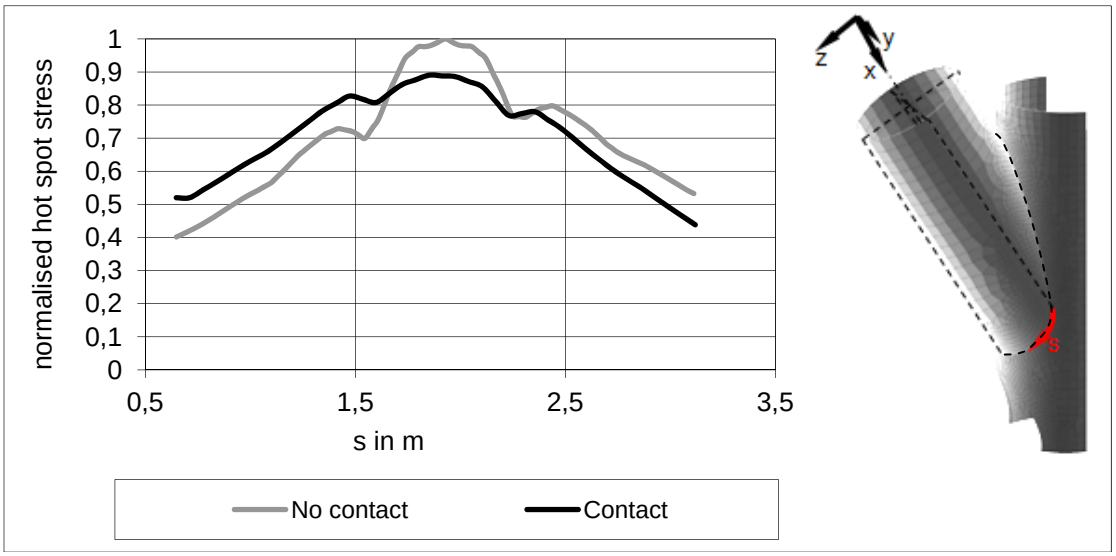

Figure 4-5: Comparison of "contact" and "no contact" hot spot stresses along the connection line (the starting point and direction is indicated with the red arrow).

Another aspect is the influence of applying a solid or a shell model for the stress calculation. The displacement based solid elements are able to model linear stress variations due to the quadratic interpolation functions. This applies also to the thickness direction. However, in the vicinity of the connection between the tubes non-linear stress fractions over the thickness are present. Hence, for modeling these, at least three element layers through the thickness are used. The element mesh is highly refined along the connection lines of the tubes. The same boundary conditions for the foundation are applied modeling the reinforced concrete using a contact formulation. The load introduction is modeled as described in Section 4.2.2.

For comparing the stresses between the shell and the solid model the hot spot stress distribution over the thickness computed with the solid model is linearized. This means

that a constant stress fraction is calculated by computing the mean normal stress and the linear varying stress fraction is computed by requiring equivalency of the moments.

For both considered connections, namely the connection tower-upper brace and the connection pile guide-upper brace the hot spot stresses calculated with the solid model are lower than the stresses which are calculated using the shell model (Figure 4-6). For the connection tower-upper brace the hot spot stress is a factor of 0.95 lower whereas the stress in the connection pile guide-upper brace is a factor of 0.84 lower. The significant reduction of the stress for the connection pile guide-upper brace can be explained by the fact that the solid models allows the stresses in the thickness direction to be transferred which is not the case for the shell model. The shell model leads to conservative hot spot stresses.

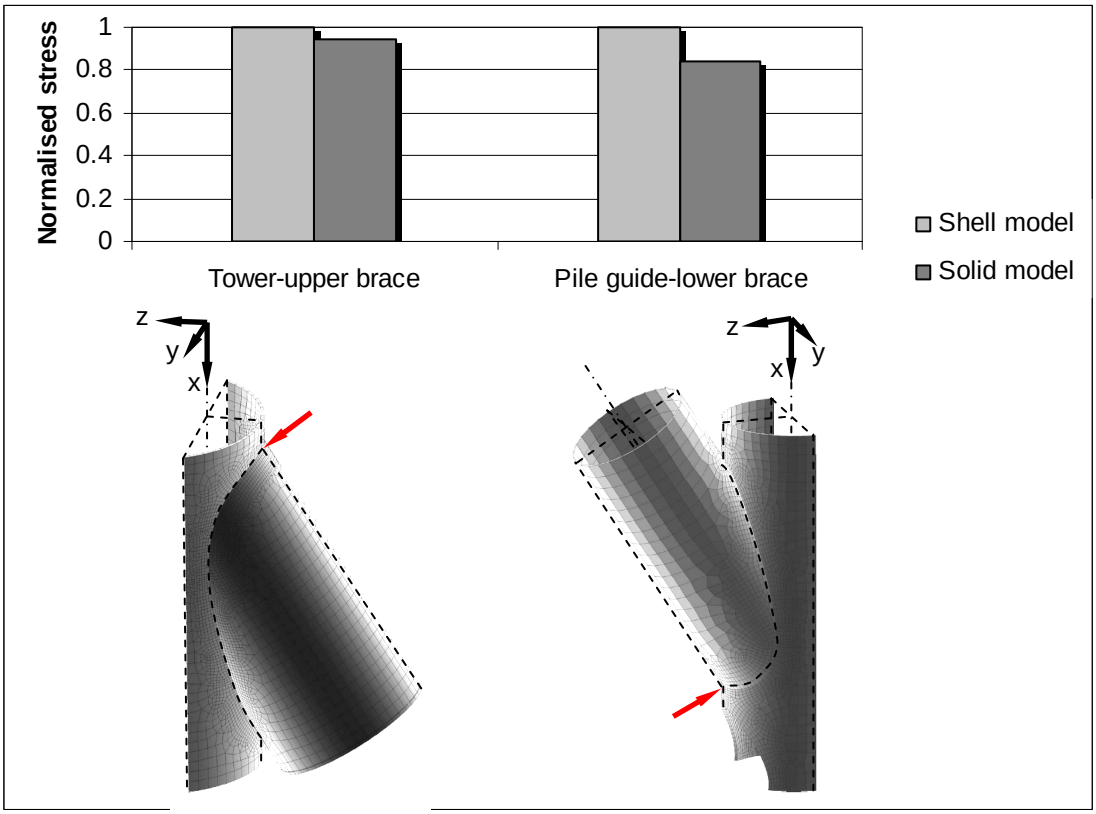

Figure 4-6: Comparison of hot spot stresses calculated with the shell and the solid model.

4.2.3.2 Modeling consideration for the serviceability limit state

Two models are compared here which have the same support structure model but differ in the modeling of the rotor. The overall model (Figure 4-3), as introduced in Section 4.2.1, contains a distributed rotor model with point masses for the nacelle and the hub in their center of gravity. These mass elements are rigidly connected to the top of the support structure where a ring flange connects the support structure with the nacelle. The discrete rotor model is different in the way that also the rotor beside the nacelle and the hub is modeled by point masses.

The mode shapes equated for the discrete rotor model are illustrated in Figure 4-7. The first two as well as the third and the fourth natural frequencies are very close together (see mode shapes in Figure 4-7a and Figure 4-7b). The deflection of the first mode shape is nearly in direction of the Y-axis (perpendicular to the X-Z plane, see Figure 4-7a) and the deflection of the second mode shape is in the X-direction. The cause for the slightly higher natural frequency is that the stiffness in the X-direction is higher because there is an upper brace in this direction. In contrast, in the deflection direction of the first mode shape there is no upper brace causing a lower natural frequency. The same consideration applies to the third and fourth mode shape (Figure 4-7b) where the foundation is deflected. The fifth mode is a torsional mode (Figure 4-7c) and the sixth mode is the second tower bending mode (Figure 4-7d).

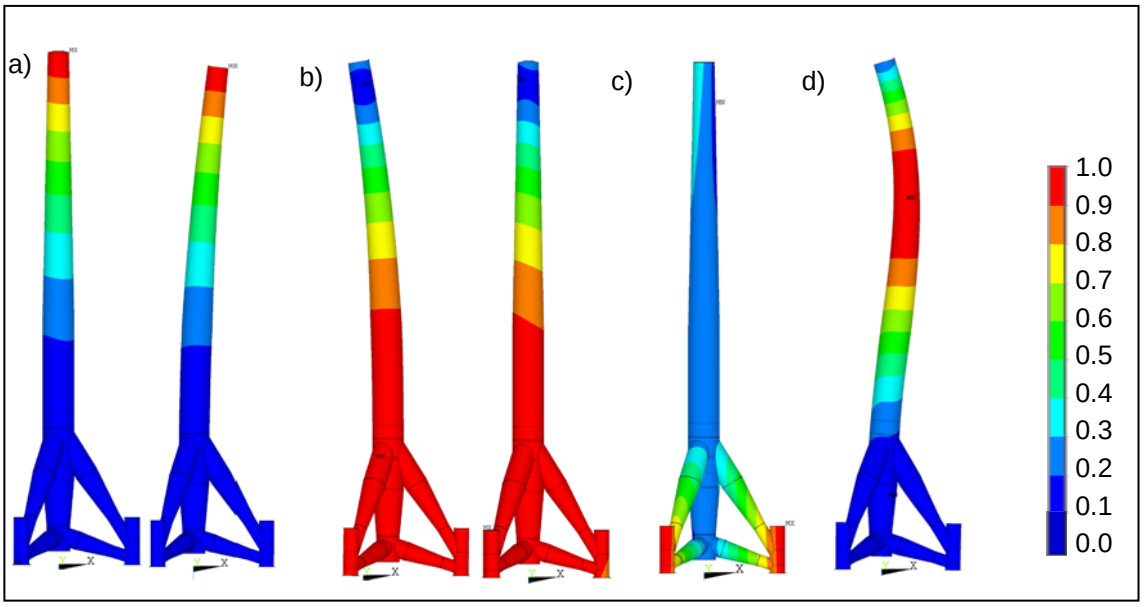

Figure 4-7: Mode shapes of the discrete rotor model with colored displacement vector sum in ascending order

Most of the mode shapes calculated with the discrete rotor model are found in the mode shapes of the overall model (Figure 4-8). However, the overall model contains various modes of the rotor and rotor blades with low support structure interaction. These modes are excluded here. They are however of significant importance for the identification of all mode shapes and natural frequencies of the structure.

The natural frequencies belonging to the considered mode shapes are only slightly influenced by the variation in the modeling alternatives with the exception of the torsional mode shape in Figure 4-7c and Figure 4-8c. The natural frequency calculated using the discrete rotor model is lower than the natural frequency calculated using the overall model. Further the mode shape in Figure 4-7c contains only a slight twist between the gravity center of the rotor and the support structure whereas in Figure 4-8c this twist is significantly larger which can be seen in the pictures by comparing the displacement vector sums along the tower. A further difference is that third mode shape of the discrete rotor model (Figure 4-7b left) is not calculated with the overall model

(Figure 4-8b). It is understood here that the different edgewise and flapwise stiffness of the rotor blades causes this mode shape to disappear.

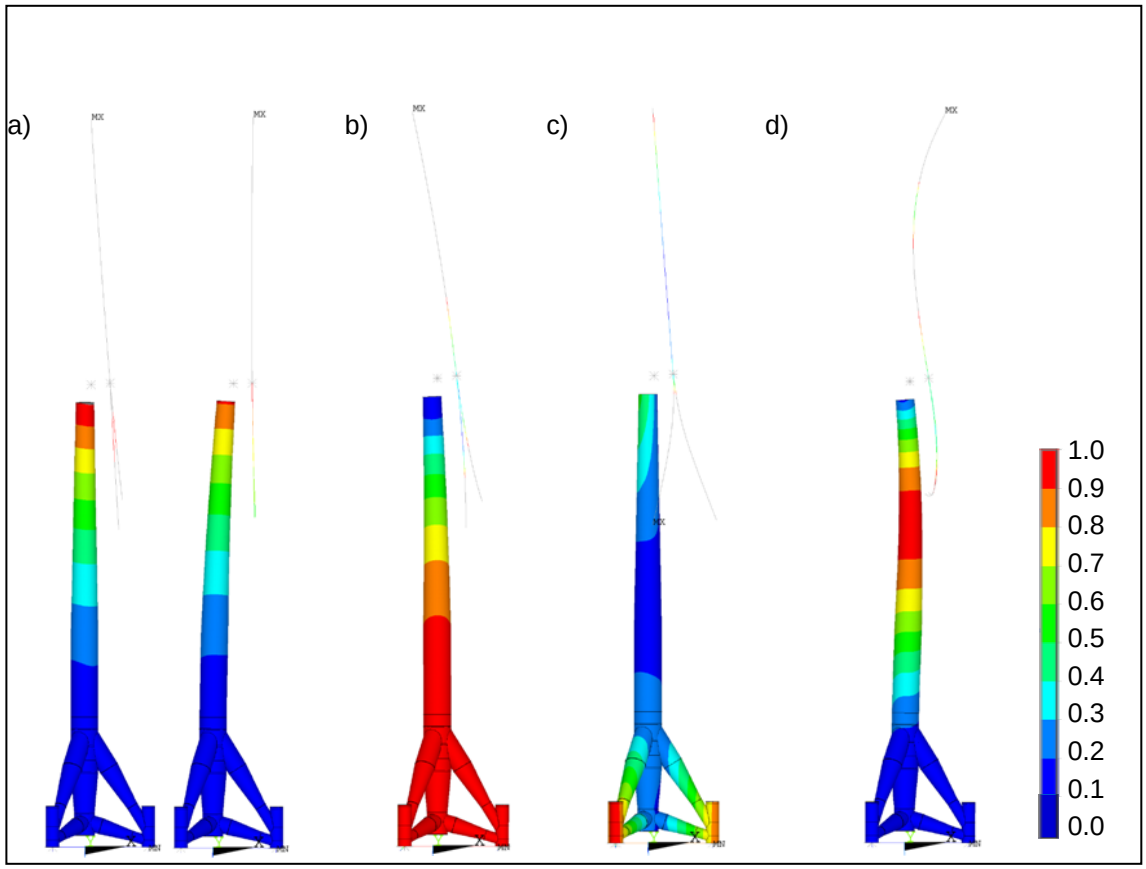

Figure 4-8: Mode shapes in ascending order using the overall model with colored displacement vector

Another aspect which is investigated with the overall model is the influence of the rotor and nacelle position on the results of the modal analysis of the support structure. It is observed that there are only minor influences on the considered natural frequencies and mode shapes. The analyses include nacelle positions between 0 and 120 degrees about the vertical axis and rotor movements about the rotor axis within the same angles. Despite the fact that it is important to model the rotor continuously, the first 10 natural frequencies are only influenced slightly by the change of the rotor and nacelle angle in the system.

4.2.4 Probabilistic model

The probabilistic model was introduced in detail in Thöns, Faber et al. (2009b) and is here taken as basis. The random variables representing uncertainties of the global structural system variables over load variables to model uncertainties are summarized in Table 4-1. The probabilistic modeling is adapted to the probabilistic model code (PMC) of the Joint Committee on Structural Safety JCSS (2006) in combination with design documents (e.g. DIBt (2004)) and experimental investigations.

Table 4-1: Common probabilistic models for fatigue and serviceability limit states

Parameter	Distr.	Mean	Standard deviation	Reference
Foundation stiffness factor f_g	LN	1.0	0.6	JCSS (2006)
Thickness-deviation f_t (mm)	N	1.2	0.7	JCSS (2006), Meas. on prototype
Modulus of elasticity E (N/mm²)	LN	210000	6300	JCSS (2006)
Misalignment α (rad)	N	0.0	0.0048	JCSS (2006); DIBt (2004)

N: Normal distribution; LN: Lognormal distribution

For the fatigue and the serviceability limit states two further random variables are introduced. The random variable $f_{M\,\mathrm{od}}$ represents the model uncertainty associated with the process of the preceding overall dynamic analysis for the fatigue limit state and includes random effects that are neglected in the models and simplifications in the mathematical relations (compare Thöns, Faber et al. (2009b)). The time series of the loading vectors are multiplied with the factor $f_{M\,\mathrm{od}}$ determined using the probabilistic model code (JCSS (2006), Part 3.09 Model Uncertainties). For the serviceability limit state calculation the model uncertainty is not introduced since it does not built upon any preceding analysis.

A material damping ratio with a mean of 0.05 and standard deviation of 0.01 is used for the serviceability limit state calculation, i.e. the modal analysis, following a discussion of measured variations of this factor in Kühn (2001).

Table 4-2: Additional probabilistic models

Parameter	Distr.	Mean	Standard deviation	Reference
Damping ratio d_r	N	0.05	0.01	Kühn (2001)
Model uncertainty $f_{M\,\mathrm{od}}$	LN	1.0	0.1	JCSS (2006)

N: Normal distribution; LN: Lognormal distribution

4.2.5 Computational aspects

The finite element models developed incorporate geometrical and material non-linearity in combination with a substantial number of degrees of freedom resulting in demanding computations. For illustration the solid model of the tripod (Figure 4-4b) possesses 5 100 000 degrees of freedom. For the calculation of one load case with such a model incorporating the contact non linearity 12 hours are needed using 10 GB RAM with one E5450 XEON processor.

The reliability problem requires around 30 to 150 calculations of the structural and loading model with defined random variables realizations according to the design of experiments. This restricts the time of an individual model calculation and is the reason why the solid model of the tripod is used only as a reference but not in the further. The other models, especially concerning the support structure and the tripod are refined including only the necessary non-linearity and further by choosing an appropriate solution strategy with the most efficient solvers for the specific problems.

For solving the steady state equation (Equation (4.2)) of the tripod shell model (Figure 4-4b) incorporating a relatively large number of nodes, higher order shell elements and non-linearity due to the contact formulation an iterative approach using a Newton-Rapson line search is applied (ANSYS (2006)). The convergence criteria incorporate a force, a moment and a degree of freedom criteria. For all criteria the Euclidian vector norm is checked at each load step with an allowance of 5% in regard to a model based reference value. The individual load steps are solved with an iterative solver namely the preconditioned conjugate gradient solver. The contact problem is solved utilizing an augmented Lagrangian method combining the penalty method and the Lagrange multiplier method (ANSYS (2006)).

The modal analysis with the overall beam/shell (Figure 4-4a) is solved with the QR-damped method combining the Block-Lanczos algorithm and the complex Hessenberg method by using the modal damped matrix to calculate the complex frequency in modal coordinates (ANSYS (2006)).

4.3 Sensitivity analysis

The sensitivity of the random variables in regard to the relevant responses is determined by quantifying the degree of functional dependency by the calculation of the coefficient of correlation. This analysis involving the structural, loading and uncertainty models introduced in the foregoing is documented in this section. After defining the relevant responses for subsequent reliability calculation, the Spearmen rank correlation is introduced. The results of the sensitivity study are documented and a refinement of the probabilistic models is discussed.

4.3.1 Definition of responses and solution strategies

The responses are defined for the individual limit states having in mind that this sensitivity study will be followed by reliability calculations. For this purpose the solution strategies are developed for the specific failure mechanisms hence facilitating the definition of relevant responses.

For the fatigue limit state the response damage equivalent stress range $\Delta\sigma_{eqv}$ is calculated for all tube connections applying a Rainflow algorithm (Clormann U. H. and Seeger T. (1986)) for the stress range classification of the time series. The residuals are included corresponding to the half of the damage of a complete hysteresis. The equivalent stress range (Equation (4.7)) is calculated by the damage equality corresponding to the multi-stage spectrum determined by the Rainflow analysis consisting of the number of stress ranges n_i and the allowed number of the stress ranges N_i according to an SN curve with the parameters C and m (Equations (4.5) and (4.6)). The number of equivalent stress cycles n_{eqv} is assumed to be equal to $2 \cdot 10^6$ for an easy

calculation of the damage. The damage equivalent stress range is independent of the parameter C implying that $\Delta\sigma_{eqv}$ is independent of the welded detail. The stress time series of the tube connections are calculated using the tripod shell model (Figure 4-4b) applying the fatigue loading time series corresponding to the load cases as specified in Section 4.2.2.

$$\frac{n_{eqv}}{N_{eqv}} = \sum_i \frac{n_i}{N_i} \tag{4.5}$$

$$N = C \cdot \Delta\sigma^{-m} \tag{4.6}$$

$$\Delta\sigma_{eqv} = \left(\frac{\sum_i n_i \cdot \Delta\sigma_i^m}{n_{eqv}} \right)^{\frac{1}{m}} \tag{4.7}$$

For the purpose of modeling the serviceability limit state a modal analysis is performed as outlined in Section 4.2.1. The modal analysis is important to avoid resonance of the support structure with the excitations caused by the wind speed depending rotor revolutions and the blade passing frequency. The first two natural frequencies for this support structure lie between these two excitation mechanisms since they are very close together. So the most important responses for the serviceability limit state are the natural frequencies close to the excitations meaning for this specific case (see Figure 4-8) the first two and the third natural frequency.

4.3.2 Measures of correlation and design of experiments

The Spearman rank correlation coefficient ρ_{xy} is defined as the ratio of the covariance to the product of the standard variations and of the considered random variables applying the rank operation (rg) to the n realizations of the random variables x and y (Equation (4.8)). The rank operation converts values of a function in a number according to a rank in an ordered row and effectively means that any biunique function dependency between the random variables x and y (e.g. parameters and responses) is linearized. Therefore any biunique dependency between the random variables x and y leads to Spearman rank coefficient equal to one.

$$\rho_{xy} = \frac{\sum_{i=1}^{n} \left(rg(x_i) - \overline{rg}_x \right) \left(rg(y_i) - \overline{rg}_y \right)}{\sqrt{\sum_{i=1}^{n} \left(rg(x_i) - \overline{rg}_x \right)^2} \sqrt{\sum_{i=1}^{n} \left(rg(y_i) - \overline{rg}_y \right)^2}} \tag{4.8}$$

Restricted by the complexity and numerical efforts associated with the finite element calculations predetermined designs of experiments for the random variables are used namely a Central Composite Designs consisting of 2^{k-f} points of a k-dimensional hypercube, one centre point and $2k$ axis points. Fractional designs with a resolution of V are applied, which facilitates the modeling of non-linear responses.

For the sensitivity analysis conducted here a guess of the design point is used by classifying the random variables into resistance and load variables. The centre point is

selected as $x_{C_i} = \mu_{X_i} \mp 3s_{X_i}$ (with μ_{X_i} as the mean and s_{X_i} as the standard deviation) for load variables with the plus and resistance variables with the minus and a range for both of $x_{C_i} \mp s_{X_i}$ for the fatigue limit state calculations. Because of the application of non-symmetrical probability distribution functions in the probabilistic modeling the probabilities determined with a standard normal distribution are used. The serviceability limit state implies in general a lower probability of failure. Hence the centre point is determined by using the probability levels $\mu_{X_i} \mp 2s_{X_i}$. The same range of two standard deviations is used for the experimental design.

4.3.3 Results

The Spearman rank correlation matrix for the fatigue limit state (Figure 4-9) includes the random variables f_g, f_t, E, α, and f_{Mod} and the responses namely the damage equivalent stresses $\Delta\sigma_{eqv}$. The responses of the relevant connections regarding the subsequent reliability calculations are included. The connections with the highest stresses comprise the connections of the upper brace (see Figure 4-4a). These include the connection upper brace – tower (UBT), both section changes (cylindrical to conical (UB1) and conical to cylindrical (UB2)) and the connection pile guide – upper brace (PGUB).

The relation of the damage equivalent stresses to random variables is rather complex having in mind the internally highly statically undetermined structure. Shifting the level of the forces in the time series with the model uncertainty factor, representing the model uncertainty of the overall dynamic analysis leads to a nearly fully positive correlation with all responses. Stiffness variations of the constraints with the foundation stiffness factor f_g and the stiffness variation of the sections with the thickness deviation f_t are also correlated with the responses. It is observed that the correlation of the thickness deviation to the responses is lower for sections with larger thicknesses. Minor correlation to the responses shows the modulus of elasticity E whereas the misalignment α shows no practically significant correlation. The reason for the insignificant influence of the misalignment is that the fatigue loading is dominated by the misalignment independent horizontal forces (see also Schaumann, Böker et al. (2007)).

	f_g	f_t	E	α	$f_{M\,od}$	$\Delta\sigma_{eqv,UBT}$	$\Delta\sigma_{eqv,UB1}$	$\Delta\sigma_{eqv,UB2}$	$\Delta\sigma_{eqv,PGUB}$
f_g	1,00	0,00	0,00	0,00	0,00	-0,14	-0,14	0,15	-0,14
f_t	0,00	1,00	0,00	0,00	0,00	-0,24	-0,35	-0,27	-0,24
E	0,00	0,00	1,00	0,00	0,00	0,08	0,08	-0,08	0,08
α	0,00	0,00	0,00	1,00	0,00	-0,02	-0,02	-0,01	0,01
$f_{M\,od}$	0,00	0,00	0,00	0,00	1,00	0,95	0,90	0,94	0,95
$\Delta\sigma_{eqv,UBT}$	-0,14	-0,24	0,08	-0,02	0,95	1,00	0,99	0,94	1,00
$\Delta\sigma_{eqv,UB1}$	-0,14	-0,35	0,08	-0,02	0,90	0,99	1,00	0,93	0,99
$\Delta\sigma_{eqv,UB2}$	0,15	-0,27	-0,08	-0,01	0,94	0,94	0,93	1,00	0,94
$\Delta\sigma_{eqv,PGUB}$	-0,14	-0,24	0,08	0,01	0,95	1,00	0,99	0,94	1,00

Figure 4-9: Spearman rank correlation matrix for fatigue limit state random variables and responses.

Whereas the responses of the ultimate and the fatigue limit state are nearly fully correlated (positively or negatively) the responses of the serviceability limit state, i.e. the natural frequencies (λ_1, λ_2, λ_3, λ_4 and λ_5), are not all fully correlated (Figure 4-10). These natural frequencies belong to the mode shapes depicted in Figure 4-8. However, for different realizations of the random variables it has been observed that the three last mode shapes can change the order. In such a case the natural frequencies are rearranged to fit to the considered mode shapes.

The modulus of elasticity E has the largest influence on the most important first natural frequency followed by the foundation stiffness factor f_g. The third and fourth natural frequency exhibit the highest correlation to the foundation stiffness which is explained by the fact that the corresponding mode shapes contain displacements of the individual foundations. An interesting observation is that the thickness deviation f_t is positively correlated with the first two and the fifth natural frequency and is negatively correlated with the third and fourth natural frequency. Clearly the thickness deviation affects both the stiffness and the mass. Hence observing that for the third and fourth natural frequency the tripod is deflected which is not the case for the other mode shapes and considering that the tripod is much stiffer than the tower it becomes clear that for mode shape three and four the mass influence on the frequency is active whereas for the other mode shapes the stiffness influence on the natural frequencies play the major role. The misalignment and the material damping ratio d_r have no influence.

	f_g	f_t	E	α	d_r	λ_1	λ_2	λ_3	λ_4	λ_5
f_g	1,00	0,00	0,00	0,00	0,00	0,39	0,39	0,90	0,90	0,75
f_t	0,00	1,00	0,00	0,00	0,00	0,16	0,16	-0,18	-0,08	0,17
E	0,00	0,00	1,00	0,00	0,00	0,86	0,86	0,09	0,14	0,52
α	0,00	0,00	0,00	1,00	0,00	-0,01	-0,01	-0,01	0,00	-0,02
d_r	0,00	0,00	0,00	0,00	1,00	-0,01	-0,01	-0,02	-0,02	-0,02
λ_1	0,39	0,16	0,86	-0,01	-0,01	1,00	1,00	0,49	0,55	0,81
λ_2	0,39	0,16	0,86	-0,01	-0,01	1,00	1,00	0,49	0,55	0,81
λ_3	0,90	-0,18	0,09	-0,01	-0,02	0,49	0,49	1,00	0,99	0,71
λ_4	0,90	-0,08	0,14	0,00	-0,02	0,55	0,55	0,99	1,00	0,75
λ_5	0,75	0,17	0,52	-0,02	-0,02	0,81	0,81	0,71	0,75	1,00

Figure 4-10: Spearman rank correlation matrix for serviceability limit state random variables and responses

The random variable with the highest correlation to the responses of the fatigue limit state is the model uncertainty associated with the overall dynamic analysis. For the serviceability limit state the foundation stiffness and the modulus of elasticity have the highest correlation to the responses. The random variable representing the thickness deviation has a relatively low correlation to the limit state response. Random variables with minor i.e. negligible influences are the misalignment angle for both limit states and the structural damping ratio for the serviceability limit state.

4.3.4 Refinement of probabilistic model

The probabilistic model is discussed in conjunction with the individual limit state responses to refine the specific characteristics of the random variables which are relevant for the limit states. Clearly for the fatigue limit state local stress variations as e.g. caused by local thickness changes implying small reference areas play a role. For the failure mechanism yielding in the ultimate limit state such local thickness variation is of minor importance since plastic strains leads to stress redistribution. Therefore only an average value of the spatial thickness variation in the section determines the yielding capacity of the section. For buckling applying the EC3-concept (DIN EN 1993-1-6 (2007)) again the yielding capacity plays a role and in addition the geometrical imperfections. The latter is associated with imperfections in regard to the section geometry (as there are strict production rules in DIN EN 1993-1-6 (2007)) rather than local thickness variations. For the serviceability limit state the important lower natural frequencies are determined by the overall stiffness and mass distribution and hence are not dependent on the local mass and local thickness variations, i.e. the local stiffness distribution.

The random variable thickness deviation is modeled neglecting the spatial variation and independent of the thickness. It is applied to the structural finite element models for the

fatigue and serviceability limit state here and for the ultimate limit state in Thöns, Faber et al. (2009b). Measurement data taken with a small probe implying a small reference area are utilized for the derivation of the parameters of the PMC model (JCSS (2006)).

Considering the characteristics of the limit states a refinement of the probabilistic model is suggested. For the fatigue limit state the model based on the PMC (JCSS (2006)) is maintained but used for the fatigue relevant locations in the limit state functions. Further the thickness dependency is introduced deriving the parameters of the normal distribution using the measurements of the corresponding thickness. For the ultimate limit state, as the local spatial variation is of minor interest, the statistical model according to PMC is applied to the limit state functions of the individual sections separately assuming no spatial variation within the section, but spatial variations due to different realizations for the individual section thicknesses. For the serviceability limit state the probabilistic model for the thickness deviation is applied for the finite element model using spatial variation for the different sections. As this would introduce a large number of random variables it is suggested introduce groups of sections for computational feasibility. As more measurement data become available the statistical model can be further refined which applies especially to the derivation of a statistical model including the reference area characteristics of the individual limit states.

4.4 Conclusions

The model basis for the assessment of offshore wind energy converters has been completed with the introduction of the fatigue and serviceability model basis. The ultimate limit state basis was introduced in Thöns, Faber et al. (2009b). With this work the mechanical and probabilistic aspects of the models developed have been analyzed in detail resulting in a computational efficient basis for the modeling of the relevant mechanical and probabilistic characteristics of this type of wind energy converter.

The model basis is established for calculation of the prior reliabilities of the support structure components for assessment by monitoring providing local and continuous information meaning e.g. strain gauge data or acceleration sensor data which are itself associated with measurement uncertainties. When utilizing the developed model basis for the assessment of the structural characteristics incorporating monitoring data it seems appropriate to take benefit from a Bayesian probabilistic modeling.

The model basis should include all relevant information of the structure as designed including the production and construction data. The latter provides important information about the involved uncertainties and can be used as a basis for the derivation of probabilistic models. The deterministic part of the model basis meaning the structural responses and the loading models should be clearly physically determined. Engineering models are limited in the way they cover system effects and may incorporate substantial conservativeness.

The sensitivity study conducted here for the fatigue and serviceability limit state is based on the Spearmen rank coefficient of correlation. With this coefficient the degree of any biunique functional dependency of the random variables to the responses is quantified and hence random variables possessing a low coefficient of correlation can be neglected. The refined probabilistic model regarding the structural and loading model

of the support structure is summarized in Table 4-3 including also the ultimate limit state model basis (Thöns, Faber et al. (2009b)). Further random variables might be used with the limit state functions of the individual limit states. This applies to the random variable thickness deviation which will be used within the limit state functions for the ultimate and fatigue limit state.

Table 4-3: Refined probabilistic model for the structural and loading models

Random Variables	Distr.	Mean	Standard deviation	Limit state
Foundation stiffness factor f_g	LN	1.0	0.6	ULS, FLS, SLS
Modulus of elasticity E (N/mm²)	LN	210000	6300	ULS, SLS
Loading Model Uncertainty $f_{M\,\mathrm{od}}$	LN	1.0	0.1	ULS, FLS
Wind load factor f_w	WB	0.4891	0.2256	ULS
Thickness-deviation f_t (mm)	N	1.2	0.7	SLS

N: Normal distribution; LN: Lognormal distribution; WB: Weibull distribution

Certain aspects of the underlying structural and loading models have been analyzed including the effect of the contact formulation, the application of a solid model for hot spot stress calculation and modeling of the mass distribution of the overall model. The influence of the contact formulation was explained and with examples it was shown that the hot spot stresses are lower when a contact formulation is applied. Therefore it can be concluded that this refinement affects both the fatigue and the ultimate limit state. Furthermore this modeling aspect applies not only to the considered type of foundation but especially to the grout connections envisaged used for the offshore version on of this support structure. The application of a solid model is considered even more sophisticated to calculate the stresses in the pile guide-upper brace connection due to the inclusion of stresses in thickness direction which is assumed to be the cause for significantly lower hot spot stresses in comparison to the shell model.

For the modal analysis it was concluded that an overall model is important first to facilitate the assessment of all structural natural frequencies and secondly to model the rotational masses properly. It has also been observed that a part of the mode shapes change when the overall model is applied. The analysis of different rotor angles and angles of the nacelle showed only minor influence on the important lower natural frequencies and on the mode shapes.

4.4.1 General insights gained

The process of analyzing both the deterministic and probabilistic models contributed to deep insight of the rather complex structural, loading and probabilistic models. The assessment of the Spearmen rank correlation leads to the quantification of functional dependencies on which the relevance of certain parameters can be assessed. Since the

functional dependency is based on structural mechanics the interpretation of the results provides an enhanced understanding of the structural responses. In this regard the choice of the design of experiments especially affects the representation of non-linear dependencies.

In developing the uncertainty model it was found of particular value to have measurement data of the structure as constructed. In this way certain parameters of relevance to the responses were included in the probabilistic model; others were excluded. Production data, i.e. quality control data could contribute to further refinement of the probabilistic models. When assessing structures for one or more wind parks, rather than only one structure, these data become even more important.

5 Support Structure Reliability of Offshore Wind Turbines Utilizing an Adaptive Response Surface Method (Paper IV)

S. Thöns

BAM Federal Institute for Materials Research and Testing, Berlin, Germany and

Swiss Federal Institute of Technology, Zurich, Switzerland

M. H. Faber

Institute of Structural Engineering, ETH Zurich, Zurich, Switzerland

W. Rücker

BAM Federal Institute for Materials Research and Testing, Berlin, Germany

Proceedings of the 29th International Conference on Ocean, Offshore and Arctic Engineering (OMAE 2010). 06.-11.06.2010, Shanghai, China.

Abstract

This paper focuses on a reliability analysis of an offshore wind turbine support structure which is part of an assessment and monitoring framework for wind turbines in operation.

The reliability analysis builds upon structural, loading, limit state and uncertainty models comprising design, production and construction data. This model basis facilitates the reliability analysis of the ultimate, the fatigue and the serviceability limit states utilizing stochastic finite elements. The complexity of the individual models dictates an efficient solution scheme for the reliability analysis. Such an algorithm is developed in the present paper consisting of an adaptive response surface algorithm and an importance sampling Monte-Carlo algorithm. The response surface algorithm is based on predetermined experimental designs and facilitates the adjustment of design parameters for an optimized prediction variance in the design point region. Approaches for the consideration of multiple design points and the augmentation of the design for reduction of the prediction variance are introduced.

In this paper, a reliability analysis for a tripod support structure of a Multibrid M5000 wind turbine is performed. A comparison with the target reliabilities specified in DIN EN 1990 (2002) shows that the requirements are fully met. However, the consideration of system reliability leads to the conclusion that at the end of the service life there is a significant probability of fatigue damages. The quantification of the reliability for the individual structural components for all limit states facilitates an identification of sensitive components.

The results of this study can support the targeted application of monitoring systems, the optimization of the support structures and additionally highlight the need for criteria to the systems reliability.

5.1 Introduction

This paper contains a reliability analysis of the support structure of offshore wind turbines which is part of an assessment and monitoring framework for wind turbines in operation (see Thöns, Faber et al. (2008)). This assessment and monitoring framework consists of a combination of a risk analysis with monitoring algorithms aiming to provide continuous condition information and decision support for inspection and maintenance planning.

The study documented in this paper builds upon the model basis described in Thöns, Faber et al. (2009a) and Thöns, Faber et al. (2009b) consisting of probabilistic models for the structural performance, the loads and the associated model uncertainties. These models are derived from constitutive physical equations for a wind turbine system and the methodology for their solution which then in combination with the individual limit state requirements lead to the specific constitutive stationary and general eigenvalue relations. The uncertainty models contain the probabilistic models for the random variables.

The model basis is here completed with the introduction of the limit state models for the ultimate, the fatigue and the serviceability limit states as well as the associated probabilistic models.

The solution algorithm is described subsequently addressing its theoretical foundations such as the regression analysis, the experimental design generation and augmentation, the design point calculation and the applied importance sampling scheme. Approaches for the consideration of multiple design points and the augmentation of the design for reduction of the prediction variance are introduced.

The paper continues with the results of the reliability analysis for a prototype offshore wind turbine support structure and the comparison to target reliability criteria specified in DIN EN 1990 (2002) and the Joint Committee on Structural Safety Probabilistic Model Code (JCSS (2006)). The results are followed by the conclusions.

5.2 Model basis and limit state models

The model basis for the support structure of a prototype of a Multibrid M5000 wind energy converter comprises all models necessary for the reliability assessment. This includes probabilistic models for the structural performance, the loading, the limit state models as well as the associated model uncertainties. The structural and loading models have been developed in Thöns, Faber et al. (2009a) and Thöns, Faber et al. (2009b) with the help of a sensitivity study and analyzing various modeling aspects. This model basis is completed with limit state models and associated probabilistic models in the present paper.

5.2.1 Structural model and loading models

The support structure of the wind energy converter consists of a tower divided in segments by ring flanges, the tripod consisting of upper braces, lower braces, the pile guide as well as the foundation, which consists of circular reinforced concrete slabs attached to a pile group (Figure 5-1). This support structure is represented by means of several finite element models for the specific limit state requirements developed and described in detail in Thöns, Faber et al. (2009b) and Thöns, Faber et al. (2009a). For easy reference, the main aspects of the models are summarized in the subsequent.

The finite element models developed incorporate iso-parametric displacement based shell elements (SHELL 181: ANSYS (2006)) combining plate and membrane theory with linear interpolation functions. At geometrical discontinuities, especially at the tube connections within the tripod, the mesh is refined until the resulting stresses become independent of the mesh. The support structure is connected to the foundation through the pile guides (Figure 5-1). The inside of the pile guide and the outside of the reinforced concrete is meshed with contact elements (CONTA173/174 and TARGE170: ANSYS (2006)).

The loading model consists of the loading vectors calculated by the preceding time domain analysis and a distributed wind loading including a gust response factor on the support structure in the ultimate limit state. The loading vectors at the top of the support structure for the ultimate limit state are provided as min/max matrices (OWT (2009)). Within this matrix all load cases are selected resulting in the high structural demands including the load case with maximum horizontal force and therefore with the highest overturning moment.

For the fatigue limit state, the loading vectors on top of the support structure and on top of the tripod consist of time series representing the fatigue loading scenarios. They

include normal power production operating conditions as well as start and stop operations.

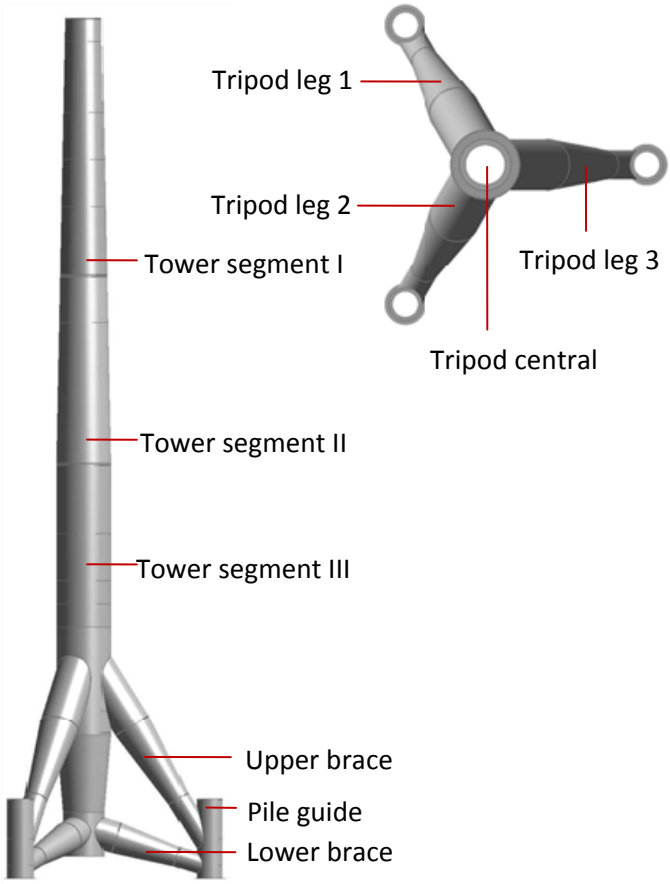

Figure 5-1: Support structure of the Multibrid M5000 wind turbine

5.2.2 Uncertainties associated with structural model and loading models

The uncertainty model comprises random variables associated with the structural model and the loading model. It is derived and described in detail in Thöns, Faber et al. (2009a) and Thöns, Faber et al. (2009b). This model is summarized in Table 5-2 comprising the ultimate limit state (ULS), the fatigue limit state (FLS) and the serviceability limit state (SLS).

Compared to the uncertainty model presented in Thöns, Faber et al. (2009a) the model uncertainty for the fatigue limit state $f_{M,FE,FLS}$ has been further refined. The most sophisticated approach regarding the fatigue model uncertainty has been developed in Folsø, Otto et al. (2002) distinguishing four types of uncertainties related to the load calculation, the stress calculation and the stress concentration calculation. For these sources of uncertainties, two different models are developed considering a basic case and an improved case. As the improved case incorporates direct load and finite element calculations the statistical models for this case are used (see Table 5-1 and Equation (5.1)).

Table 5-1: Model uncertainty of the fatigue limit state (Folsø, Otto et al. (2002))

Random Variable		Mean	St. dev.
Load calculation factor B_L	LN	0.696	0.216
Stress calculation factor B_σ	LN	1.000	0.050
Stress concentration factor calculation B_H	LN	1.011	0.150

LN: Lognormal distribution

The random variables of the individual model uncertainties are multiplied for determination of the fatigue model uncertainty (Equation (5.1)) which is then multiplied by the calculated stresses. The models applied here following (Folsø, Otto et al. (2002)) yield results very similar to the uncertainty model introduced by Wirsching (1984).

$$f_{M,FE,FLS} = B_L B_\sigma B_H \tag{5.1}$$

Table 5-2: Uncertainty model of the structural and loading model (Thöns, Faber et al. (2009a))

Random Variable		Mean	St. dev.	
Foundation stiffness factor f_g	LN	1.0	0.6	ULS, FLS, SLS
Modulus of elasticity E (N/mm²)	LN	210000	6300	ULS, SLS
Thickness-deviation f_t (mm)	N	1.2	0.7	SLS
Loading Model Uncertainty $f_{M,FE}$	LN	1.0	0.1	ULS
Wind load factor f_w	WB	0.4891	0.2256	ULS

N: Normal distribution; LN: Lognormal distribution; WB: Weibull distribution

5.2.3 Limit state models

The limit state models represent the failure mechanisms of the support structure and comprise the ultimate, the fatigue and the serviceability limit states. For these failure mechanisms the limit state equations are derived in the following.

The considered failure mechanisms for the ultimate limit state are yielding, shell buckling and support structure buckling. The failure mode yielding is directly accounted for in the finite element model and includes section yielding as well as punching shear at the tube connections. The corresponding limit state function g_y containing the

component capacity C_c as a function of the yield stress f_y and the component force A may be written as:

$$g_y = C_c(f_y) - A \tag{5.2}$$

The shell buckling failure mode is accounted for based on DIN EN 1993-1-6 (2007). For this study the plastic reference capacity and the ideal buckling resistance are computed with a nonlinear finite element analysis using an approach based on a nonlinear finite element and an eigenvalue analysis (MNA / LBA see DIN EN 1993-1-6 (2007)).

The respective limit state function for component buckling contains the plastic reference resistance R_{Pl}, the buckling reduction factor χ_{ov} and the buckling model uncertainty $f_{M,B}$:

$$g_B = f_{M,B}\chi_{ov}R_{Pl} - 1 \tag{5.3}$$

The plastic reference resistance is defined by the ratio of the yield strength f_y to the membrane equivalent stress σ_{EQ}:

$$R_{Pl} = \frac{f_y}{\sigma_{EQ}} \tag{5.4}$$

The value of the membrane equivalent stress σ_{EQ} is determined by a nonlinear finite element analysis. The buckling reduction factor χ_{ov} is determined through the slenderness ratios $\bar{\lambda}_{ov}$ (related overall slenderness), $\bar{\lambda}_0$ (fully plastic slenderness) and the $\bar{\lambda}_p$ (partly plastic slenderness):

$$\chi_{ov} = 1 \text{ if } \bar{\lambda}_{ov} \le \bar{\lambda}_0 \tag{5.5}$$

$$\chi_{ov} = 1 - \beta\left(\frac{\bar{\lambda}_{ov} - \bar{\lambda}_0}{\bar{\lambda}_p - \bar{\lambda}_0}\right)^{\eta} \text{ if } \bar{\lambda}_0 < \bar{\lambda}_{ov} < \bar{\lambda}_p \tag{5.6}$$

$$\chi_{ov} = \frac{\alpha}{\bar{\lambda}_{ov}^2} \text{ if } \bar{\lambda}_p \le \bar{\lambda}_{ov} \tag{5.7}$$

Here, η is the buckling curve exponent, α is the reduction factor for imperfections and β is the plastic region factor. The related slenderness ratio for the overall shell is assessed from the plastic reference resistance and the ideal buckling load R_{cr} determined by an eigenvalue analysis:

$$\bar{\lambda}_{ov} = \sqrt{R_{pl} / R_{cr}} \tag{5.8}$$

Buckling of the structure, i.e. buckling of the tower as a cantilever, is accounted for with the limit state function g_{os} (Equation (5.9)). This limit state function contains the loading factor f determined by a generalized eigenvalue analysis (see Equation (3.3)) in Thöns, Faber et al. (2009b)). The loading factor represents the first mode shape associated with the stability of the structure.

$$g_{OS} = f - 1 \tag{5.9}$$

The fatigue limit state functions are based on SN models and the assumption of linear damage accumulation known as Miners rule. The SN curves are empirical models relating the number of cycles to failure N to different (constant) stress ranges $\Delta\sigma$ with the parameters C, m, $\Delta\sigma_q$ and $\Delta\sigma_0$ (Equation (5.10)). The parameters $\Delta\sigma_q$ and $\Delta\sigma_0$ are defined to $\Delta\sigma_q = 2 \cdot 10^6$ and $\Delta\sigma_0 = 0$ for offshore structure design purposes (see GL Wind IV - Part 2 (2005) and DIN EN 1993-1-9 (2005a)).

$$N = C \cdot \Delta\sigma^{-m} \tag{5.10}$$

The hot stress concept (see e.g. Niemi, Fricke et al. (2006)) is applied for this study and hence the stresses caused by the local geometry but without taking into account the nonlinear stress concentrations due e.g. the welding geometry are calculated. The linear damage accumulation, i.e. the Miners rule, is the summation of the individual damages which are defined as the ratio of the cycles n_i and the cycles to failure N_i.

Fatigue failure is reached when the accumulated damage D reaches Δ, the damage criteria. The SN limit state function is thus:

$$g_F = \Delta - D \tag{5.11}$$

Eigenfrequency control is essential for operation; design is thus restricted by the excitation frequencies caused by varying rotor revolutions and multiples of the rotor revolutions. According to design codes and guidelines (e.g. GL Wind IV - Part 2 (2005)) the natural frequencies should have a distance of 5 % to the excitation frequencies. Considering the design with the specified first natural frequency of the support structure f_s, it is assumed that natural frequencies lower than $0.95 \cdot f_s$ and higher than $1.05 \cdot f_s$ cause resonance. Therefore the limit state function is zero for all calculated first natural frequencies f_n outside this region (see Equations (5.12) and (5.13)).

$$g_S = 1 \text{ for } 0.95 \cdot f_s \le f_n \le 1.05 \cdot f_s \tag{5.12}$$

$$g_S = 0 \text{ for all other cases} \tag{5.13}$$

5.2.4 Uncertainty models for the limit state models

The uncertainty model for the ultimate limit state includes random variables which have directly assigned distributions and random variables with distributions which depend on the responses of the finite element analysis (Table 5-3). The latter random variables are modeled with a response surface s depending on the random variables specified in the uncertainty models of the loading and structural models. The response model applied is a fully quadratic polynomial function (see details in Section 5.3.1).

The production thickness deviation (which is added to the nominal thickness of the individual sections) and the yield strength are modeled according to the Joint Committee on Structural Safety Probabilistic Model Code (JCSS (2006)). For the derivation of thickness deviation model, measurement data were additionally used. The models are discussed in detail in Thöns, Faber et al. (2009b).

A model uncertainty $f_{M,B}$ for the prediction of the buckling capacity is introduced based on a statistical study by Das, Thavalingam et al. (2003). In this study, predicted

buckling capacities of shells and experimental capacities are statistically analyzed. A normal distribution of the buckling model uncertainty has been assumed.

Table 5-3: Uncertainty model for the ultimate limit state model

Parameter		Mean	St. dev.
Thickness-deviation t_d (mm)	N	1.2	0.7
Yield strength f_y (N/mm²)	LN	370.0	24.2
Buckling model uncertainty $f_{M,B}$	N	1.06	0.076
Stress ratio σ_M / σ	$s_{\sigma_M/\sigma}(f_g, E, f_{M,FE}, f_w)$		
Ideal elastic buckling load r_{Rcr}	$s_{r_{Rcr}}(f_g, E, f_{M,FE}, f_w)$		
Membrane equivalent stress σ_{EQ}	$s_{\sigma_{EQ}}(f_g, E, f_{M,FE}, f_w)$		

N: Normal distribution; LN: Lognormal distribution

The uncertainty in the SN model is related to the linear damage accumulation and to the empirical nature of the SN curves. Whereas the latter uncertainty is introduced by the random variable $\log C$, the uncertainty due to the damage accumulation is introduced by the damage at failure Δ following Folsø, Otto et al. (2002) (Table 5-4).

Table 5-4: Uncertainty model for the fatigue limit state model

Parameter		Mean	St. dev.
Stress range $\Delta\sigma$ (N/mm²)	$s_{\Delta\sigma}(f_g, f_{M,FE,FLS})$		
Uncertainty due to Miners rule Δ	LN	1.00	0.30
SN curve parameter $\log C$	N	12.80	0.25

N: Normal distribution; LN: Lognormal distribution

For the serviceability limit state, the uncertainty model includes as a random variable the natural frequencies modeled with response surfaces (Table 5-5).

Table 5-5: Uncertainty model of the serviceability limit state model

Parameter		Mean	St. dev.
Natural frequencies f_n	$s_{f_n}(f_g, E, f_t)$		

5.3 Solution algorithm

In this section the applied algorithm for the reliability calculation is introduced consisting of an adaptive response surface algorithm and an importance sampling algorithm. These algorithms as well as methods for reducing the prediction variance in the area of the design point and an approach for the consideration of multiple design points are the focus of the next sections.

The description of the solution algorithm starts with the theoretical background, namely the regression analysis, the theory of experimental designs and design efficiency criteria as well as the design point calculation and importance sampling. Consecutively, the algorithm itself and the application of the methods are described.

5.3.1 Regression analysis

The regression analysis is described in the view of the application to the response surface methodology and therefore focuses on the two main aspects, namely, the description of the response prediction variance and the augmentation of the experimental design.

The fully quadratic response model is characterized by Equations (5.14) and (5.15) containing the $1\text{x}\,n$ vector of the responses $\mathbf{y}$ in terms of the $n\,\text{x}\,r$ experimental design matrix $\mathbf{X}$ with the $1\text{x}\,n$ vector of regression coefficients $\boldsymbol{\beta}$ and the $1\text{x}\,n$ vector of the error term $\boldsymbol{\varepsilon}$. The errors are assumed to be independent and normally distributed with zero mean and a variance of σ^2.

$$\mathbf{y} = \mathbf{X}\boldsymbol{\beta} + \boldsymbol{\varepsilon} \tag{5.14}$$

The experimental design matrix $\mathbf{X}$ contains the r combinations of the individual terms of the response model for the number of random variables l and the of samples n. The quadratic response model applied here leads to an experimental design matrix with interaction terms (Equation (5.15)).

$$\mathbf{X}_A = \begin{bmatrix} 1 & x_{11} & x_{12} & \cdots & x_{1l} & x_{11}x_{12} & \cdots & x_{11}x_{1l} & x_{11}^2 & \cdots & x_{1l}^2 \\ 1 & x_{21} & x_{22} & \cdots & x_{2l} & x_{21}x_{22} & \cdots & x_{21}x_{2l} & x_{21}^2 & \cdots & x_{2l}^2 \\ \vdots & \vdots & \vdots & & \vdots & \vdots & & \vdots & \vdots & & \vdots \\ 1 & x_{n1} & x_{n2} & \cdots & x_{nl} & x_{n1}x_{n2} & \cdots & x_{n1}x_{nl} & x_{n1}^2 & \cdots & x_{nl}^2 \end{bmatrix} \tag{5.15}$$

Given a process of unknown precision, an experimental design $\mathbf{X}$ with the (calculated) responses $\mathbf{y}$ the marginal predictive distribution of the responses $\bar{\mathbf{y}}$ for any points contained in $\mathbf{X}_S$ is a multivariate Student t-distribution with the expected values in Equation (5.16) and the covariance matrix in Equation (5.17). These equations are taken as a basis for augmenting the experimental design in the adaptive response surface algorithm as they contain the variances of the response prediction at the trace of the covariance matrix.

$$E\left(\bar{\mathbf{y}}\middle|\mathbf{X},\mathbf{X}_S\right) = \mathbf{X}_S\mathbf{b} \tag{5.16}$$

$$Cov\left(\bar{\mathbf{y}}\middle|\mathbf{X},\mathbf{X}_S\right) = \left(\mathbf{X}_S\mathbf{N}^{-1}\mathbf{X}_S^T + \mathbf{I}\right)\upsilon \tag{5.17}$$

$$\upsilon = \frac{1}{\nu}\left(\mathbf{y} - \mathbf{Xb}\right)^T \left(\mathbf{y} - \mathbf{Xb}\right) \tag{5.18}$$

$$\nu = n - p \text{ and } p = rank(\mathbf{X}) \tag{5.19}$$

The case that a new matrix of points $\mathbf{X}_N$ with the dimensions $m \text{ x } r$ and a responses vector $\mathbf{y}_N$ with the dimension m are added to the experimental design is defined as augmenting the experimental design leading to the augmented experimental design matrix $\mathbf{X}_A$ and the response vector $\mathbf{y}_A$. The marginal predictive distribution can then be calculated applying Equations (5.16) to (5.19) to the augmented experimental design matrix and the augmented responses.

5.3.2 Experimental design and design efficiency criteria

For this study the experimental design is built upon a central composite design (CCD) consisting of $F = 2^k$ factorial points of a k-dimensional hypercube, n_0 centre points and $2k$ axis points. This design belongs to the class of so-called factorized designs (Myers and Montgomery (2002)).

The experimental design is usually defined in coded design coordinates c_i, the space of the experimental design. Depending on the width of the experimental design in the standard normal space $w_{ED,u}$ and in the coded the design space $w_{ED,c}$ the coordinates can be directly transformed with Equation (5.20).

$$u_i = \frac{w_{ED,u}}{w_{ED,c}} c_i \tag{5.20}$$

The two basic properties of an experimental design are that the design is orthogonal (Equation (5.21)) and rotatable (Equation (5.22)). An orthogonal design allows for ease in computations and uncorrelated estimates of the response model coefficients. A rotatable design has the property that the scaled prediction variance v_S (Equation (5.23)) is the same at any location with the same distance $r(\mathbf{x})$ to the design origin. The scaled prediction variance is a scale free experimental design property (due to the division by σ^2) relative to the available information (due to the multiplication by number of sample points n). The requirement of a rotatable design for a CCD leads to Equation (5.22) where the level α is calculated depending on the number of factorial points F. Taking this level, the number of centre points n_0 for an orthogonal design can be calculated (Equation (5.21)).

$$\alpha = \left(\frac{\sqrt{F\left((F + 2k + n_0\right)} - F}{2} \right)^{\frac{1}{2}} \tag{5.21}$$

$$\alpha = F^{1/4} \tag{5.22}$$

The variance expression in Equation (5.24) is contained in the equation for the covariance matrix of the marginal predictive distribution (see Equation (5.19)). In Equation (5.24) the variance is given for one point $\mathbf{x}^{(m)}$ assuming known precision.

$$v_S = \frac{n \cdot Var\left(\bar{y}\left(\mathbf{x}\right)\right)}{\sigma^2} = const. \text{ when } r\left(\mathbf{x}\right) = const. \tag{5.23}$$

$$Var\left(\bar{y}\left(\mathbf{x}\right)\right) = \mathbf{x}^{(m)T}\left(\mathbf{X}^T\mathbf{X}\right)^{-1}\mathbf{x}^{(m)} \cdot \sigma^2 \tag{5.24}$$

The variance property of an experimental design can be depicted with a variance dispersion graph, where the variance V^I is plotted against the dimensionless distance in the coded design space $r\left(\mathbf{x}\right)$. The variance V^I (Equation (5.25)) is defined as the integrated scaled prediction variance over the region U_r with the same distance to the design origin.

$$V^I = \frac{n\psi}{\sigma^2}\int_{U_r} Var\left(y\left(\mathbf{x}\right)\right)d\mathbf{x} \tag{5.25}$$

The variance V^I is complemented by a minimum and a maximum variance graph. These minimum and maximum variance graphs are defined as the integrated values of the respective maximum and minimum scaled prediction variances over the region U_r.

As an example, the variance dispersion graphs for an orthogonal and rotatable CCD with a dimension of four, 12 centre points and a fully quadratic response model is depicted in Figure 5-2. Because of the fact that the design is rotatable all variance dispersion graphs are identical. The integrated variance increases from 3.0 near the centre of the design to 21.0 at a distance of 2.0 in coded design coordinates. Such a distribution of the prediction variance is desirable for application to structural reliability problems since the variance of the prediction around the design point, i.e. the centre of the design, determines the quality of the solution. This property is achieved through 12 centre points, as a CCD with only one centre point has a considerably larger prediction variance in the design centre.

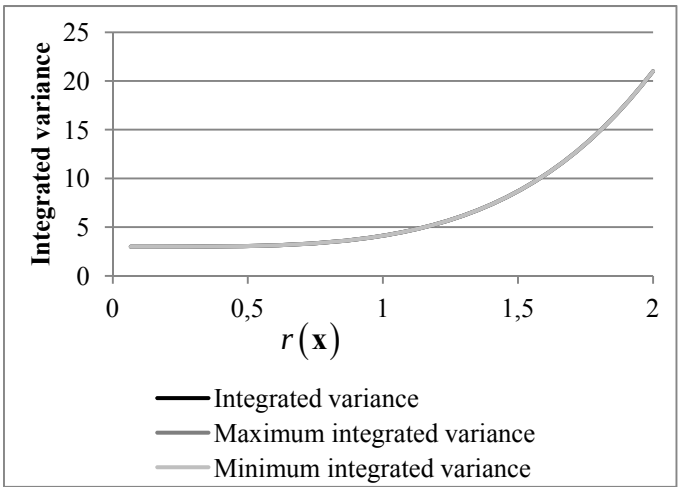

Figure 5-2: Example for variance dispersion graphs (in this case identical).

The variance dispersion graph is closely related to the alphabetic experimental design efficiency criteria called *Q*-efficiency. The *Q*-optimality, which represents the basis for the *Q*-efficiency, is defined as the minimum of an integral value of the scaled prediction

variance over a region of interest (Equation (5.26)). The *Q*-efficiency of a design ζ^* is then defined in relation to the *Q*-optimality (Equation (5.27)). The *Q*-efficiency is used consecutively for updating experimental designs making sure that the updating is contributing to a reduction of the prediction variance in the region of the design point.

$$Q_{opt} = \underset{\zeta}{Min}\left(\frac{1}{K}\int_R n \cdot \mathbf{x}^{(m)T}\mathbf{N}^{-1}\mathbf{x}^{(m)} d\mathbf{x} \right) \text{ with } K = \int_R d\mathbf{x} \tag{5.26}$$

$$Q_{eff} = \frac{\underset{\zeta}{Min}\left(Q(\zeta)\right)}{Q\left(\zeta^*\right)} \tag{5.27}$$

5.3.3 Design point calculation and importance sampling

The design point calculation is necessary for two reasons, namely, to assess the location of the response surface centre and for the importance sampling density. The calculation of the design point, i.e. the point with the shortest distance β to the origin of the u-space, leads to an optimization problem. This problem can be formulated as a Langrange function which is then solved with the Rackwitz-Fiessler algorithm (Bucher (2009b)).

Once the design point is found, an importance sampling Monte Carlo scheme is utilized. The approach applied here uses as the weighting function a multidimensional Gaussian distribution with the expected values equal to the design point.

5.3.4 Approach for multiple design points

A reliability calculation can involve multiple design points corresponding to the number of structural components. This can lead to a substantial number of necessary runs when this problem is approached by the calculation of experimental designs for each design point.

The approach developed here is based on clustering the individual component design points taking basis in the k-means algorithm (e.g. Abonyi and Feil (2007)). This algorithm leads to k clusters C where each component design point $\mathbf{u}_{CDP,j}$ belongs to the cluster with the nearest mean $\mathbf{u}_{DP,C,i}$ (Equation (5.28)).

$$\arg\min_{C} \sum_{i=1}^{k} \sum_{\mathbf{u}_{CDP,j} \in C} \left\| \mathbf{u}_{CDP,j} - \mathbf{u}_{DP,C,i} \right\|^2 \tag{5.28}$$

$$\mathbf{u}_{DP,C} = \frac{1}{n_{CDP,C}} \sum_i \mathbf{u}_{CDP,C,i} \tag{5.29}$$

The calculation of the cluster design point $\mathbf{u}_{DP,C}$ which serves as the origin for the cluster CCD applied for next iteration is calculated as the centre of gravity of all $n_{CDP,C}$ component design points belonging to the cluster with the origin $\mathbf{u}_{CDP,C}$ (Equation (5.29)).

5.3.5 Description of the algorithm

The algorithm is divided into the adaptive response surface algorithm and the reliability analysis. The adaptive response surface algorithm includes four steps namely the

experimental design generation for determining or augmenting central composite designs, the finite element calculation, the regression analysis for the calculation of the regression coefficients and the design point calculation with the Rackwitz-Fiessler optimization algorithm. These steps are repeated until convergence of the calculated design points is achieved. The structural model, the loading model and their associated uncertainty models (as described in the previous sections) are applied in this part of the solution algorithm. The reliability calculation is then performed with the converged design points and the importance sampling. Here only the limit state model and the associated uncertainty model are applied since the response surfaces contain all further information.

The adaptive response algorithm is subdivided in the cluster search and the design augmentation. The cluster search starts with a guess of the design point and a generation of an orthogonal and rotatable central composite design with a width of two standard deviations in the u - space. In the first run, the component design points are assigned to clusters for which new central composite designs are generated. This step is illustrated in Figure 5-3 for the two dimensional case in the *u*-space and three design points. Here the three design points are assigned to two clusters.

The cluster search has converged when a) the clusters do not change, b) the cluster design points have converged and c) all component design points are situated within a distance of $d_{Cl,DP,c} = 0,5\sqrt{k}$ to the respective cluster design point. For the case that the component design points are not located within $d_{Cl,DP,c}$ the width of the design can be enlarged as an alternative to the introduction of a further cluster.

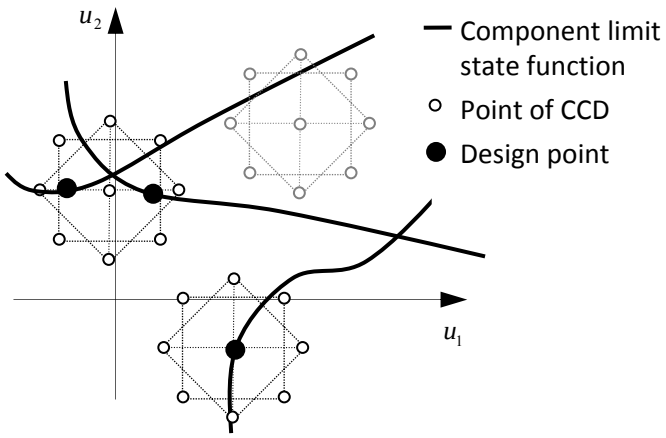

Figure 5-3: Illustration of cluster search with a starting CCD (grey) and the actual clusters consisting of two CCDs (black)

Once the cluster search is converged, the next step, the cluster design augmentation, is performed. Here the component design points are added to the corresponding cluster CCDs. This step is repeated until the component design points are converged and still located within $d_{Cl,DP,c}$.

The augmentation of a CCD in the region around the cluster design point with a distance smaller than $d_{Cl,DP,c}$ (Figure 5-4) leads in almost any cases to an improvement of the Q-efficiency (Equation (5.27)). However, the design then only results in a nearly

rotatable design. To monitor this property, further criteria are introduced, namely, the ratios of the maximum and minimum integrated prediction variances to the integrated prediction variances. These ratios are kept smaller than 1%.

Once the iteration has finished, the importance sampling Monte Carlo scheme is applied and the probabilities of failure are calculated.

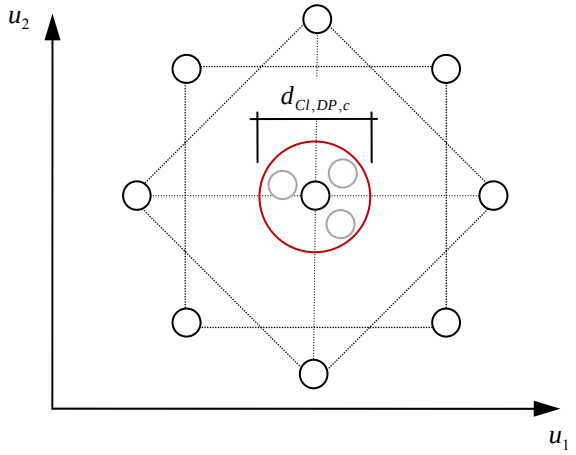

Figure 5-4: Augmentation of a cluster CCD with three component design points (grey)

5.4 Results and discussion

The solution algorithm as described in the previous sections is applied to the structural, loading, limit state and uncertainty models with the aim of the calculation of the reliability of the individual components of the structure. The overall support structure involves 11 tower components assigned to three tower segments and 24 tripod components as parts of the tripod legs and central tube (see Figure 5-1) as well as their connections.

In the ultimate limit state, significant probabilities of failure are only calculated for the buckling failure mechanism. The probabilities of failure of the mechanisms yielding and overall stability are not significant and are consequently not considered further.

All tower components and 7 tripod components are considered in the ultimate limit state. The yearly probabilities of failure of the individual tower components increase from the first to the ninth component where the maximum probability of failure is reached (Table 5-6). The tripod cone components have very low probabilities of failure.

Table 5-6: Yearly component probabilities of failure $p_{f,B}$ for the ultimate limit state

Segment		Comp.	$p_{f,B}$
Tower segment I		1	$< 10^{-9}$
		2	1.20×10^{-9}
		3	5.35×10^{-9}
		4	1.06×10^{-8}
		5	2.35×10^{-8}
Tower segment II		6	1.29×10^{-8}
		7	4.44×10^{-8}
Tower segment III		8	**2.78×10^{-7}**
		9	**5.38×10^{-7}**
		10	**5.07×10^{-7}**
		11	3.18×10^{-8}
Tripod	Cone	12	$< 10^{-9}$
	Leg 1, upper brace cone	13	$< 10^{-9}$
	Leg 1, lower brace cone	14	$< 10^{-9}$
	Leg 2, upper brace cone	15	$< 10^{-9}$
	Leg 2, lower brace cone	16	$< 10^{-9}$
	Leg 3, upper brace cone	17	$< 10^{-9}$
	Leg 3, lower brace cone	18	$< 10^{-9}$

The probability that the support structure fails can be calculated with the simple bounds of system reliability theory. This system can then be modeled as a series system (Equation (5.30)) taking basis in the fact that if one component fails due to buckling the support structure as a whole fails.

The system failure probability of this serial system is between 5.38×10^{-7} for the uncorrelated failure events and 1.46×10^{-6} for correlated failure events. To the system probability of failure clearly the tower segment III with the components 8 to 10 contributes most. Besides the number of components n_C plays a role for correlated probability failure.

$$\max_{i=1}^{n_C} \left\{ P(F_i) \right\} \le P_F \le 1 - \prod_{n_C}^{i=1} (1 - P(F_i)) \tag{5.30}$$

Previous analyses showed similar results, e.g. that the failure mode with lowest reliability for the ultimate limit state is shell buckling (see Thöns, Faber et al. (2008) and Thöns, Faber et al. (2009b)) and that the components of the tower segment III (Figure 5-1) have the highest probabilities of failure.

The calculation of the probabilities in the fatigue limit state involves the connections of all tower components and 13 tripod components which have been identified to have significant probabilities of failure (see Thöns, Rohrmann et al. (2008)). The considered tripod components comprise the upper brace and the pile guides of all three tripod legs as well as one component of the central tube.

Table 5-7: Tower Component probabilities of failure $p_{f,F,T}$ in the fatigue limit state referring to a 20 year service life

Comp.	Location	$p_{f,F,T}$	Comp.	$p_{f,F,T}$
1	Top weld, inside	$< 10^{-6}$	7	1.06×10^{-6}
	Top weld, outside	$< 10^{-6}$		3.49×10^{-5}
	Bottom weld, inside	$< 10^{-6}$		$< 10^{-6}$
	Bottom weld, outside	1.63×10^{-5}		$< 10^{-6}$
2	Top weld, inside	$\mathbf{1.66 \times 10^{-3}}$	8	$< 10^{-6}$
	Top weld, outside	$< 10^{-6}$		$< 10^{-6}$
	Bottom weld, inside	6.12×10^{-5}		$\mathbf{2.47 \times 10^{-4}}$
	Bottom weld, outside	1.32×10^{-6}		2.62×10^{-5}
3	Top weld, inside	$< 10^{-6}$	9	7.36×10^{-6}
	Top weld, outside	1.96×10^{-5}		$\mathbf{1.33 \times 10^{-4}}$
	Bottom weld, inside	4.25×10^{-5}		$\mathbf{2.72 \times 10^{-4}}$
	Bottom weld, outside	1.21×10^{-6}		3.57×10^{-5}
4	Top weld, inside	$< 10^{-6}$	10	1.10×10^{-5}
	Top weld, outside	1.53×10^{-5}		$\mathbf{1.60 \times 10^{-4}}$
	Bottom weld, inside	2.92×10^{-5}		$\mathbf{1.25 \times 10^{-3}}$
	Bottom weld, outside	1.24×10^{-6}		$< 10^{-6}$
5	Top weld, inside	$< 10^{-6}$	11	$< 10^{-6}$
	Top weld, outside	1.41×10^{-5}		$\mathbf{2.40 \times 10^{-4}}$
	Bottom weld, inside	$< 10^{-6}$		$\mathbf{7.92 \times 10^{-4}}$
	Bottom weld, outside	$< 10^{-6}$		$< 10^{-6}$
6	Top weld, inside	$< 10^{-6}$		
	Top weld, outside	$< 10^{-6}$		
	Bottom weld, inside	8.52×10^{-5}		
	Bottom weld, outside	4.32×10^{-6}		

The yearly probabilities of failure shown in Table 5-7 refer to a 20 year service life. The highest probabilities of failure (Table 5-7 bold numbers) were calculated for component two (tower segment I, see Figure 5-1) and the components eight to eleven (tower segment III) with the maximum of 1.66×10^{-3} for component two. The connections, i.e. the welds of the tower segment II show relatively low probabilities of failure.

The connections of the tripod components have probabilities of failure ranging from 9.28×10^{-4} to 1.83×10^{-5} (Table 5-8). Here the highest probability of failure is calculated for the connection upper brace with the pile guide. The probabilities of failure for leg 2 and 3 are lower than for leg 1 because of the direction distributed wind loading.

Table 5-8: Tripod component probabilities of failure $p_{f,F,Tr}$ in the fatigue limit state referring to a 20 year service life

	Connection	$p_{f,F,Tr}$
Leg 1	Tower - upper brace	7.26×10^{-4}
	Upper brace, upper kink	3.05×10^{-4}
	Upper brace, lower kink	2.69×10^{-5}
	Upper brace - pile guide	9.28×10^{-4}
Leg 2	Tower - upper brace	2.41×10^{-4}
	Upper brace, upper kink	9.60×10^{-5}
	Upper brace, lower kink	7.04×10^{-6}
	Upper brace - pile guide	3.15×10^{-4}
Leg 3	Tower - upper brace	2.41×10^{-4}
	Upper brace, upper kink	9.60×10^{-5}
	Upper brace, lower kink	7.04×10^{-6}
	Upper brace - pile guide	3.15×10^{-4}

For determining the system probability of fatigue failure the simple bounds of system reliability theory (e. g. Equation (5.30)) necessitate a system model. In contrast to the buckling failure mechanism the fatigue failure of one component does not necessarily lead to a failure of the whole support structure. The system probability of failure of the tripod caused by fatigue is therefore without further studies hardly determinable. However, the tripod is a highly statically undetermined system and the stress concentrations are located in a small area of the connection in comparison to the overall length of the tube connections. Both facts indicate that the tripod is a damage tolerant system.

Fatigue failure of the tower components also occurs very locally because of its dimensions. As the tower is a statically determined system it is not as damage tolerant as the tripod.

As the system for the calculation of system failure can only be modeled qualitatively for fatigue so far, the probability that a fatigue failure occurs can be calculated with the simple bounds of system reliability theory taking basis in a serial system (Equation (5.30)). Then the probability that fatigue failure occurs results for the tower in the bounds of 1.66×10^{-3} and 5.15×10^{-3}, for the tripod in the bounds of 9.28×10^{-4} and 3.30×10^{-3} and for the support structure in the bounds of 1.66×10^{-3} and 8.43×10^{-3}.

For the serviceability limit state, a probability of exceeding the frequency bounds, of 1.56×10^{-1} is calculated. Here the first two mode shapes (see Thöns, Faber et al. (2009a)) were considered. It is observed that the lower bound of the limit state equation (Equation (5.12) and (5.13)) contributes more in comparison to the upper bound to the calculated probability of failure.

The calculated probabilities of failure should be in accordance with acceptance criteria such as target probabilities of failure given e.g. in the DIN EN 1990 (2002) and in the Probabilistic Model Code (JCSS (2006)). For the ultimate limit state, the DIN EN 1990 (2002) gives annual probabilities of failure for the individual components of 1.00×10^{-7} for consequence class 3, 1.30×10^{-6} for consequence class 2 and 1.33×10^{-5} for consequence class 1. Considering an offshore wind park, the consequence class 2 with minor consequences for life and limb but considerable economic consequences should be envisaged. The component probabilities of failure in the ultimate limit state are below this specified value with a maximum of 5.38×10^{-7}.

For the fatigue limit state, probability of failure bounds between 6.68×10^{-1} and 7.23×10^{-5} for a 50 year service life depending on accessibility, maintainability and damage tolerance are given. The support structure of an offshore wind turbine has clearly limited accessibility and maintainability due to the offshore environment. The tower of the support structure can be considered as better accessible (as it is not under water) but not damage tolerant whereas the tripod can be considered as hard accessible but due to the high degree of statical indeterminacy damage tolerant. The maximum component probabilities of failure of 1.66×10^{-3} for the tower and 9.28×10^{-4} for the tripod are situated approximately in the middle of these bounds for a service life of 20 years.

The probability of un serviceability is situated between the probability of failure of 6.68×10^{-1} referring to a 1 year reference period and 1.87×10^{-3} referring to a 50 year reference period as specified in DIN EN 1990 (2002). The calculated probability of failure (1.56×10^{-1}) is here closer to the reference period of 1 year.

Considering the Probabilistic Model Code (JCSS (2006)) the target probabilities of failure are distinguished in the ultimate (which includes the fatigue limit state) and the serviceability limit states. In opposite to the DIN EN 1990 (2002) requirements these probabilities refer to the structure as a whole i.e. to the system probability of failure. For

the ultimate limit state, the probabilities of failure have a range from 1.00×10^{-6} for low cost of safety and high consequences of failure from 1.00×10^{-3} for high cost of safety and low consequences of failure. For the serviceability limit state, values of 1.00×10^{-1} for high cost of safety and 1.00×10^{-2} for low cost of safety are given.

In regard to the target probabilities of failure specified in the Probabilistic Model Code (JCSS (2006)), the system probability of failure in ultimate limit state is with a value between 5.38×10^{-7} and 1.46×10^{-6} significant lower than the value of 1.00×10^{-5}, specified for medium cost of safety and moderate consequences.

The comparability of the system probabilities of failure in the fatigue limit state is limited because here only the probability that fatigue failure occurs rather than the probability of system failure (as specified in the Probabilistic Model Code) is calculated. The target probability of failure for the serviceability limit state is slightly exceeded.

5.5 Conclusions

A reliability analysis for a tripod support structure of a Multibrid M5000 wind turbine has been performed utilizing a model basis consisting of structural, loading, limit state and uncertainty models as well as an adaptive response surface solution algorithm. Furthermore, the limit state models, the associated uncertainty models and the solution algorithm have been developed.

The results presented here show in detail that the reliability of the support structure is in accordance with the requirements of DIN EN 1990 (2002). The reliability is especially high at the beginning of the service life as the reliability in the ultimate limit state is very high and the fatigue loading is low.

With increasing service life of the support structure the probability of fatigue failure increases, which leads at the end of the service life to a significant probability that fatigue failure occurs. Two facts contribute to this situation, namely, the relatively high probabilities of fatigue failure and the high number of locations where fatigue can occur.

A significant probability of fatigue failure at the end of the service life is found despite the conformity with the design requirements of DIN EN 1990 (2002). This is caused by the fact that the target reliabilities are only specified for the components in DIN EN 1990 (2002) and no system reliability or robustness requirements are given. This example clearly shows why offshore structures in general often exhibit at the end of the service life fatigue problems.

The component reliabilities provide a basis for the design of a monitoring system, as sensitive components with the highest probabilities of failure comprising all limit states have been identified. These are the tower segment III for the ultimate and the fatigue limit state and the tower component 2 for the fatigue limit state. Furthermore the connection of the tripod upper brace belongs to the components with a relatively high probability of failure.

The adaptive response surface algorithm was applied for this reliability analysis and hence utilized for complex finite element models. Especially the clustering algorithm turned out to be efficient for reducing the number of experimental designs and, in connection with the Q-efficiency criteria, an improvement the prediction variance of the experimental design is achieved. For the cases considered, fast convergence was observed. However, the proposed algorithm and its efficiency should be further studied and analyzed in detail.

Furthermore, the developed model basis and the algorithms can be utilized for studies such as the reliability and production cost optimization of the support structure.

6 On measurement uncertainties, monitoring data and structural reliability

Abstract

This chapter introduces an approach for structural reliability analysis utilizing monitoring data and the associated measurement uncertainties. Furthermore, a new approach for the determination of measurement uncertainties building upon the framework of the Guide for Uncertainties in Measurements (GUM) is presented. GUM distinguishes two types of measurement uncertainty namely the uncertainty based on a statistical analysis of observations (Type A) and the uncertainty derived from a process equation as well as an uncertainty model of the parameters (Type B). The approach introduced in this chapter utilizes both types for the derivation of a posterior measurement uncertainty by Bayesian updating. This facilitates the quantification of a measurement uncertainty using all available data of the measurement process. The measurement uncertainty models derived in this chapter are analysed with a sensitivity study and discussed in detail resulting in an identification of the most relevant sources of measurement uncertainty. Furthermore all types of measurement uncertainties are utilised the for a generic fatigue reliability analysis. It is shown that accounting for the measurement uncertainties has an influence on the reliability.

6.1 Introduction

A recent research challenge is the application of monitoring data for a reliability analysis in various fields of engineering (see e.g. Enright, Hudak et al. (2006), Liu, Frangopol et al. (2010) and Thöns, Faber et al. (2008)). The most relevant question of the application of monitoring data is: Which uncertainties should be applied to the monitoring data when utilized in a reliability analysis? This question is answered with the present chapter by building upon two existing frameworks: The framework for the determination of measurement uncertainties based on ISO/IEC Guide 98-3 (2008a) and reliability analysis framework of the JCSS Joint Committee on Structural Safety.

The framework of the JCSS Joint Committee on Structural Safety (PMC JCSS (2006)) constitutes one of the most sophisticated frameworks for the reliability analysis. An essential statement of the basis of design of this framework constitutes that all essential sources of uncertainty have to be evaluated and integrated in the utilized models.

An established framework for the determination of measurement uncertainties constitutes the ISO/IEC Guide 98-3 (2008a) developed from the Guide for the expression of Uncertainties in Measurements (GUM), published in 1995. Since then, the Joint Committee for Guides in Metrology (JCGM) leads the development of GUM and has released several accompanying documents such as the ISO/IEC Guide 98-3/Suppl.1 (2008b) and JCGM (2009). The approaches developed in this chapter built upon this framework.

The chapter starts with a description of methods for the determination of the measurement uncertainty for strain measurements following ISO/IEC Guide 98-3 (2008a). Subsequently these methods are extended to account for model uncertainties and a probabilistic model assignment uncertainty. Furthermore, the measurement uncertainties based on a process equation and based observations are derived.

In the third section the core of the introduced concept is derived and discussed, namely the posterior measurement uncertainty.

The fourth section contains a generic reliability analysis. Here, the measurement uncertainty for strain measurements is determined for the specific example followed by a sensitivity analysis to identify the parameters contributing most to the measurement uncertainty. The fatigue reliability is calculated then with a mechanical model, a limit state model and with the associated probabilistic models. The results for the reliability considering the derived types of measurement uncertainties are compared. The fifth section contains the summary and conclusions.

6.2 Measurement uncertainties and model assignment uncertainty

The measurement uncertainty following ISO/IEC Guide 98-3 (2008a) is determined with a measurement equation which yields the measurand. The uncertainties of the input quantities, i.e. the (random) variables, determine the uncertainty of the measurand. The estimation of the uncertainty model of the random variables is distinguished into two types. Type A measurement uncertainties are derived by assigning a statistical model to observations. This derivation follows the frequentistic definition of probability. Type B measurement uncertainties are derived with the help of a process equation modeling physically the measurement process. The probabilistic models of the associated random variables are “evaluated by scientific judgment based on all of the available information” (ISO/IEC Guide 98-3 (2008a)) implying a Bayesian definition of probability.

Taking these concepts as a basis, the measurement uncertainty, defined here as the distribution of the measurand, is determined for a generic example: The strain measurement with a strain gauge.

For such an application the measurand is the mechanical strain E_{mech}. The mechanical strain is defined as the sum of the amplifier strain E_{amp} and the apparent strain E_{app} leading to the measurement equation (Equation (6.1)). Here, the mechanical strain is the strain in the structure. The amplifier strain denotes the strain which is measured with the amplifier and the apparent strain is the strain which is caused by temperature effects in the strain gauge.

$$E_{mech} = E_{amp} + E_{app} \tag{6.1}$$

6.2.1 Measurement uncertainty based on a process equation

Based upon the physical properties of the measurement process, the process equation is derived and uncertainty models are introduced for the associated random variables. This derivation takes basis in the concept for the determination of Type B uncertainties

according to ISO/IEC Guide 98-3 (2008a). In addition to this concept, a model uncertainty and an assignment uncertainty are introduced.

The starting point for the derivation of the process equation is the measurement equation (Equation (6.1)). The Introduction of the model uncertainty $\theta_{E_{mech}}$, which describes the uncertainty associated with the physical formulation of the problem, leads to Equation (6.2).

$$E_{mech} = \theta_{E_{mech}} + E_{amp} + E_{app} \tag{6.2}$$

The process of a strain measurement is an electrical process where specifically the voltage differences in an electrical circuit are measured. These voltage differences change, as the strain gauge, an electrical conductor, changes its resistance with elongation or compression, i.e. with mechanical strain. For a quarter Wheatstone Bridge with the measured voltages U_A and U_B and the gauge factor k, the measured strain ε_{meas} is described with Equation (6.3).

$$\varepsilon_{meas} = \frac{4}{k}\frac{U_A}{U_B} \tag{6.3}$$

Two corrections for the k-factor, namely the transverse strain correction factor $f_{s,q}$ (Equation (6.5)) and the temperature coefficient of the strain gauge $\alpha_{s,k}$ with the temperature difference $\Delta T_{20°C}$, are introduced. The transverse strain correction takes basis in the quality testing procedure of the strain gauges in a one dimensional stress field. This one-dimensional stress field causes due to the Poisson ratio of the calibration beam ν_0 a two dimensional strain field. In case the ratio of the transverse to the longitudinal strain $\varepsilon_q / \varepsilon_l$ differs from the calibration procedure, a correction according to Equation (6.5) is considered depending on the transverse sensitivity of the strain gauge q. Furthermore, the gauge factor variation $f_{s,v}$ and an associated model uncertainty of the gauge factor variation $f_{s,s}$ are introduced leading to Equation (6.4).

$$E_{amp} = \frac{4}{k\left(1 + f_{s,v} + f_{s,s} + f_{s,q} + \alpha_{s,k}\Delta T_{20°C}\right)}\frac{U_A}{U_B} \tag{6.4}$$

$$f_{s,q} = \frac{q}{1 - q\nu_0}\left(\frac{\varepsilon_q}{\varepsilon_l} + \nu_0\right) \tag{6.5}$$

The calibration and amplifying process is modeled with the zero deviation $f_{a,z}$ (dependent on the measurement range) and the amplifier deviation $f_{a,a}$ (dependent on the measured value) are multiplied and added to Equation (6.4) respectively. This results in the process equation for the amplifier strain (Equation (6.6)).

$$E_{amp} = f_{a,a}\frac{4}{k\left(1 + f_{s,v} + f_{s,s} + f_{s,q} + \alpha_{s,k}\Delta T_{20°C}\right)}\frac{U_A}{U_B} + f_{a,z} \tag{6.6}$$

The apparent strain describes the temperature-dependent change of the measurement signal without a mechanical stress. The process equation for the apparent strain is

readily defined with Equation (6.7). The temperature-variation curve $\varepsilon'_{app}(\Delta T_{20°C})$ describes the strain depending on a temperature difference with a basis of 20 degrees Celsius $\Delta T_{20°C}$. The tolerance of the temperature-variation curve ε_T characterizes the uncertainty of the apparent strain increasing with temperature.

$$E_{app} = \varepsilon'_{app}(\Delta T_{20°C}) + \varepsilon_T \Delta T_{20°C} \tag{6.7}$$

With an associated uncertainty model, the measurement uncertainty can be derived e.g. with a Monte Carlo simulation. The uncertainty model can be derived by considering the product information of the measurement system. The product information is usually valid for all strain gauges of the same type, all amplifiers of the same type and for all surrounding and application conditions as documented in the manufacturer specifications according to standardized rules.

It is observed from (Equations (6.6) and (6.7)) that the measurement uncertainty depends on the ratio of measured voltages and the temperature. The fact of the voltage ratio dependency implies dependency on the measured value itself. It follows that the assignment of the measurement uncertainty model to a measured value is uncertain. This assignment process can be modeled and is introduced in the next section.

6.2.1.1 Uncertainty model for measurement uncertainty assignment

A measurement value constitutes a realization of the measurement uncertainty. Because of the fact that the measurement uncertainty is dependent on the measurement value, a probabilistic for the assignment of the measurement uncertainty is derived in this section based on De Sanctis (2009).

The application of the process equation (Equation (6.6)) produces i measurement uncertainty models $M_{u,i}$ for i different strains (Equation (6.8)).

$$E_{amp} \,|\, U_A / U_B \sim M_{u,i}(\mu_i, \sigma_i) \tag{6.8}$$

The parameters of these models μ_i and σ_i are considered as uncertain to account for the assignment uncertainty. A prior probability density function for these parameters is derived by calculating the individual probability densities f_j (Equation (6.9)) by associating j different reference strains $\hat{\varepsilon}_{R,j}$ (Equation (6.9)) with the parameter μ_j. The distribution of σ follows then the same distribution.

$$f'(\mu_i, \sigma_i \,|\, M_{u,i}) = f(M_{u,i} \,|\, \hat{\varepsilon}_{R,j}) \tag{6.9}$$

$$\hat{\varepsilon}_{R,j} = \frac{4}{k}\left(\frac{U_A}{U_B}\right)_j \tag{6.10}$$

The likelihood estimate of the parameters is derived based upon observations of the measurement process $\hat{\varepsilon}_1 \ldots \hat{\varepsilon}_n$ and is readily defined with Equation (6.11).

$$L(\mu_i, \sigma_i \,|\, \hat{\varepsilon}_1 \ldots \hat{\varepsilon}_n) = \prod_{j=1}^{n} f(\hat{\varepsilon}_j \,|\, \mu_i, \sigma_i) \tag{6.11}$$

The posterior distributions of the parameters are derived with Bayesian updating (Equation (6.12)) and the marginal distribution of the mechanical strain is calculated with Equation (6.13).

$$f''\left(\mu_i,\sigma_i \mid \hat{\varepsilon}\right) = f'\left(\mu_i,\sigma_i \mid M_{u,i}\right)\cdot L\left(\mu_i,\sigma_i \mid \hat{\varepsilon}\right)\cdot const. \tag{6.12}$$

$$f\left(E_{amp}\right) = \int_{-\infty}^{+\infty} f\left(E_{amp} \mid \mu,\sigma\right)\cdot f''\left(\mu\right)\cdot f''\left(\sigma\right) d\mu d\sigma \tag{6.13}$$

Having performed these steps, the uncertainty of the assignment has been calculated and is contained in E_{amp}. The process equations (Equations (6.6) and (6.7)) are inserted into Equation (6.2) and the measurand can be determined.

6.2.2 Measurement uncertainty based on observations

Here, the amplifier strain and the apparent strain are determined based on observations ε taking basis in the definition of Type A measurement uncertainties stated in ISO/IEC Guide 98-3 (2008a). The measurement equation (Equation (6.1)) is rewritten for distinguishing the different concept of uncertainty determination and to account for the model uncertainty $\theta_{\varepsilon_{mech}}$ (Equation (6.14)).

$$\varepsilon_{mech} = \theta_{\varepsilon_{mech}} + \varepsilon_{amp} + \varepsilon_{app} \tag{6.14}$$

It is assumed that n realizations of the amplifier strain ε_{amp} follow a normal distribution with the parameters μ and σ (Equation (6.15)).

$$\varepsilon_{amp} \sim N\left(\mu,\sigma\right) \tag{6.15}$$

The parameters of the distribution are estimated with the method of Maximum Likelihood. For the calculation of the marginal distribution, the statistical uncertainties of the parameters are integrated (Equation (6.16)).

$$f_{\varepsilon_{amp}}\left(\varepsilon_{amp}\right) = \int_{-\infty}^{+\infty} f\left(\varepsilon_{amp} \mid \mu,\sigma\right)\cdot f\left(\mu\right)\cdot f\left(\sigma\right) d\mu d\sigma \tag{6.16}$$

Together with temperature data, the distribution of ε_{app} can be determined leading to the distribution of ε_{mech}, the measurement uncertainty.

As the dependencies of the measurement uncertainty on the measured voltages and the temperature are observed in the last section, the measurement uncertainty based on the observation can determined for different reference strains (Equation (6.9)) and temperatures.

The measurement uncertainty obtained by observations has different boundary conditions associated with the probabilistic models. In contrast to the process equation based measurement uncertainty, the observation based measurement uncertainty applies to the utilised type of the sensor, the amplifier and to the specific application and surrounding conditions.

6.3 Derivation and definition of the posterior measurement uncertainty

As described in Section 6.2.1, the measurement uncertainty derived with a process equation and an associated uncertainty model is valid for all strain gauges and all amplifiers of the same type and for all application conditions as stated in the manufacturer specifications. However, a measurement is conducted with a certain type of a sensor and a certain type of an amplifier under specific application conditions. This leads to a different and unknown, presumably lower, measurement uncertainty. Thinking in terms of the process equation, the probabilistic models of the random variables have changed and some random variables may have realized, i.e. may have transformed to deterministic values.

The observations applied for the determination of the measurement uncertainty must not necessarily cover all surrounding conditions but the conditions which apply for the situation where the observations are generated. This clearly constitutes a limitation of the observation based measurement uncertainty as typically experienced in measurement projects (see e.g. Thöns, Rohrmann et al. (2008)).

It becomes clear that the measurement uncertainty for a specific application is not exactly determinable and that furthermore both concepts for the determination of the measurement uncertainty have their different boundary conditions and their limitations. The latter is also true for the probabilistic concepts as the definitions of Type A and Type B measurement uncertainties originally take basis in a frequentistic and a Bayesian definition of the probability respectively. In this way it is natural to distinguish between these concepts as done in ISO/IEC Guide 98-3 (2008a).

Both concepts aim at the determination of the measurement uncertainty for a considered application, but following the characteristics described, the process equation based measurement uncertainty should give an upper boundary and the observation based measurement uncertainty may give a lower boundary.

Having established the boundaries of the measurement uncertainty, a new type is now suggested to estimate the measurement uncertainty for a specific application. That is the posterior measurement uncertainty, based upon Bayesian updating, utilizing all available information and data, i.e. informative distributions for the prior and the likelihood.

The process equation based measurement uncertainty is seen as the accumulation of the prior knowledge of the measurement process and therefore constitutes the prior measurement uncertainty (Equation (6.17)).

$$f'\left(E_{mech}\right) = f\left(\theta, E_{amp}, E_{app}\right) \tag{6.17}$$

The measurement uncertainty derived from observations, constitutes the likelihood of the measurement uncertainty, i.e. the distribution of the observations given the prior knowledge $L\left(\varepsilon_{mech} \mid E_{mech}\right)$. It is derived for the specific measurement application and surrounding conditions.

With Bayesian updating the posterior measurement uncertainty, i.e. the distribution of the measurement uncertainty accounting for prior knowledge and observations, is derived (Equation (6.18)).

$$f''(E_{mech} \mid \varepsilon_{mech}) = f'(E_{mech}) \cdot L(\varepsilon_{mech} \mid E_{mech}) \cdot const. \tag{6.18}$$

This posterior measurement uncertainty is interpreted as an estimate of the measurement uncertainty for an application which should be situated between the boundaries established by the process equation based and the observation based measurement uncertainty. This clearly takes basis in the boundary condition of the involved models as described.

6.4 On the assignment of measurement uncertainties to measurements

The framework for the determination of probabilistic models for measurement uncertainties has been introduced and the individual probabilistic models comprising three concepts can be derived. Together with the measurement data the reliability can be calculated.

However, the measurement data constitute the realizations of the process as described by the probabilistic model leading to the question which probabilistic model should be assigned to a measurement value. Since the assignment uncertainty has already been accounted for (see Section 6.2.1.1), it is now possible to assign the probabilistic model to the measurement value which equals the reference value.

The second aspect is the treatment of the random variables in the reliability calculation. For this purpose, general model uncertainties are considered. This type of uncertainties is applied in a reliability analysis as it is an element of the framework of the PMC (JCSS (2006)) and it constitutes the uncertainties with the application of e.g. a mechanical model. Here, we have also the situation that to account for an uncertainty and we practically deal with a realization, i.e. with the utilized model. These uncertainties are introduced in the PMC (JCSS (2006)) either by addition or multiplication or a combination of both.

The measurement uncertainties are treated similarly as the measurement equals the reference value and is then directly replaced with the derived probabilistic model. This could be equally rewritten in the form of addition of the measurement uncertainty to the measurement.

6.5 Generic fatigue reliability analysis

For a generic reliability analysis, a structural detail of detail category 3 (DIN EN 1993-1-9 (2005a)) is considered. This detail is assumed to have been designed, built and the loading of this detail then has been measured.

It is assumed that the specimen is designed applying the hot spot concept in combination with the SN approach and the linear damage accumulation (DIN EN 1993-1-9 (2005a)).

Further, it is assumed that the strain history is measured with strain gauges at the hot spot location of the detail (see Figure 6-1). These strain gauges measure the strains $\varepsilon_{0.4t,i}$ at position $0.4t$ and $\varepsilon_{t,i}$ at position t form the notch root.

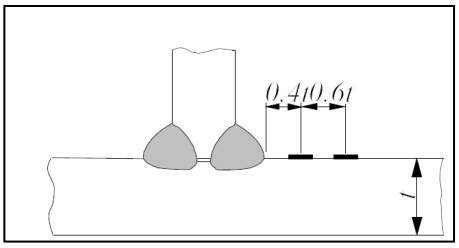

Figure 6-1: Position of strain gauges at the detail

The measurement system applied, consists of HBM MGC plus amplifier (HBM (2008)) with a ML55B card and a strain gauge of type WFLA 6-17 (TML (2008)).

6.5.1 Mechanical, limit state and associated probabilistic models

The mechanical models for the fatigue reliability calculation comprise models for the fatigue reliability as designed and for the fatigue reliability based on the strain measurements; further models are the limit state model and the associated probabilistic models.

The mechanical model for the fatigue reliability calculation as designed involves the random variable generic stress range $\Delta\sigma_{gen}$ and is assumed to follow a Weibull-distribution (see Table 6-1). Its parameters are adjusted according to Straub (2004) with a scale parameter of 20 and a shape parameter of 0.6. Furthermore, the model uncertainties for the stress calculation and for the hot stress calculation are multiplied to the generic stress ranges to calculate the stress ranges for the reliability analysis $\Delta\sigma_{rel}$ (Equation (6.19)). The probabilistic models are chosen following Folsø, Otto et al. (2002) as described in Thöns, Faber et al. (2010).

$$\Delta\sigma_{des} = B_\sigma B_H \cdot \Delta\sigma_{gen} \tag{6.19}$$

Table 6-1: Uncertainty model for the design stress calculation (Equation (6.19))

Random variable		Scale par.	Shape par.	
Generic stress ranges $\Delta\sigma_{gen}$	WB	20	0.6	Straub (2004)
Random variable		Mean	St. dev.	
Stress calculation factor B_σ	LN	1.000	0.050	Folsø, Otto et al. (2002)
Hot spot stress calculation factor B_H	LN	1.011	0.150	Folsø, Otto et al. (2002)

LN: Lognormal distribution; WB: Weibull distribution

For the fatigue reliability calculation based on the measurements, the mechanical model for the calculation of the hot spot stress time series consists of a linear extrapolation model of the strain (see e.g. Niemi, Fricke et al. (2006)) and a multiplication with the modulus of elasticity E (Equation (7.4)). The n strain measurements contained in the time series contain the measurement datum dependent (index i) measurement uncertainties ($\varepsilon_{0.4t,i}^{M}$ and $\varepsilon_{t,i}^{M}$). A one dimensional stress state is assumed as typical in the regions of stress concentrations.

$$\Delta\sigma_{RF} = \overset{n}{\underset{i=1}{F_{RF}}}\left[E\cdot(1.67\varepsilon_{0.4t,i}^{M} - 0.67\varepsilon_{t,i}^{M})\right] \tag{6.20}$$

$$\Delta\sigma_{meas} = B_{H,meas}\cdot\Delta\sigma_{RF} \tag{6.21}$$

The stress ranges $\Delta\sigma_{RF}$ as well as the number of cycles are calculated with a Rainflow algorithm (here denoted with F_{RF}) which is implemented based on Clormann U. H. and Seeger T. (1986). The stress ranges are then multiplied with the model uncertainty $B_{H,meas}$ accounting for the hot spot stress calculation uncertainty (Equation (6.21)) to calculated the distribution of measured stress ranges $\Delta\sigma_{meas}$.

The associated probabilistic model for the fatigue reliability calculation based on the measurements is summarized in Table 6-2. The model uncertainty is derived following Folsø, Otto et al. (2002). However, the case here differs from the analyses of Folsø, Otto et al. (2002) in the way that strain gauges are directly applied to the detail and no uncertainties for the load and the stress calculation have to be considered. It follows that only the uncertainty model for the hot spot stress calculation is considered. In this study a standard deviation of 0.05 instead of 0.15 is assumed because of the fact that this model is extensively applied in scientific studies for the derivation of fatigue life models for structural details (e.g. Schumacher and Nussbaumer (2006)) and should therefore be associated with rather low model uncertainties. The probabilistic model for the modulus of elasticity is introduced as specified in JCSS (2006). The strains $\varepsilon_{0.4t}$ and ε_{t} at position $0.4t$ and t are assumed to be fully correlated and to follow a Weibull distribution. The scale and the shape parameter of the Weibull distribution are numerically adjusted in a way that the distributions of the measured stress ranges and the design stress ranges are approximately equivalent (Equation (6.22)) and that these distributions result in the same damage equivalent stress ranges $\Delta\sigma_{eq}$ (Equation (6.23)). For the adjustment the measurement uncertainty and the probabilistic model of the modulus of elasticity are not considered.

$$\Delta\sigma_{RF} \sim WB\left(\Delta\sigma_{gen}\right) \tag{6.22}$$

$$\Delta\sigma_{gen,eq} = \Delta\sigma_{RF,eq} \tag{6.23}$$

Table 6-2: Uncertainty model for the hot spot stress calculation model (Equation (6.21))

Random variable		Mean	St. dev.	Reference
Modulus of elasticity E (N/mm²)	LN	2.10×10^5	6.30×10^3	JCSS (2006)
Model uncertainty B_H	LN	1.00	0.05	Folsø, Otto et al. (2002)
Random variable		Scale par.	Shape par.	
Measured strain $\varepsilon_{0.4t}$	WB	20	0.4	Equations (6.22) and (6.23)
Measured strain ε_t	$\varepsilon_t = 0.5 \cdot \varepsilon_{0.4t}$			
Strain with measurement uncertainty $\varepsilon_{0.4t}^M$	$f\left(\varepsilon_{0.4t,i}\right)$			Section 6.2
Strain with measurement uncertainty ε_t^M	$f\left(\varepsilon_{t,i}^M\right)$			Section 6.2

LN: Lognormal distribution; WB: Weibull distribution

The limit state model is based upon the SN-model for hot spot stresses as specified in DIN EN 1993-1-9 (2005a), see Equations (6.24) and (6.25)). The SN-curves are empirical models relating the number of cycles to failure N to different stress ranges $\Delta\sigma$ with the parameters C_1 and m_1.

$$N = C_1 \cdot \Delta\sigma_{eq}^{-m_1} \tag{6.24}$$

Linear damage accumulation, i.e. the Miners rule is assumed (Equation (6.25)) leading to the limit state function with the accumulated damage D, the damage criteria Δ and the number of cycles n_i.

$$g_F = \Delta - D \text{ with } D = \frac{n_{eq}}{N} \tag{6.25}$$

The uncertainties of the limit state model (Table 6-3), i.e. the SN model, consists of the probabilistic models for the parameter $\log C_1$ and the Miners rule Δ. These uncertainty models are discussed in detail in Thöns, Faber et al. (2010).

Table 6-3: Uncertainty model for the limit state model

Parameter		Mean	St. dev.	Reference
SN curve parameter m_1	D	3.0		DIN EN 1993-1-9 (2005a)
SN curve parameter $\log C_1$	N	12.80	0.25	DIN EN 1993-1-9 (2005a)
Equivalent stress ranges n_{eq}	D	2.0×10^6		
Uncertainty due to Miners rule Δ	LN	1.00	0.30	Folsø, Otto et al. (2002)

D: Deterministic ; N: Normal distribution; LN: Lognormal distribution

6.5.2 Probabilistic models for the derivation of the measurement uncertainty

Following the developed process equation in Section 6.2.1, the probabilistic models are summarized in Table 6-4. The uncertainty model of the gauge factor takes basis in the product specification (TML (2008)) and the guideline VDI/VDE/GESA 2635, Part 1 (2007). According to VDI/VDE/GESA 2635, Part 1 (2007), the specified uncertainty is the statistical uncertainty of the mean of the strain gauge factor and a factor for the consideration of systematic effects. The factor for the systematic effects $f_{s,s}$ is here considered as a model uncertainty. Information about the size are taken from VDI/VDE/GESA 2635, Part 1 (2007). Following the principle of maximum entropy (e.g. ISO/IEC Guide 98-3/Suppl.1 (2008b)) a rectangular distribution is assigned to the random variable $f_{s,s}$.

The uncertainty model for the variation of the strain gauge factor $f_{s,v}$ is assumed normally distributed, as it is derived by repeated measurements (VDI/VDE/GESA 2635, Part 1 (2007)). The parameters of the distribution of the variation of the strain gauge factor are calculated from the distribution of the mean of the strain gauge factor assuming a 95% confidence interval and a sample size of 10 strain gauges according to VDI/VDE/GESA 2635, Part 1 (2007). The gauge factor k is taken as the mean specified in the product information (TML (2008)).

Table 6-4: Uncertainty model of the strain gauge

Random Variable		Mean	St. dev.	Reference
Gauge factor variation $f_{s,v}$	N	0.00	7.00×10^{-3}	TML (2008), VDI/VDE/GESA 2635, Part 1 (2007)
Model uncertainty of gauge factor variation $f_{s,s}$	R	0.00	4.16×10^{-4}	TML (2008), VDI/VDE/GESA 2635, Part 1 (2007)
Gauge factor k	D	2.12		TML (2008)
Transverse sensitivity q	D	5.00×10^{-4}		Keil (1995)
Specimen Possion Ratio ν	LN	3.00×10^{-1}	9.00×10^{-3}	JCSS (2006)
Poisson's Ratio of gauge calibration beam ν_0	D	2.85×10^{-1}		Keil (1995)
Temperature coefficient of gauge factor α_k in %/10°C	N	0.10	6.99×10^{-2}	TML (2008), VDI/VDE/GESA 2635, Part 1 (2007)
Tolerance of temperature-variation curve ε_T in µm/m	N	0.00	1.19	TML (2008), VDI/VDE/GESA 2635, Part 1 (2007)

N: Normal distribution; LN: Lognormal distribution; R: Rectangular distribution, D: Deterministic

The probabilistic model for the temperature coefficient of the gauge factor α_k and the tolerance of temperature-variation curve ε_T are derived based on the product information and considering VDI/VDE/GESA 2635, Part 1 (2007) assuming also a 95% confidence interval and a sample size of 10 strain gauges.

The transverse sensitivity q and the Poisson's Ratio of gauge calibration beam ν_0 is described with deterministic values according to Keil (1995). The Poisson's Ratio of the specimen ν is modeled according to JCSS (2006), Part 3.02.

The probabilistic model of the zero amplifier deviation $f_{a,z}$ and the amplifying deviation $f_{a,a}$ is assumed to follow a rectangular distribution. This distribution is assigned considering the ISO/IEC Guide 98-3/Suppl.1 (2008b) utilizing the principle of maximum entropy and the product information data (HBM (2008)).

The model uncertainties $\theta_{E_{mech}}$ and $\theta_{\varepsilon_{mech}}$ are added to the amplifier strain and the apparent strain. The distribution of the model uncertainty for this process equation is assumed as a normal distribution with a standard deviation of 1 micro strain. Both facts are analyzed in De Sanctis (2009).

Table 6-5: Uncertainty model of the amplifier

Random Variable		Mean	St. dev.	Reference
Zero deviation $f_{a,z}$ in µm/m	R	0.00	6.93×10^{-1}	ISO/IEC Guide 98-3/Suppl.1 (2008b), HBM (2008)
Amplifying deviation factor $f_{a,a}$	R	1.00	1.73×10^{-4}	ISO/IEC Guide 98-3/Suppl.1 (2008b), HBM (2008)
Model uncertainty $\theta_{E_{mech}}$ in µm/m	N	0.00	1.00	Estimated

N: Normal distribution; R: Rectangular distribution

The parameters in Table 5-2 and Table 6-5 are all uncorrelated since the dependencies are explicitly modeled with the process equations (Equations (6.2), (6.6) and (6.7)).

With the specified measurement equipment, amplifier strain readings for different reference values $\hat{\varepsilon}_R$ were taken under the same conditions as for the experiment. The temperature was kept constant at 20 degrees. For these measurements, a strain, i.e. the reference value, was assumed and the strain gauge was replaced with a very precise resistance. In total 4 different strains from 170 µm/m to 820 µm/m were simulated in this way and 10000 readings of the amplifier strain for each were taken. Each of the data series is modeled as described in Section 6.2.2 leading to the amplifier strain distribution and, since the apparent strain is zero, to the distribution of the measurand, i.e. the mechanical strain. The parameters of the probabilistic model for other reference values than measured are linearly interpolated.

6.5.2.1 Sensitivity analysis

For the quantification of the influences of the individual parameters on the mechanical strain a sensitivity analysis is performed, applying the process equations (Equations (6.2) and (6.6)) and the observation based Equation (6.14). Here, the Spearman rank coefficient of correlation is applied accounting for any biunique functional dependencies.

The sensitivity analysis in regard to the amplifier strain process equation (Equation (6.6)) shows a high correlation of the strain gauge factor variation $f_{s,v}$ for high reference values and for the amplifier zero deviation $f_{a,z}$ for low reference values (Figure 6-2). The model uncertainty of the gauge factor variation $f_{s,s}$ shows a low coefficient correlation which slightly increases with an increasing reference value. The transverse strain correction factor $f_{s,q}$ and the amplifying deviation factor $f_{a,a}$ have practically no correlation with the amplifier strain E_{amp}.

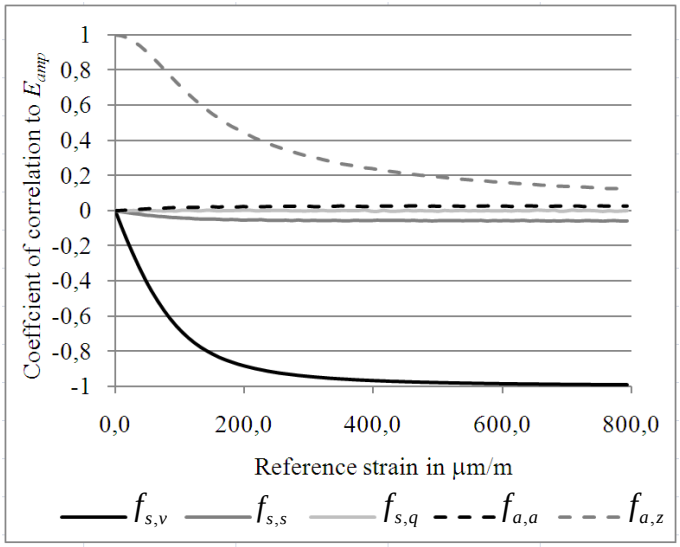

Figure 6-2: Coefficient of amplifier strain correlation applying the process equation

With this sensitivity analysis the random variables of the process equation contributing most to the measurement uncertainty are identified on a quantitative basis.

A further sensitivity analysis is performed for the process equation based mechanical strain E_{mech} and observation based mechanical strain ε_{mech} applying Equations (6.2) and (6.14). The coefficients of correlation of the amplifier strains and the model uncertainties to the mechanical strain are significant for both cases (Figure 6-3).

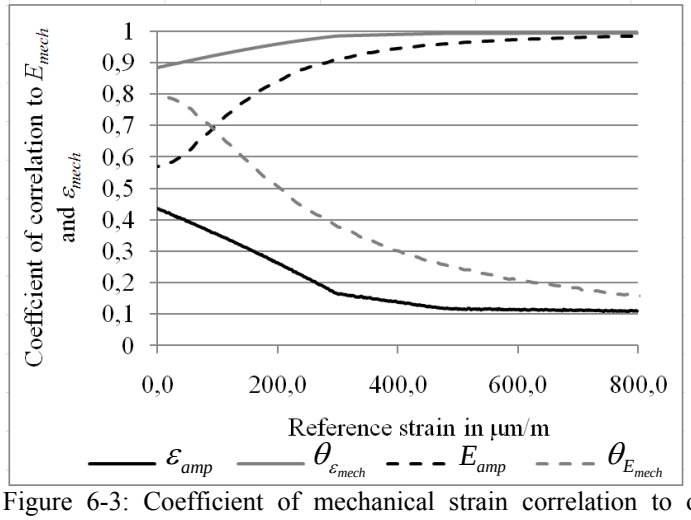

Figure 6-3: Coefficient of mechanical strain correlation to observation and process equation based amplifier strain and model uncertainty applying the measurement equation

The standard deviation of the process equation based amplifier strain E_{amp}, containing the assignment uncertainty, increases with higher reference strains resulting in increasing coefficients of correlation. The standard deviation of the observation based amplifier strain ε_{amp}, however, decreases with higher reference strains leading to decreasing coefficients of correlation.

6.5.3 Derivation and assignment of the measurement uncertainty

All three outlined concepts (Sections 6.2 and 6.3) are applied to determine the measurement uncertainty. For the process equation based measurement uncertainty, the uncertainty associated with the assignment of a probabilistic to a measured strain is modeled as described in Section 6.2.1.1. In Figure 6-4 the probability densities for the mean of the statistical model are depicted. This encloses the prior density (see Equation (6.9), I in Figure 6-4), the likelihood (see Equation (6.11), II in Figure 6-4) and the posterior density (see Equation (6.12), III in Figure 6-4). It is observed, that for a measured strain of 300 µm/m, the likelihood density of the mean is more peaked than the prior density. The likelihood density has a slightly shifted mean. The posterior density, calculated with Bayesian updating, is then orientated closer to the likelihood with a slightly higher density.

The distribution of the mean and the standard deviation of the measurement uncertainty is integrated to calculate the marginal distribution of the process equation based measurement uncertainty applying Equation (6.13).

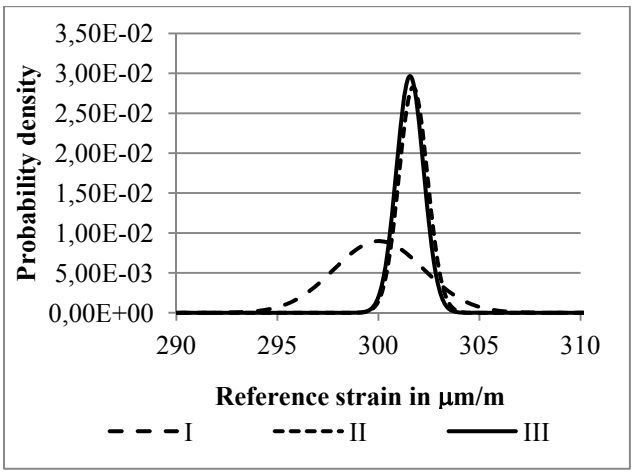

Figure 6-4: Probability densities of the measurement uncertainty mean: I) prior density; II) likelihood density; III) posterior density for a reference value of 300 µm/m (Section 6.2.1.1)

The results for all types of the measurement uncertainty for a reference strain of 400 µm/m are summarized in Figure 6-5. The measurement uncertainty model based on observations (II in Figure 6-5) has smaller standard deviation than the measurement uncertainty model based on the process equation (I in Figure 6-5). Between these standard uncertainties lies the standard deviation of the posterior measurement uncertainty (III in Figure 6-5).

It is further observed that the mean of the observation based measurement uncertainty is shifted to the left accounting for systematic effects of the measurement uncertainty. Due to the Bayesian updating, the mean of the posterior measurement uncertainty (III in Figure 6-5) is situated between the observation based and the process equation based mean, but closer to the observation based mean of the measurement uncertainty. As the densities of the observation based distribution near the mean are higher than for the process equation based distribution, the distribution of the posterior measurement uncertainty is situated closer to the observation based distribution with a slightly higher maximum density.

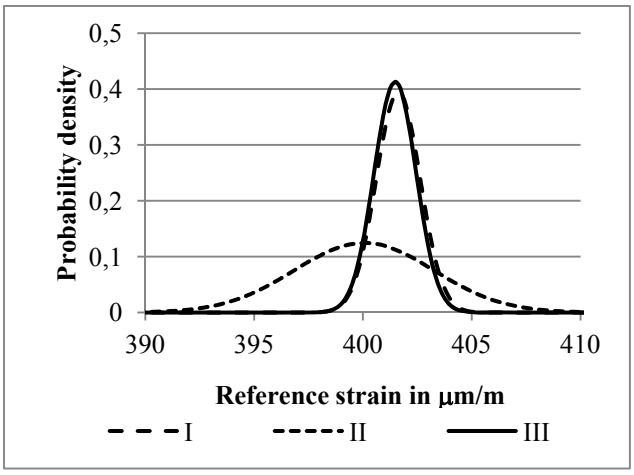

Figure 6-5: Probability densities of the measurement uncertainty based on the process equation (I, Section 6.2.2), based on observations (II, Section 6.2.1) and with the new concept (III, Section 6.3) for a reference value of 400 μm/m

The standard uncertainties reflect the boundary character of the process equation based (upper boundary) and the observation based measurement uncertainty (lower boundary) as outlined in Sections 6.2 and 6.3. This boundary character also applies to the means of the distribution as it reflects the systematic errors identified with the process equation and the observations.

6.5.4 Fatigue reliability

The fatigue reliability of the detail is calculated first as designed and then based upon the assumptions of the measured strains with consideration of the all the three concepts of the measurement uncertainty.

The probability of failure for the detail as designed is calculated utilizing Equation (6.19) for the calculation of the stress ranges and then the limit state model (Equation (6.25)). With these assumptions a fatigue reliability of 4.90×10^{-3} is calculated for the detail (Figure 6-6 (IV)).

For the calculation of the fatigue reliability with consideration of the measurement uncertainty, the predetermined probabilistic models are assigning to each of the individual measurements. By sampling from these probabilistic models the samples of the strain time series are generated. With these samples of the time series and the mechanical model (Equation (6.20)), the hot spot stress range distributions are

computed. The limit state model (Equation (6.25)) is then used with to calculated the probability of fatigue failure.

The probability of failure for the example is calculated with a Latin Hypercube Monte Carlo method. The sample size was chosen to achieve a standard deviation of the failure probability lower than 1%.

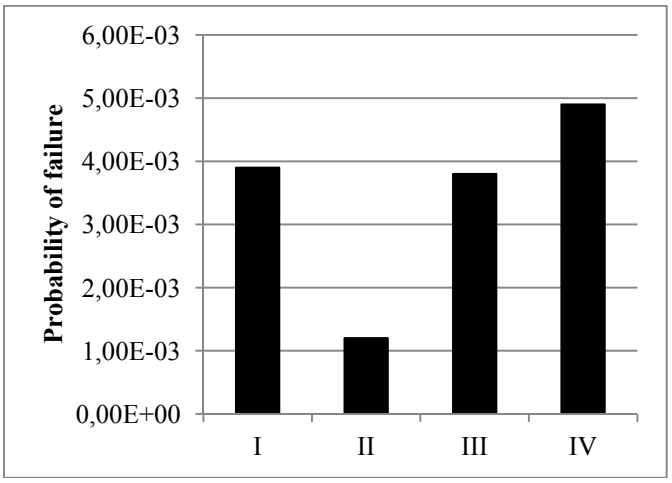

Figure 6-6: Probabilities of failure: with measurement uncertainties based on observations (I, Section 6.2.2); with measurement uncertainties based on process equation (II, Section 6.2.1) and with the new concept (III, Section 6.3). For comparison the probability of failure of the design of the detail is shown (IV).

The probabilities of failure of the detail considering the different types of measurement uncertainties are shown in Figure 6-6. It is observed that the probabilities of failure applying the observation based measurement uncertainty (column I in Figure 6-6) and the posterior measurement uncertainty (column III in Figure 6-6) are higher than the probability of failure applying the process equation based measurement uncertainty (column II in Figure 6-6). On the first sight this might be contradictory since the standard deviation of the process equation based measurement uncertainty is significantly higher. However, this can be explained by the shift of the observation based and the posterior measurement uncertainty (see Figure 6-5) leading to slightly higher stress ranges which are then exponentiated for the damage calculation (Equation (6.25)).

It is further observed, that the probabilities of failure applying the observation based measurement uncertainty (column I in Figure 6-6) and the posterior measurement uncertainty (column III in Figure 6-6) have nearly the same value. The reason for this is here, that the observation based measurement uncertainty and the posterior measurement uncertainty are very similar and have almost the same shift (because of the dominance of the likelihood due to the small uncertainties in the derivation of the posterior measurement uncertainty).

The probabilities of failure based on the measured strains are significantly lower in comparison to the design probability of failure (column IV in Figure 6-6). The difference in the probability of failure originates from the different structural and loading models (Equation (6.19) and Equations (6.20), (6.21)) and the associated probabilistic models. This can be concluded because of the fact that the measured stress ranges and the design stress ranges are adjusted to follow the same distribution and possess the same damage equivalent stress (see Equations (6.23) and (6.22)). For the calculation of the design stress ranges two model uncertainties are considered (stress calculation and hot spot stress calculation) whereas for the calculation of the measured stress ranges one model uncertainty and the measurement uncertainties are considered.

6.6 Summary and Conclusions

A framework for the determination of measurement uncertainties is introduced building upon the successor documents of the Guide for the Expression of Uncertainty, namely the ISO/IEC Guide 98-3 (2008a) and ISO/IEC Guide 98-3/Suppl.1 (2008b). This framework, which is elaborated on the example of strain measurements, accounts explicitly for the assignment uncertainty of a probabilistic model to a measurement value and for model uncertainties.

A new type of measurement uncertainty, the posterior measurement uncertainty, is derived by Bayesian updating. Both, the prior and the likelihood are informative distributions as the prior measurement uncertainty is associated with prior knowledge about the measurement process, i.e. with a process equation and an associated uncertainty model. The likelihood is associated with probabilistic models of observations. This approach facilitates to use all information of the measurement process which comprises the theoretical knowledge of the process including the physical and probabilistic nature as well as the observations of the process.

It is suggested to use the framework for the determination of measurement uncertainties for the further development of the ISO/IEC Guide 98-3 (2008a) as the concept is based on a Bayesian definition of probability and this is a possible direction for further development seen by the Joint Committee for Guides in Metrology (Bich (2008)).

A typical engineering situation which involves the fatigue reliability of detail based on the design process and the reassessment with the help of measurement data was chosen as a generic example and illustrates the application of the developed framework. As herewith a further source of uncertainty for the structural reliability framework of the JCSS has been identified, it is thus suggested to extend the framework of the Probabilistic Mode Code (JCSS (2006)) to measurement uncertainties.

The calculation of the fatigue reliability for the design and with measurement data for assessment is performed consequently with different approaches and probabilistic models. It has been specifically demonstrated that the reliability calculated with the measurement data can be higher than with the design data taking basis in the same distribution of the stress ranges.

The generic fatigue reliability analysis has shown that the consideration of measurement uncertainties is significant for the reliability analysis because of the fact that it is also significant for the calculation of the stress ranges with the Rainflow algorithm. Further, it can be concluded that the bias and standard deviation of the measurement uncertainty can influence the fatigue reliability.

The measurement uncertainties were determined and a sensitivity analysis of the involved models was performed. With the results of this sensitivity analysis, a monitoring system can be designed for a minimum measurement uncertainty as the probabilistic models of the random variables are directly linked to product specification data. The model uncertainties introduced for calculating the measurement uncertainties can have a significant sensitivity as it is the case for the observations based measurement uncertainty. Because of this situation the model uncertainties of the utilized models should be further investigated.

With this chapter the first step has been taken towards the application of the developed framework to in situ measurement systems and to further measurement technologies for monitoring structural systems. The chapter focuses on the comparison of the reliabilities calculated with the design models and data as well as with monitoring models and data to illustrate the characteristics of the models. However, for specific application purposes, updating of the probabilistic design models with the probabilistic models of the monitoring data can be the next step for the further development.

7 Structural integrity management utilizing the developed concepts

The purpose of this chapter is to illustrate the application of the developed methods for the management of the structural integrity, i.e. in the context of a life cycle cost benefit analysis.

Structural integrity management requires information on the state of structures. Monitoring, whether it is performed continuously or at discrete point in time, provides measurement data which can be utilized to update probabilistic models of the performance of structures.

The approaches elaborated in the following specifically address the field of structural reliability which is characterized by very low probabilities of failure, little or no available relevant data concerning failure rates and by very specific failure mechanisms. The application of the methods of structural reliability, in contrast to classical reliability analysis, necessitate the development and application of probabilistic models for the structural performance, the loading and the limit states defining structural performance which are associated with consequences. The classical reliability theory is based upon statistical data of the behaviour of technical systems and their characteristics include the expected failure rate, the expected life and the mean time between failures.

To illustrate the contrast to the classical reliability this chapter starts out with damage detection procedures as they are understood to originate from classical reliability theory. A description of methods for utilization of monitoring data in reliability analysis then follows comprising two concepts for the ultimate limit state reliability analysis as well as a discussion of the serviceability limit state. The concepts are illustrated with generic examples. The discussion of the serviceability limit state refers to the reference case: a support structure of an offshore wind turbine.

With a life-cycle cost-benefit analyses it is shown how to apply the Bayesian pre-posterior decision theory for the design of a monitoring system and how to achieve a benefit for the expected life-cycle costs.

7.1 Damage detection procedures

Damage detection procedures aim directly at the identification and localization of structural damages. Such methods are usually referred to as structural health monitoring (SHM). Structural health monitoring focuses on the detection of changes in the static and dynamic structural performance caused by damages. At the algorithmic level an inverse problem is solved using modal information as well as directly forced and/or ambient vibrations in the time and frequency domains (e.g. Fritzen and Kraemer (2009) and Basseville, Mevel et al. (2004)).

The efficiency of the approaches and technical systems for damage detection is an important factor in structural health monitoring. The most common approach for assessing the efficiency is through the conditional probability of damage given an indication $P(D|I)$. If the damage detection system is efficient this probability is close to one. Of course the efficiency also depends on the costs of the system, however, this

issues is set aside in the following. The conditional probability of damage given an indication of damage may be taken as a basis for formulating quality criteria to monitoring systems. It can easily be calculated using rule of Bayes (Equation (7.1)). This probability then depends on the prior probability of damage $P(D)$ and on the probabilities of indication for both the situations of damage and no damage, i.e. $P(I \mid D)$ and $P(I \mid \bar{D})$.

$$P(D \mid I) = \frac{P(I \mid D)P(D)}{P(I \mid D)P(D) + P(I \mid \bar{D})P(\bar{D})} \tag{7.1}$$

Structural health monitoring systems work well, where a significant probability for a defect exists (see e.g. Visser Consultancy Limited (2000)). However, a problem arises when a monitoring system is used for the detection of damages and failures in building structures as in these cases very often the probability of damage is rather low. In such cases, in order to achieve a reasonable probability of damage given an indication, a very low probability of indication given no damage is thus necessary. To determine such probabilities, however, for a damage detection system on the basis of frequentistic information, as this is the common approach in quality assurance, becomes a rather non-trivial task. This can be illustrated with help of generic assumptions for the probabilities in Equation (7.1). It is assumed that damage occurs with a probability of $P(D) = 1.00 \cdot 10^{-3}$ and that the damage detection system indicates this with a probability of $P(I \mid D) = 0.95$. To achieve now a probability of damage given an indication of $P(D \mid I) = 0.90$ a very low probability of indication given no damage of $P(I \mid \bar{D}) = 1.00 \cdot 10^{-4}$ is required. This is a very low probability and is hardly determinable with a quality assurance procedure implying a frequentistic basis. A further remedy is that this probability cannot directly be utilized for the structural reliability.

A workaround, if this straightforward calculus is to be applied, is to calculate the probability of damage given no indication ($P(D \mid \bar{I})$, Equation (7.2)) as this represents the general approach in risk based inspection planning (originally by Madsen, Skjong et al. (1987)). The probability of damage given no indication can additionally be utilized e.g. in a risk analysis for a structure which is equipped with a damage detection system. This approach is of a general character because the probabilistic models for the structural performance; the loading and the limit states are not directly addressed as it is the case for the risk based inspection planning.

$$P(D \mid \bar{I}) = \frac{P(\bar{I} \mid D)P(D)}{P(\bar{I} \mid D)P(D) + P(\bar{I} \mid \bar{D})P(\bar{D})} \tag{7.2}$$

Equation (7.2) is evaluated taking basis in the above example, i.e. with $P(D) = 1.00 \cdot 10^{-3}$ and assuming the damage detection system indicates no damage given no damage with a probability of $P(\bar{I} \mid \bar{D}) = 0.95$ and no damage given damage with a probability of $P(\bar{I} \mid D) = 0.10$. This leads to a probability of damage given no indication of $P(D \mid \bar{I}) = 1.05 \cdot 10^{-4}$.

The probability of damage given no indication shows, on the basis of generic probabilities, that the information of no indication can be utilized to substantially reduce the probability of damage. Another important aspect is that the quality criteria

associated with the monitoring system are reformulated. These quality criteria are defined as the probability of no indication given damage ($P(\bar{I} \mid D)$) and given no damage ($P(\bar{I} \mid \bar{D})$). The approach of Equation (7.2) then facilitates that the probabilities can be determined on frequentistic basis within a quality assurance process.

It is suggested to apply the introduced concept as a general approach for the utilization of structural health monitoring information for the structural reliability. Then the introduced concept can be further developed and the structural health monitoring information should be explicitly connected to the structural reliability theory as this is the case for the inspection system information in the framework of the risk based inspection planning.

However, the focus of this thesis is on monitoring systems and thus the utilization of such systems within the framework of structural reliability methods is addressed in more depth in the following.

7.2 Ultimate limit state reliability analysis and monitoring

In this section the framework for the determination of measurement uncertainties is applied to structural reliability theory through observations of performance characteristics considering the ultimate limit state. The first approach described, is to interpret monitoring data as loading data of a component. The second approach interprets monitoring data as proof loading data and thus associates these data to the resistance model. The characteristics of the specific models involved are described and the effect of these on the probability of failure is shown on an exemplary basis.

7.2.1 Monitoring data as a probabilistic loading model

Monitoring data provide e.g. strains at a component of a structural system. A straight forward approach is to consider the monitoring data as loading model information for a structural reliability analysis. This approach is discussed here on the basis of an example.

The example regards the ultimate limit state taking basis in the buckling reliability model (e.g. Thöns, Faber et al. (2010)) and the structural reliability is calculated "as designed" (with design information) and "as measured" (with monitoring information). Thereby the probabilistic models are adjusted to account for comparability of the structural reliabilities. The structural reliabilities utilizing design and monitoring information illustrate effects caused by the different modelling.

A steel cylinder is assumed to be designed and consecutively monitored with strain gauges. It has a length of 10 m, a radius $r = 2.00$ m and a wall thickness of $t = 20.00$ mm. The cylinder is loaded in axial direction with the force F.

For the design of this cylinder, the equivalent membrane stress $\sigma_{EQ,des}$, as required for the reliability calculation (Equation (7.8)), is calculated by Equation (7.3) where B denotes the model uncertainty of this mechanical model.

$$\sigma_{EQ,des} = B \cdot \frac{F}{2\pi r t} \tag{7.3}$$

It is further assumed that monitoring provides the measured strain ε. This strain (in μm/m) refers to the maximum of the daily time intervals with a reference period of one year and follows a Weibull distribution with the scale and shape parameters equal to

450.0 and 2.0, respectively. Above a threshold of 800 µm/m the measured strain follows a Generalized Pareto distribution with a shape parameter of -0.11 and scale parameter of 84.11. The measured equivalent membrane stress $\sigma_{EQ,meas}$ is directly calculated with the modulus of elasticity E and the strain containing the measurement uncertainties ε^M (Equation (7.4)) for a one dimensional stress state.

$$\sigma_{EQ,meas} = E \cdot \varepsilon^M \tag{7.4}$$

The strain containing the measurement uncertainties ε^M is derived based on Thöns, De Sanctis et al. (2010). For each of the strain data – as the measurement uncertainty is dependent on the measured strain itself (Equation (7.5) with index i referencing a measurement datum) - the distribution of the posterior measurement uncertainty $u_i''(\varepsilon_i)$ is calculated. This measurement uncertainty contains the assignment uncertainty of a probabilistic model to the measurement data (see Section 6.2.1.1) and the posterior measurement uncertainty (see Section 6.3) which is derived on the basis of the process equation and is then updated with the observation based measurement uncertainty. The measurement uncertainties are added to the individual strain data and the marginal distribution of the strain containing the measurement uncertainty ε^M is derived (Equation (7.6)).

$$u_i''(\varepsilon_i) \sim N_i(\mu_i, \sigma_i) \tag{7.5}$$

$$f(\varepsilon^M) = \int_{-\infty}^{+\infty} f(\varepsilon \mid u''(\varepsilon)) \cdot f(u''(\varepsilon)) du'' \tag{7.6}$$

To account for the comparability of the calculated probabilities of failure for the design and for the monitoring, it is assumed that the distribution of the axial force follows the distribution of the measured strain multiplied by the mean of the modulus of elasticity E and the cross sectional area (Equation (7.7)).

$$F \sim Dist(\varepsilon \cdot E \cdot 2\pi rt) \tag{7.7}$$

The probabilistic models for the determination of the equivalent membrane stress are summarized in Table 7-1 as described and on the basis of the Probabilistic Model Code (JCSS (2006)).

Table 7-1: Probabilistic model for the determination of the membrane equivalent stress

Random Variable		Scale par.	Shape par.	
Measured strain ε	WB	450	2.0	≤ 800 µm/m
	GP	-0.11	84.11	> 800 µm/m
Random Variable		Mean	St. dev.	
Modulus of elasticity E (N/mm²)	LN	2.10×10^5	6.30×10^3	JCSS (2006)
Model uncertainty for stress calculation B	LN	1.000	0.050	JCSS (2006)

GP: Generalized Pareto distribution; LN: Lognormal distribution ; WB: Weibull distribution

The limit state function (Equation (7.8)) for buckling of the cylinder contains the plastic reference resistance R_{Pl}, the buckling reduction factor χ_{ov} and the buckling model uncertainty $f_{M,B}$. This limit state model is described in detail in Thöns, Faber et al. (2010) which is here abbreviated.

$$g_B = f_{M,B}\chi_{ov}R_{Pl} - 1 = f_{M,B}\chi_{ov}\frac{f_y}{\sigma_{EQ}} - 1 \tag{7.8}$$

The probabilistic models (Table 7-2) associated with this limit state model consist of a Lognormal distribution for the random variable yield stress f_y (JCSS (2006)) and a normal distribution for the buckling model uncertainty, see Thöns, Faber et al. (2010).

Table 7-2: Probabilistic model for the limit state model

Random Variable		Mean	St. dev.	
Yield strength f_y (N/mm²)	LN	370.0	24.2	JCSS (2006)
Buckling model uncertainty $f_{M,B}$	N	1.06	0.076	Thöns, Faber et al. (2010)

N : Normal distribution ; LN: Lognormal distribution

With the models described, a probability of failure of $8.79\text{x}10^{-4}$ is calculated with design models and a probability of failure of $7.58\text{x}10^{-4}$ based on the monitoring data and models. The difference of the probability of failure is caused by the different models to determine the distribution of the membrane equivalent stress. As here exemplarily shown, the design case involves a more complex structural model (Equation (7.3)) which results due to the model uncertainties in higher uncertainties of the membrane equivalent stress than for the case where monitoring data and models are applied (Equation (7.4)), despite the additional measurement uncertainties.

7.2.2 Proof loading utilizing monitoring data

The interpretation of monitoring data as proof loading facilitates an alternative utilization of monitoring information for the structural reliability analysis. Here, the resistance model is modified with the information the monitoring data provide. A new concept is introduced starting with a discussion of previous approaches and the characteristics of proof loading. Further this new concept is applied to the reliability analysis of an axially loaded steel cylinder; the example of the last section. The effect of the monitoring data, i.e. the proof loading information, on the structural reliability in conjunction with the framework for the determination of measurement uncertainties is illustrated with a parameter study. Finally, a criterion for the application of an alternative concept is introduced.

7.2.2.1 Derivation of the concept

An early approach for considering proof loading within a reliability analysis was described by Shan and Nowak (1984). It was suggested to truncate the density distribution of the resistance model at the proof loading level to integrate a deterministic proof loading information in the reliability analysis. This method has then be cited by various authors, e.g. Faber, Val et al. (2000) and JCSS (2001).

In Nishijima and Faber (2007) it is suggested to apply Bayesian updating to this problem implying that the proof loading has a probabilistic characteristic. The approach is to update the parameters of the resistance distribution with the parameters of the proof loading distribution. Further, an approach to exploit the system reliability information to determine the number of proof loading tests in the framework of pre-posterior decision theory is presented.

Historically, proof loading is either conducted as a field experiment, e.g. when a bridge is tested with defined weights, or as a laboratory experiment, when the structure to assess consists e.g. of many components. In both cases the loading and the strains of the components are measured and in this way the condition of the tested structure is monitored. As this process involves measurements, the measurement uncertainty should be explicitly accounted for. Hence, the concept introduced by Thöns, De Sanctis et al. (2010) can be used to determine the measurement uncertainty as this facilitates the determination of the parameters of the probabilistic model for all measurement data.

It is important to note that proof loading involves a specific loading situation and thus not necessarily represent all load cases of the ultimate limit state or the ultimate capacity. However, for the specific loading situation it delivers valuable information of the resistance of the structure usually near the characteristic level of the resistance and this information is usually associated with rather low uncertainties.

Based on the consideration above, a new truncation concept is suggested namely the probabilistic truncation of the resistance model, taking basis in the fact that we have a probabilistic proof loading information due to the measurement uncertainties. The probabilistic truncation of the resistance model is seen as being compatible with the characteristics of the proof loading, i.e. that proof loading delivers additional information beside the resistance model. In contrast, if Bayesian updating is applied to this situation, it would usually result in the dominance of the proof loading information because this is the information with the higher likelihood and would thus result in almost a replacement of the resistance model.

The approach to truncate the probabilistic model of the resistance with the probabilistic model of the proof loading is illustrated in Figure 7-1. Here, the density of the resistance distribution f_R is replaced below the level l with the density of the proof loading distribution f_{PL}. The resulting density function is then adjusted accounting for the reduction of the area below this curve leading to the truncated density function f_R^T.

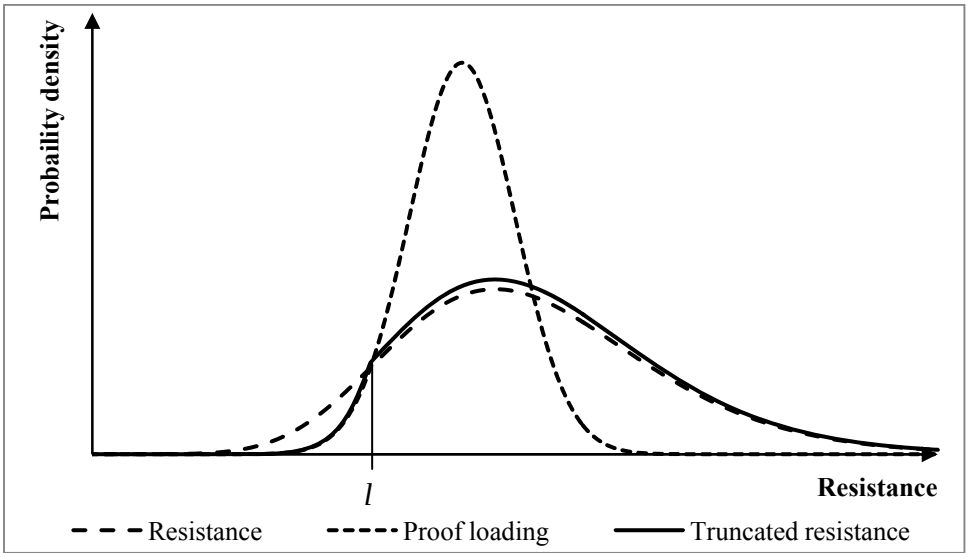

Figure 7-1: Approach for probabilistic truncating the resistance model

The mathematical formulation of this concept is expressed with Equation (7.9) and the position of the level l is determined according to Equation (7.10).

$$f_R^T(x) = \begin{cases} f_R(x) / \left(1 - F_R(l) + F_{PL}(l)\right) & for \quad x > l \\ f_{PL}(x) / \left(1 - F_R(l) + F_{PL}(l)\right) & for \quad x \le l \end{cases} \tag{7.9}$$

$$f_{PL}(l) = f_R(l) \ \wedge \ l \le \mu_{PL} \tag{7.10}$$

The modified resistance distribution for the reliability analysis is then applied in a typical limit state function with the resistance distribution R and the loading distribution S (Equation (7.11)).

$$g(\underline{x}) = R - S \tag{7.11}$$

7.2.2.2 Application of the concept to the shell buckling limit state function

The formulation of the shell buckling limit state function (Equation (7.12)) is different from the general concept and requires some additional thoughts. For including the proof loading information in this concept, it is suggested to truncate the distribution of the term $f_{M,B}\chi_{ov}f_y$ as this represents the resistance consisting of the random variables buckling model uncertainty $f_{M,B}$, the buckling reduction factor χ_{ov} and the yield stress f_y.

$$g_B = f_{M,B}\chi_{ov}R_{Pl} - 1 = f_{M,B}\chi_{ov}\frac{f_y}{\sigma_{EQ}} - 1 \tag{7.12}$$

Coming back to the example from Section 7.2.1 a parameter study is performed. Here the design reliability calculation serves as a basis for the modification of the resistance model with proof loading information. The proof loading event constitutes here a monitored extreme loading event a structure has experienced and survived.

It is assumed that the uncertainty of a proof load event follows a normal distribution in accordance with the concept for the determination of the measurement uncertainties

(Thöns, De Sanctis et al. (2010)). To estimate the effect on the probability of failure (originally 8.79×10^{-4}, see Section 7.2.1) the mean and the standard deviation of the normal distribution of the force F are varied.

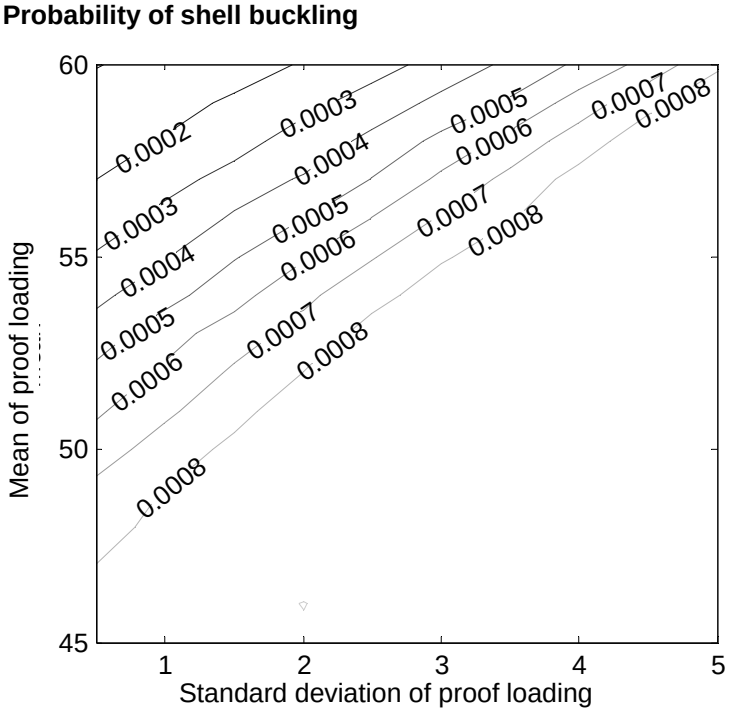

Figure 7-2: Probability of failure dependent on the standard deviation and the mean of the proof loading

It can be seen that high loading levels, i.e. high means of the proof load, as well as low standard deviations have a significant effect on the probability of failure (Figure 7-2). In this example the minimum probability of failure is calculated to 9.7×10^{-5} for a standard deviation of 0.5 and a mean of 60 the force F.

This example illustrates that these results can serve as an information in regard to which loading event can be utilized as a proof loading event; the modification of the resistance model leads to a higher reliability of the monitored component.

7.2.2.3 Bayesian updating versus truncating the resistance model

The approach elaborated here for proof loading is based on the modification of the resistance model, specifically on the probabilistic truncation of the resistance model. This is consistent with the approach of determining the measurement uncertainties (Thöns, De Sanctis et al. (2010)) and can be seen as further development of the approach to truncate the resistance model with a deterministic model as e.g. in JCSS (2001).

Clearly a Bayesian updating of the (prior) resistance information with the (likely) resistance information by proof loading is an alternative approach as e.g. introduced by Nishijima and Faber (2007). This alternative approach necessitates the development of a criterion for the application of these concepts.

As a criterion it is suggested to consider the boundaries of the probabilistic proof loading information and thus to differentiate complete resistance model information and incomplete resistance model information. Complete resistance model information in the context of proof loading is defined as comprehensive ultimate capacity data of statistical significance. These data can then be used to derive a statistical model with reasonably low statistical uncertainties. All other information about the resistance model, e.g. when only a survival of the tested components is observed, are defined as incomplete resistance model information.

It is suggested to apply the Bayesian updating of the resistance model (e.g. Nishijima and Faber (2007)) to complete the resistance model information. Consequently, the probabilistic truncation of the resistance model as developed here should be applied for the case of incomplete resistance model information.

7.3 Serviceability limit state reliability analysis and monitoring

The serviceability limit state comprises all mechanisms which might lead to a limited functionality of the support structure and thus of the wind turbine operation. Most significant for the operation is that the natural frequencies of the support structure, the nacelle and the rotor do not coincide with the varying excitation frequencies of the machinery and of the rotor evolutions as well as of the blade passing frequency. This is accounted for in the complex design process by the criteria that the natural frequencies of the support should be situated within an envelope of ±5% within the envisaged natural frequencies (Thöns, Faber et al. (2010)).

The probability of unserviceability for the reference case is found to be significant (Thöns, Faber et al. (2010)), mainly dependent on the uncertainties of the foundation stiffness as this was confirmed with a sensitivity analysis.

Applying monitoring techniques, the determination of the natural frequencies is usually performed with an experimental modal analysis which principally transforms velocity, acceleration or strain time series with a Fourier transformation into a frequency spectrum. Such procedures are usually robust against measurement uncertainties as this was confirmed with a study applying the Fourier transformation and the framework for the determination of measurement uncertainties to various time series of measurement data.

Applying the experimental modal analysis, the first natural frequencies can be determined with low uncertainties (e.g. Rohrmann, Thöns et al. (2010), BAM (2009)) which consequently leads to a significant drop of the probability of unserviceability. This results then for the reference case in a negligible probability of unserviceability.

7.4 Life-cycle cost-benefit optimization applying monitoring systems

In the Sections 6.5, 7.2 and 7.3 it is discussed and exemplarily quantified how monitoring data can be utilized to contribute to the structural reliability and thus to the reduction of the associated risks. But can monitoring furthermore be utilized for a reduction of the expected life-cycle costs?

The answer to this question is the aim of this section. Therefore, approaches for a life-cycle cost-benefit analysis are introduced and the relations to the design of monitoring

systems and to monitoring data are investigated on the basis of the Bayesian pre-posterior decision analysis. This section starts with a discussion and a formulation of generic decisions associated with the application of monitoring techniques. Subsequently, the approach for the life-cycle cost-benefit analysis is introduced based on Straub (2004) and is extended to account for the costs of a monitoring system. An optimization problem is then formulated and the approach is applied to the reference case for the determination of the generic decisions associated with monitoring. Simultaneously, the findings on the effect of monitoring data (as described in Sections 6.5.4) are utilized. The expected life-cycle costs are then quantified leading to the optimal decisions parameters and a reduction of the expected life-cycle costs.

7.4.1 Generic monitoring decisions and the life-cycle cost-benefit analysis

Based upon the failure mechanisms, the application of a monitoring system involves basically two decisions namely; which components to monitor and when to monitor. These generic decisions can formally written with Equations (7.13) and (7.14) where D denotes the decision set consisting of n different component sets c_{Si} and the decision set T containing monitoring periods t_{Mi} within the service life t_{SL}.

$$D = \{c_{S1}, c_{S2}, \ldots, c_{Sn}\}, \tag{7.13}$$

$$T = \{t_{M1}, t_{M2}, \ldots, t_{SL}\}, \tag{7.14}$$

A life-cycle cost-benefit analysis for the structural integrity management of a steel structure involves inspection, repair and failure costs (Figure 7-3). The net present total expected life-cycle costs can then be determined depending of the yearly probability of failure threshold. This approach is shortly described here based upon Straub (2004).

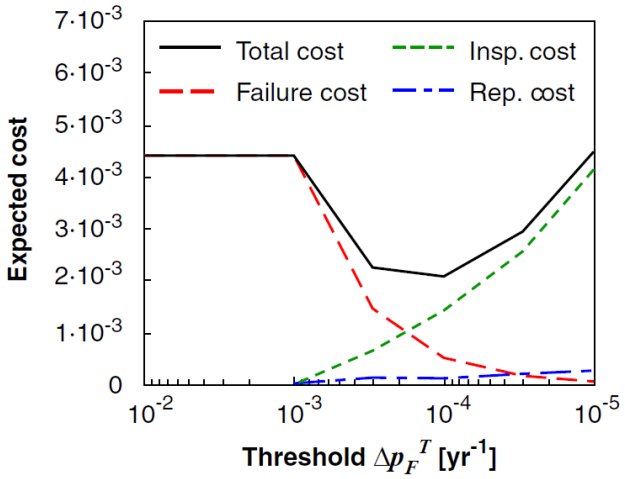

Figure 7-3: Life-cycle cost-benefit analysis in dependency of the yearly probability of failure threshold (Straub (2004)).

Such a life-cycle cost-benefit analysis involves various probabilistic and deterministic models such as degradation models, inspection models, repair models and a decision tree model applicable during the whole service life of the structure (Figure 7-4). These models and their dependencies are described in detail in Straub (2004).

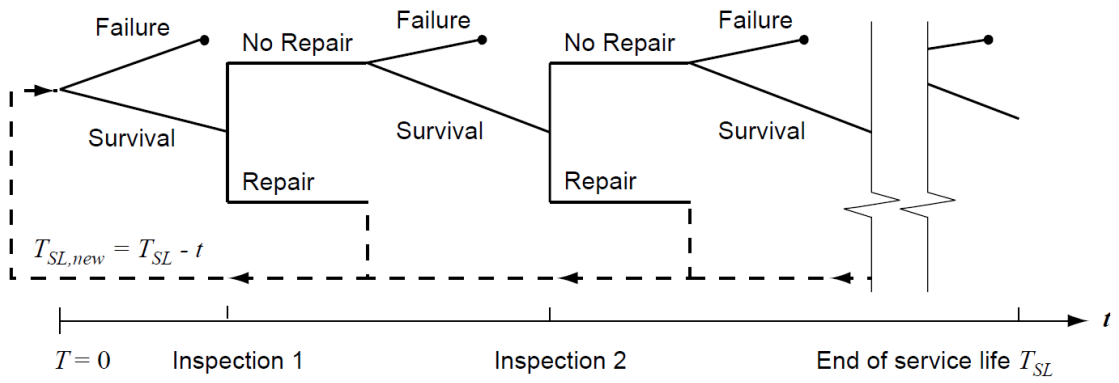

Figure 7-4: Risk based inspection decision tree (Straub (2004)).

With the decision tree the probabilities of no failure, failure and repair are determined for each service year. With these probabilities and a cost model the expected total costs are determined. An important characteristic of the decision tree is the assumption of the simplification rule which is associated with the behavior of a repaired element. The underlying assumption in Figure 7-4 is that a repaired component behaves like a new component (Straub (2004)).

The expected life-cycle costs for a steel support structure are dependent on the model for fatigue degradation, where usually the stress range information of the structural design is utilized. The fatigue limit state model then consists of fracture mechanics model which is calibrated to an SN model to facilitate the updating of the probability of failure with inspection information and information about the inspection system (e.g. Straub (2004)).

The monitoring data enable to determine the equivalent stress ranges, of course, accounting for the measurement uncertainties. As usually predetermined inspection plans are derived based on either no findings or complete repair of the damages such information enable to revise the inspection planning utilizing the monitoring information.

It has been demonstrated in Thöns, De Sanctis et al. (2010) that the application of monitoring data can substantially increase the fatigue reliability with a constant fatigue loading caused by a modification of the probabilistic models for the determination of the stress cycle uncertainties. In the following it is assumed that the increase of the fatigue reliability can be expressed with an elongation of the fatigue life as the determination of the inspection plans is based upon the fatigue reliability, i.e. specifically on the yearly probability of failure.

7.4.2 Life-cycle cost-benefit approach considering monitoring systems

The cost-benefit analysis presented here, builds upon the approach and database results documented in Straub (2004). Here, the expected value of the life-cycle costs per component $E\left[C_T(\ )\right]$ is the sum of the expected value of failure costs $E\left[C_F(\ )\right]$, the inspection costs $E\left[C_I(\ )\right]$ and the repair costs $E\left[C_R(\ )\right]$ (Equation (7.15)). The

dependency on the parameters like the inspection parameters, the repair policy and the service life is suppressed here for clarity.

$$E\left[C_T(\ )\right]=E\left[C_F(\ )\right]+E\left[C_I(\ )\right]+E\left[C_R(\ )\right] \tag{7.15}$$

The approach is to calculate the expected life-cycle costs applying a monitoring system and then to subtracted these expected costs from the original expected life-cycle costs (Equation (7.16)) to calculate the expected monitoring benefit $E\left[B_M(\ )\right]$. The expected value of the life-cycle costs applying a monitoring system are denoted with $E\left[C_T^M(\ )\right]$ and the monitoring costs with $E\left[C_M(\ )\right]$.

$$E\left[B_M(\ )\right]=E\left[C_T(\ )\right]-E\left[C_T^M(\ )\right]-E\left[C_M(\ )\right] \tag{7.16}$$

The expected value of the monitoring costs $E\left[C_M(\ )\right]$ is calculated with the channel (k) dependent, i.e. number of sensor dependent, costs of the system $C_{Sys}^M(k)$ and of the installation $C_{Inst}^M(k)$ as well as the costs of the monitoring system operation C_{Op}^M. The operation costs are discounted to the present value dependent on the time of cash flow t and are multiplied by the probability of no failure $(1-p_F)$.

$$E\left[C_M(\ )\right]=C_{Sys}^M(k)+C_{Inst}^M(k)+(1-p_F)\cdot C_{Op}^M\cdot\frac{1}{(1-i_r)^t} \tag{7.17}$$

7.4.3 Life-cycle cost-benefit analysis for the reference case

The cost-benefit analysis model introduced in the preceding section is now applied to the reference case which constitutes a support structure of a prototype offshore wind turbine (Thöns, Faber et al. (2010)). The documented probabilities of failure of the components in the fatigue limit state (Thöns, Faber et al. (2010)) in relation to their fatigue life (Figure 7-5) are applied for this analysis.

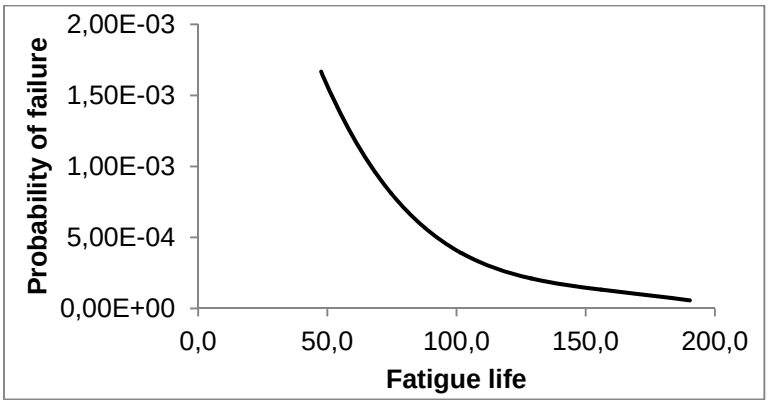

Figure 7-5: Probability of failure vs. fatigue life for the reference case

To determine the expected monitoring benefit the documentation of the generic database in Straub (2004) is applied for each of the hot spots of the support structure considered in Thöns, Faber et al. (2010). The cost model consists of failure costs $C_F=1$, inspection costs $C_I=10^{-3}$ and repair costs $C_R=10^{-2}$ per component and an interest rate of $i_r=5\%$ which represent generic assumptions (Straub (2004)).

In relation to this cost model, a monitoring cost model for the reference case is introduced. The costs of the monitoring system are assumed to $C_{Sys}^M(k)=1.33\cdot10^{-4}$ per

channel, where three channels (i.e. sensors) are associated with the monitoring of one hot spot. The costs of installation are assumed to $C_{Inst}^{M}(k) = 1.33 \cdot 10^{-4}$ per channel and the operation costs are assumed to $C_{Op}^{M} = 6.67 \cdot 10^{-4}$ per year. As an example for the cost model the reference case is considered assuming generic costs of 1,500,000 € per Megawatt (European Wind Energy Association (EWEA) (2009b)). The resulting costs for the reference case are summarized in Table 7-3; the analysis is performed with the normalized cost model as described. Further, a yearly probability of failure threshold of $1.00\text{x}10^{-3}$ and of $1.00\text{x}10^{-4}$ is considered as it encloses the minimum of the expected life-cycle costs for one component (see Figure 7-3).

Table 7-3: Example of the cost model associated with the reference case

Type of costs	Value
Failure costs C_F	7,500,000 €
Inspection costs per component C_I	7,500 €
Repair costs per component C_R	75,000 €
Costs of monitoring system per channel $C_{Sys}^{M}(k)$	1,000 €/k
Costs of system installation per channel $C_{Inst}^{M}(k)$	1,000 €/k
Cost of system operation per year C_{Op}^{M}	5,000 €/a

For this study the monitored component set c_S, i.e. the monitored hot spot locations, and the fatigue life factor (FLF) are varied. The fatigue life factor is defined as the ratio of the fatigue life applying monitoring data to the original (designed) fatigue life. It represents here the probability of failure reduction due to the application of monitoring techniques (see Section 6.5) and is varied between 1.05 and 1.50. The monitoring period is assumed to be equal to the service life of the support structure.

The monitored component sets, i.e. the monitored hot spot locations, are determined on the basis of the probabilities of failures starting with the highest probability of failure. Assuming that the probability of failure can then be reduced (e.g. Thöns, De Sanctis et al. (2010)) it is obvious that this scheme also leads to a reduction of the system probability of failure for a series system.

Equation (7.16) is now rewritten into an optimization problem where the expected benefit is to be maximized in dependency of the monitored component set and the fatigue life factor.

$$E\left[B_M\left(c_S, FLF\right)\right] = \\ = \arg\max\left(E\left[C_T\left(c_S, FLF\right)\right] - E\left[C_T^M\left(c_S, FLF\right)\right] - E\left[C_M\left(c_S\right)\right]\right) \tag{7.18}$$

Important values for the interpretation of the results are the original expected life-cycle costs, i.e. the costs without monitoring, for the service life of 20 years. For the threshold of $1.00\text{x}10^{-3}$ it is found that 5 out of 92 considered hot spots have to be inspected. This results in expected failure costs $E\left[C_F\right] = 2.8 \cdot 10^{-2}$, expected inspection costs $E\left[C_I\right] = 4.3 \cdot 10^{-3}$ and expected repair costs $E\left[C_R\right] = 1.6 \cdot 10^{-3}$ giving expected total

costs of $E[C_T] = 3.39 \cdot 10^{-2}$. For a yearly probability of failure threshold of 1.00x10^{-4} the result is 19 hot spots (out of 92 considered hot spots), $E[C_F] = 1.0 \cdot 10^{-2}$, $E[C_I] = 3.4 \cdot 10^{-2}$ and $E[C_R] = 4.0 \cdot 10^{-3}$ with total expected life-cycle costs of $E[C_T] = 4.8 \cdot 10^{-2}$.

It is very interesting to note that for the overall support structure the expected total life-cycle costs are higher for the threshold of 1.00x10^{-4} despite the fact that these costs per component are smaller (see Figure 7-3). This is due to the fact that substantially more hot spots have to be inspected for the threshold of 1.00x10^{-4}.

Figure 7-6 contains the results of the cost-benefit analysis. It can be seen that in general the expected benefit increases for both the probability of failure thresholds with an increasing number of monitored components and increasing fatigue life factors. A local maximum is observed in dependency on the number of monitored components whereas for the considered fatigue life factor no local maximum is observed.

For a yearly probability of failure threshold of 1.00x10^{-3} (Δp_{f1}) the maximum benefit is reached when five components are monitored (Equation (7.19)). This is caused by the fact that an inspection is necessary for five hot spots within the service life of 20 years. A maximum monitoring benefit of 1.65x10^{-2} can be reached which represents 48.7% of the expected total life-cycle costs (3.39x10^{-2}).

$$c_{S,opt}^{\Delta p_{f1}} = \{c_5\} \tag{7.19}$$

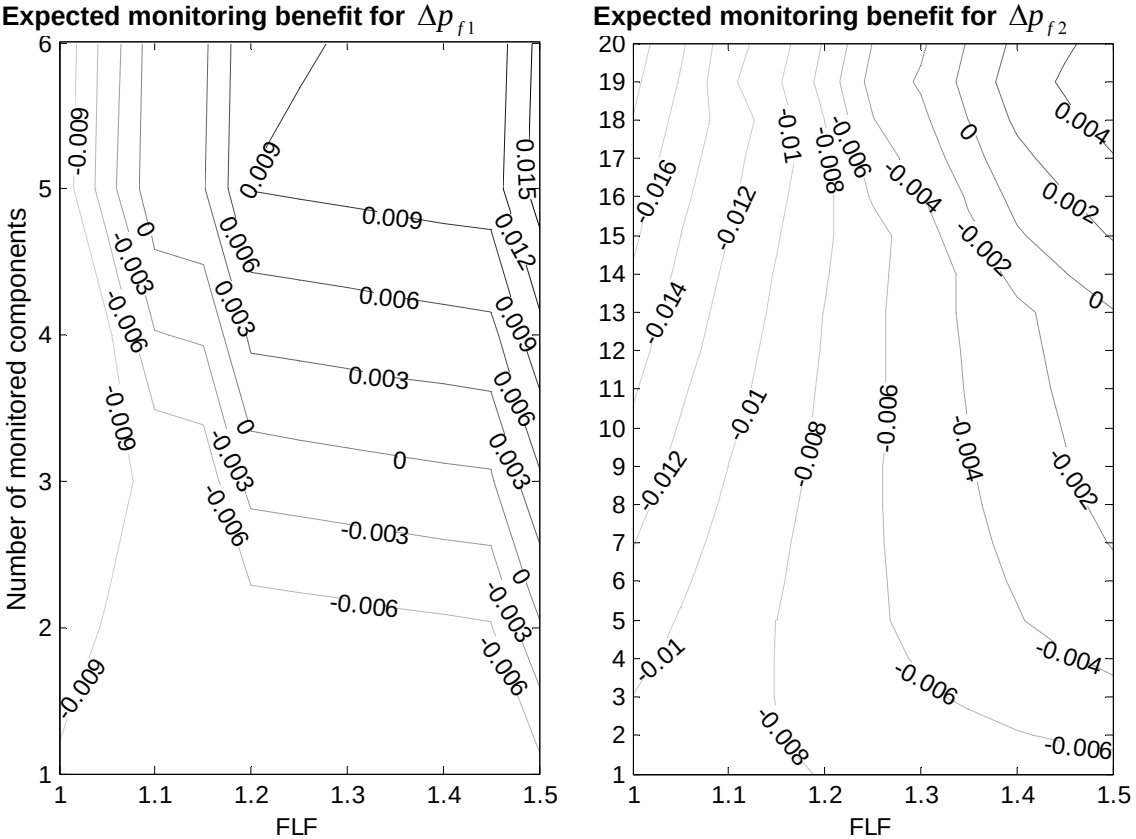

Figure 7-6: Expected monitoring benefit dependent on the number of monitored components and the fatigue life factor (FLF) with a yearly probability of failure threshold of 1.00x10^{-3} (left) and of 1.00x10^{-4} (right).

For a threshold of $1.00x10^{-4}$ (Δp_{f2}), the expected benefits are less in comparison to a threshold of $1.00x10^{-3}$. Here a maximum benefit of $5.3x10^{-3}$ (11.0%) relating to the total expected life-cycle costs of $4.8x10^{-2}$ can be reached. From the fact that 19 hot spots have to be inspected, it follows that the number of monitored hot spots is 19 to achieve the maximum benefit (Equation (7.20)).

$$c_{S,opt}^{\Delta p_{f2}} = \{c_{19}\} \tag{7.20}$$

To the monitoring benefit for the yearly probability of failure threshold of $1.00x10^{-3}$ the reduction of failure costs contributes most whereas for the case of threshold of $1.00x10^{-4}$ this applies to the inspection costs.

It should be mentioned that not for all FLF a positive benefit can be reached. This applies to FLFs lower than 1.1 for a threshold of $1.00x10^{-3}$ and to FLFs lower than 1.35 for a threshold of $1.00x10^{-4}$. Clearly, in such situation the application of monitoring is from the perspective of a cost-benefit analysis not sensible.

7.4.4 Determination of the monitoring period for the reference case

The generic decision considered in this section refers to the determination the monitoring period. Clearly, the monitoring period should be such that there is enough (statistical) significance for the modification of the probabilistic model of the equivalent stress ranges. In the following it is thus assumed that the minimum monitoring period is one year.

To find an approach for the determination the monitoring period, the inspection plans are calculated on the basis of the generic inspection plan database documented in Straub (2004). Consecutively the inspection plans are modified in each year of the service life in dependency of the fatigue life factor. The modification of the inspection plans follows the approach described in Straub (2004) based on the calculation of a fictive installation year t_{FIY} at the modification time t_{Mod} (which here equals the monitoring system installation time plus one year) for which the inspection plan is then derived (Figure 7-7). This approach accounts for the properties of the underlying fracture mechanics model. The new inspection plan for the remaining service life is derived in combination with the original inspection plan considering already performed inspections before the modification time.

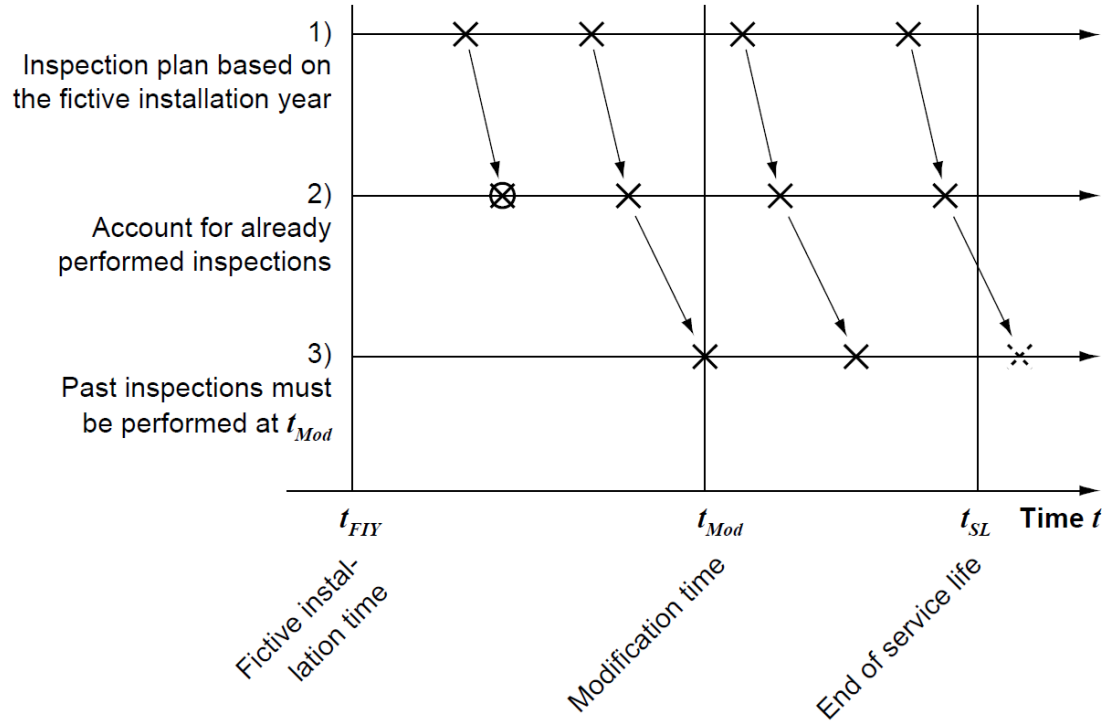

Figure 7-7: Scheme for modification of inspection plans (Straub (2004))

The modified inspection plans are calculated for the monitoring system installation years 0 to the 18th service life year of the structure. These installation years result in inspection plan modification times 1 to 19th year of the service life.

The inspection plans are derived also in dependency of the fatigue life factor, i.e. the factor which is found by analyzing the monitoring data considering the measurement uncertainties of the monitoring system and which describes the probability of failure reduction. A further dependency on threshold of the yearly probability of failure ($1.00\text{x}10^{-3}$ and $1.00\text{x}10^{-4}$) is considered.

The results are depicted in Figure 7-8 and show the cumulated number of inspection over all hot spots and over time in dependency of the modification year and the fatigue life factor. The original inspection plan derived for a yearly probability of failure threshold of $1.00\text{x}10^{-3}$ contained 6 inspections during the service life whereas the original inspection plan for a threshold of $1.00\text{x}10^{-4}$ contained 42 cumulated inspections.

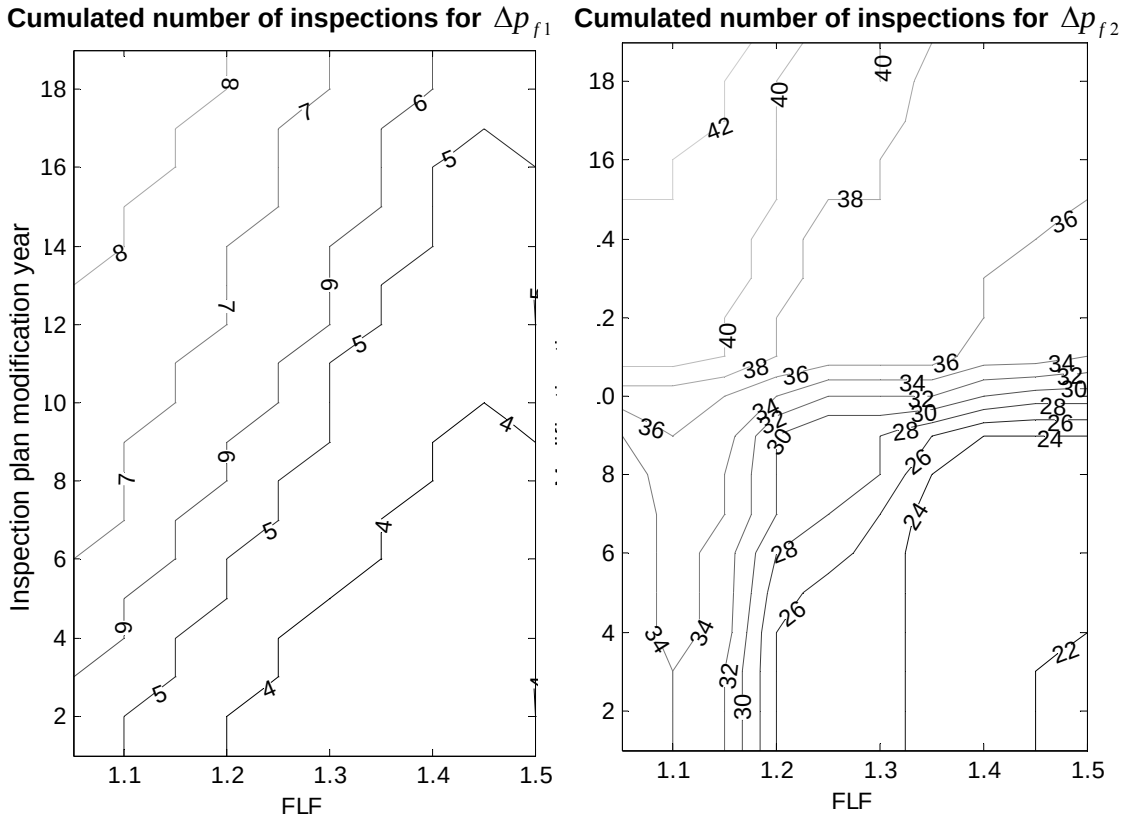

Figure 7-8: Number of inspections dependent on the modification time and the fatigue life factor (FLF) with a yearly probability of failure threshold of 1.00×10^{-3} (left) and of 1.00×10^{-4} (right).

For both thresholds it can be seen that the inspection effort, i.e. the number of the accumulated inspections, can be reduced in accordance with the results in Section 7.4.3. In general, the inspection effort decreases with higher fatigue life factors and lower modification years. For high modification years the inspection effort can increase despite a fatigue life factor higher than 1.00.

For a yearly probability of failure threshold of 1.00×10^{-3} a minimum of 3 accumulated inspections can be reached for the fatigue life factors higher than 1.2 and lower than 1.5 and the corresponding maximum modification years of 2 to 8. A reduction of the accumulated inspections can be achieved for all fatigue life factors starting with 1.05 and a modification year 1 until a fatigue life factor of 1.5 with a modification year 16.

For a threshold of 1.00×10^{-4} a minimum of 21 accumulated inspections can be reached for a fatigue life factor of 1.5 and the corresponding maximum modification year 3. A reduction of the accumulated inspections can be achieved for all fatigue life factors except 1.05 to 1.15 and the corresponding modification years 15 to 19.

The point for the further discussions is that the full reduction of accumulated inspections is achievable with modification of the inspection plans later than the first year. It can then additionally be assumed that the benefit associated with a certain fatigue life factor can be fully achieved (see Figure 7-6). Consequently, the monitoring

system does not have to be operated the full service life as assumed in the previous Section 7.4.3.

It follows that the monitoring system is operated in the first year of the service life (to acquire the data) and then from the latest modification time (corresponding to the results in Figure 7-8) to the last inspection. This is seen as an approach to determine the operation time of the monitoring system and the optimal decision in decision set in T in dependency of the fatigue life factor (see Equation (7.14)).

Considering the described approach, the expected benefit is affected due to the reduced operation costs of the monitoring system (Figure 7-9). For a threshold of $1.00\text{x}10^{-3}$ a maximum monitoring benefit of $1.71\text{x}10^{-2}$ can be reached which represents 50.4% of the total expected life-cycle costs. For a threshold of $1.00\text{x}10^{-4}$ a maximum monitoring benefit of $7.8\text{x}10^{-3}$ (16.3%) can be achieved and the least fatigue life factor for achieving a positive monitoring benefit is 1.3. The optimal decision in regard to which component set should be monitored is not affected.

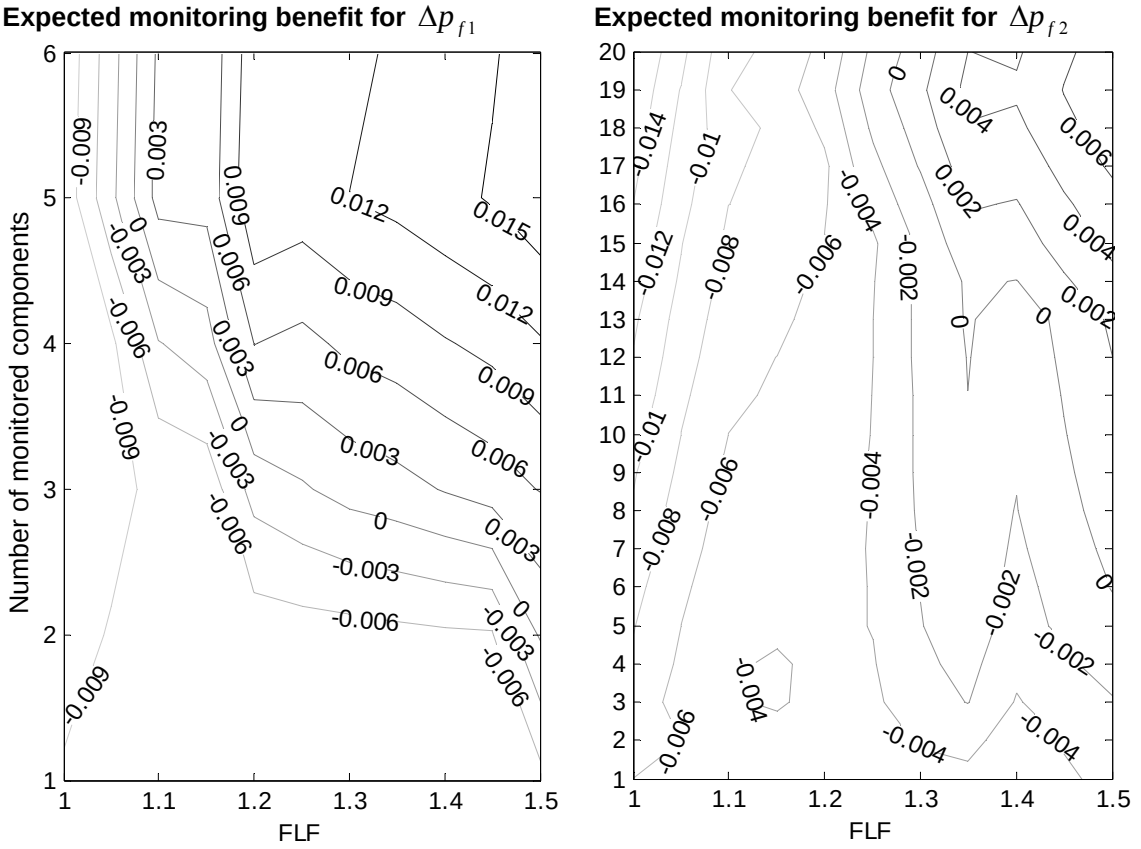

Figure 7-9: Benefit dependent on the number of monitored components and the fatigue life factor (FLF) with a yearly probability of failure threshold of $1.00\text{x}10^{-3}$ (left) and of $1.00\text{x}10^{-4}$ (right)

The results of this section can be utilized for guidance whether and when the modification of the inspection plans from a life-cycle cost-benefit perspective is

sensible. An important point here is that the probability of failure threshold is not exceeded as this is implied in the modification scheme introduced by Straub (2004).

7.5 Conclusions

In this chapter, the application of the research results of Chapter 5 and 6 for the management of the structural integrity is described. The research results of Chapter 5 regard the component reliabilities of the support structure; in Chapter 6 a framework for the determination of measurement uncertainties is introduced and the effect of applying monitoring data for the fatigue reliability analysis is discussed.

Concepts for the utilization of monitoring data in the ultimate and in the serviceability limit state are introduced. These concepts comprise the interpretation of monitoring as loading data (associated with the probabilistic loading model) and as proof loading data (associated with the probabilistic resistance model). With a life-cycle cost-benefit analysis it is shown on the basis of the reference case, how to design a monitoring system to achieve an expected life-cycle benefit.

The most significant conclusion here is that the application of the developed concepts and monitoring techniques can lead to a significant expected life-cycle benefit. It is achieved by the introduced approach to relate the monitoring techniques to the structural reliability assessment and to base the design decisions of a monitoring system upon the results of life-cycle cost benefit analysis within the framework of pre-posterior decision analysis. In order to maximize the benefit it is thus necessary to monitor all components or hot spots which are relevant for a risk based inspection scheme dependent on the probability of failure reduction. Furthermore, an approach for reducing the costs of monitoring in conjunction with a modification of inspection plans has been introduced.

Utilizing monitoring data as loading model information, the reduction of the probability of failure in regard to the design reliability assessment is caused by lower uncertainties of the structural models associated with monitoring and low measurement uncertainties. The reduction of the probability of failure is clearly dependent on the measurement data and the conservativeness of the design models and procedures.

The developed approach for utilizing monitoring data as proof loading facilitates to account for extreme loading events a support structure has survived resulting in an increased reliability in the ultimate limit state. This is would normally require additional (risky) loading experiments. The proof loading truncation concept is developed further in a way that it is accounted for a probabilistic proof loading as it is subject to measurement uncertainties. For the application of the alternative proof loading concept based on Bayesian updating in Nishijima and Faber (2007), a developed criteria enables to consistently apply the appropriate concept.

By examining the approaches of monitoring and damage detection, the relation to the structural reliability theory and classical reliability theory is identified. For the contribution of damage detection procedures to assess and to monitor the reliability of a structure, a general approach is introduced. This approach can additionally serve as the basis for the determination of the quality of a damage detection system.

8 Conclusions and outlook

One of the major challenges in the field of renewable energies represents the development of large scale offshore wind parks as this has been the research focus in the last decade. By the time this thesis is completed the commissioning of the first German commercial wind park has started in a location of significant water depths. In preparation for the next step, namely, the operation of offshore wind parks, this thesis contains conceptual and applied research results on the monitoring based condition assessment of offshore wind turbine structures.

With this thesis a framework for the monitoring based structural condition assessment and for the management of the structural integrity of offshore wind turbines is established. This framework facilitates holistically to account for monitoring information and data regarding the design, the production and the construction process. The individual achievements are:

1. The most important conceptual achievement represents the integration of monitoring data in combination with the developed framework for the determination of the measurement uncertainties in the framework for the structural reliability assessment of the Joint Committee on Structural Safety (JCSS). This facilitates to utilize monitoring data consistently for the assessment of the structural reliability building upon well established frameworks.
2. The introduced framework for the determination of measurement uncertainties represents a substantial development in regard to the established approaches of the ISO/IEC Guide 98-3 (2008a). Four facts contribute to this achievement, namely the basis of the Bayesian interpretation of probability, the introduction of the posterior measurement uncertainty, to account for the assignment uncertainty of the probabilistic models to the measurement data and to account for the model uncertainties.

   The framework for the determination of the measurement uncertainties facilitates to account for all available information of the measurement process and to model all aspects detailed and explicitly.
3. A detailed, full probabilistic performance model basis of a wind turbine structure comprising structural models, loading models and limit state models is established. This model basis constitutes a major accomplishment for the scientific community and industry as there no comparable model basis exists currently in terms of detailing and complexity.

   The full probabilistic performance model basis facilitates a detailed assessment of the structural reliability and constitutes the basis for an identification of critical components and thus for the design of monitoring systems.

4. The developed concepts for the monitoring based assessment for support structures of wind turbines can be applied to support the structural integrity management. This is achieved by the application of the Bayesian per-posterior decision analysis basing the decisions associated with the design of monitoring system on a structural reliability assessment and simultaneously to account for the characteristics of monitoring results in a life-cycle cost-benefit analysis.

   The developed concepts are based on an optimization of the expected life-cycle costs and address thus a most relevant issue for industrial application.

5. The applied research results are achieved by utilizing the conceptual findings for a complex reference case, namely an offshore wind turbine support structure. The most significant applied research accomplishment is that a substantial expected life-cycle benefit up to 50.4% can be achieved by the application of the developed concepts for the reference case. This benefit is achieved with a constant structural reliability level.

   The application of monitoring systems on structures for operation support represents a new industrial application with the potential for a substantial contribution to a more cost efficient wind energy production.

These achievements contribute directly to the objectives of the EU 7th framework research project IRIS as the reduction of the maintenance costs at equal safety level constitutes one of the main project objectives (VCE (2009)). A further project objective is the "development of embedded online risk monitoring systems for all industries" which is achieved here on a conceptual level for the wind energy industry.

Finally, these research results contribute to the aims of the European Strategic Energy Technology Plan (SET-Plan: European Union (2010)) focusing on the improvement of the competitiveness of the wind energy production. The research results also support in this way the German and European Union energy politics aiming at the establishment of renewable energies as a major component of future energy production.

8.1 Specific conclusions and limitations of the conceptual research

Of importance for the conceptual work is the developed model basis (Chapters 3 and 4). This model basis facilitates an independent reliability calculation building upon the design, production and construction information. Furthermore, the model basis relies on as few as possible assumptions because it builds upon the well developed non-linear Finite Element methods. For each of the fatigue, the ultimate and the serviceability limit state, structural and loading models are developed, analyzed and documented. With a sensitivity study the most relevant random variables are identified. The probabilistic models are derived on the basis of the Probabilistic Model Code (JCSS (2006)) and production data as available. Furthermore, the model basis facilitates to update the individual probabilistic models as additional information become available.

The approach for the structural reliability assessment facilitates the reliability analysis in conjunction with the most advanced calculation approach for the response calculation of wind turbines (Chapters 2 and 5). Furthermore, this approach facilitates that only the input of the overall dynamic analysis is necessary for the reliability calculation with the sophisticated model basis. Hence, the control unit models of the wind turbine, which are usually classified by the industrial partners as confidential, do not have to be known in detail by the analyst.

The approach for the structural reliability assessment contains an approximation, because for the realizations of the random variables associated with the structural models, the loadings are not recalculated with an overall dynamic analysis. However, this is the implication of the concept of the current structural code generation which applies to the design of offshore wind turbine structures (see e.g. BSH (2007) and GL Wind IV - Part 2 (2005)).

The developed adaptive response surface algorithm facilitates the reliability assessment with the complex model basis because of its computational efficiency (Chapter 5). This efficiency is achieved by the new approaches of clustering the design points of the multiple components structural models and by locally augmenting the experimental design for improving the prediction variance in the design point region. Both approaches facilitate to account for the specific requirements of a complex reliability analysis and to simultaneously improve the prediction variance of the response surface.

The determination of the measurement uncertainty should integrally utilize the process equation and observations of the measurement process. This constitutes the essence of the framework for the determination of the measurement uncertainty (Chapter 6). Furthermore, the specific challenge of the dependency of the probabilistic model on the measurement datum, which itself additionally represents a realization of a random process, is solved by explicitly accounting for the assignment uncertainty.

The framework for the determination of the measurement uncertainties (Chapter 6) facilitates to choose the monitoring system for operation support. This means that the sensors and measurement system can be determined with the aim of achieving a low measurement uncertainty because the framework is related to the product specification data. A low measurement uncertainty can then lead to the reduction of the uncertainties for the structural reliability assessment.

The reliability analysis utilizing monitoring data can lead for both the fatigue and ultimate limit state to lower probabilities of failure compared to the probability of failure calculated with the design data. This reduction is caused by the characteristics of the involved structural and probabilistic models (Chapters 6 and 7) and depends on the specific model uncertainties, the measurement uncertainty and the results of the measurements. It has been demonstrated that the common association to monitoring data possessing low uncertainties, can be modeled with the developed approaches. For the application of the concept Bayesian updating techniques can be applied depending on the specific boundaries of the involved probabilistic models.

The interpretation of monitoring data as proof loading data (Chapter 7) can be used to account for extreme events a structure has survived by modifying the resistance model which then can lead to an increased reliability of the structure. This approach facilitates to avoid additional (risky) proof loading tests. The common association, that structures posses a high reliability which have survived for long time and thus have experienced extreme events, can be modeled with this approach. The proof loading truncation concept itself is developed further in a way that it is accounted for a probabilistic proof loading information, namely proof loading test data subjected to measurement uncertainties. In conjunction with a proof loading method utilizing Bayesian updating techniques a developed criterion enables to consistently chose the appropriate method.

The conceptual work on the structural integrity management (Chapter 7) associates the developed approaches and results with a cost-benefit analysis for the operation of wind

turbine support structures. This conceptual work implies further that the monitoring systems should measure entities which can be used in (or transformed to) entities of the limit state equations and that the sensors should be applied to the components of the structure which are most sensitive to the system reliability. Furthermore, an approach for the monitoring system operation cost reduction is introduced. However, these results are subjected to the application of a risk based inspection procedure for the operation of wind turbine structures, the specific probabilistic models and monitoring data.

8.2 Specific conclusions in regard to the applied research

The most relevant failure mechanism and its most relevant influencing factors are identified on a quantitative and scientific basis with the analysis of the individual limit states and the sensitivity study (Chapters 3 and 4). The deterministic part of the model basis meaning the structural and the loading models should be clearly physically determined. Engineering models are limited in the way they cover system effects and may incorporate substantial conservativeness.

The results of the reliability analysis (Chapter 5) comprising the fatigue, the ultimate and the serviceability limit state have shown that that the highest probabilities of failure are associated with the serviceability limit state. For the considered resonance mechanism it is shown that the uncertainties and thus the probability of failure can be substantially reduced. This leads to a more general conclusion when it is additionally considered that the serviceability limit state is mostly associated to rather simple mechanisms, such as resonances or deflections, which can easily be monitored. Then monitoring can provide valuable information which can substantially reduce the probability of failure, i.e. the probability of unserviceability.

One of the important conclusions is that the reliability assessment of the reference case is compliant with the requirements of the “Eurocode: Basis of design” (DIN EN 1990 (2002)) (Chapter 5). However, the probability of fatigue failure increases with increasing service life of the support structure, which at the end of the service life leads to a significant probability that fatigue failure occurs within the structural system. This result is in line with the common observation for offshore structures. Two facts contribute to this situation, namely, the relatively high probabilities of local fatigue failure and the high number of locations where fatigue can occur. The probabilities of failure of a structural system are not covered by the requirements of the DIN EN 1990 (2002).

Another important conclusion can be drawn considering the fact that significant probabilities of failure relate to the fatigue limit state for the reference case (Chapter 5). The hot spot stresses for the pile guide, consisting of steel tube filled with reinforced concrete, can contain conservativeness when calculated with the Finite Element method applying shell elements. This conservativeness is caused by the three dimensional stress state in such a composite section which can only be accounted for with a solid Finite Element model (Chapter 4).

The framework for the determination of the measurement uncertainty (Chapter 6) facilitates quantification of the measurement uncertainty and of the sensitivities of its parameters based on the production specification data of the measurement equipment. For practical purposes aiming at a low measurement uncertainty quantitative criteria for

choosing the measurement equipment are thus provided. On the example of strain gage measurements the application of this framework has been demonstrated.

It is of practical relevance that the optimal decisions in regard to how many components and which locations of the support structure should be monitored can be determined on the basis of a cost-benefit analysis (Chapter 7). In order to maximize the expected benefit it is necessary to monitor all components or hot spots which are relevant for a risk based inspection planning.

Extensive knowledge of the design process and models has been gained with this thesis. The developed model basis contributes most to this fact as the limit states in combination with advanced analysis techniques are analyzed and the most relevant variables are quantitatively identified. Furthermore, the results of the reliability analysis provide an overview about the reliabilities of the components of the support structure and the relevant failure mechanisms.

8.3 Outlook

This thesis advocates a full probabilistic structural integrity assessment and thus to utilize structural monitoring techniques for the operation support of offshore wind turbines. The conceptual and applied research results have the potential for a new industrial application utilizing the theoretical framework of structural reliability theory for the operation of large scale offshore wind parks. In combination with the rapid development of the wind energy industry aiming at a major contribution to the energy mix, the industrial application can substantially contribute to the European industry development.

Furthermore, the conceptual research results can be applied in a broader perspective, i.e. in other engineering fields in the sense that a structural reliability and risk assessment is identified as an appropriate basis for the design of monitoring systems aiming to optimize the operation of the structures.

It is suggested to use the framework for the determination of measurement uncertainties for the further development of the ISO/IEC Guide 98-3 (2008a) as the concept is based on a Bayesian definition of probability and this is a possible direction for further development seen by the Joint Committee for Guides in Metrology (Bich (2008)). The measurement uncertainty constitutes a further source of uncertainty for the structural reliability framework of the JCSS. It is thus suggested to extend the framework of the Probabilistic Mode Code (JCSS (2006)) to measurement uncertainties.

The model basis can be applied to analyze and to research on issues which are beyond the focus of this thesis. Such issues can be the optimization of the system reliability, the production costs and/or the life-cycle costs of the support structure. Furthermore, the models can be modified to account for dependencies between all support structures of a wind park as further production information become available.

The application of the reliability assessment approach revealed that the partial safety factor concept is not completely consistent with calculation approach for wind turbines as it neglects the coupling to the load calculation procedure. This is reflected also by the fact that different standards are applied for the load calculation and the structural design (see e.g. BSH (2007)). This is an issue of utmost importance and further research should be concentrated in this area.

References

Abonyi, J. and B. Feil (2007). Cluster Analysis for Data Mining and System Identification, Birkhäuser Basel.

ANSYS, I. (2006). Release 11.0 Documentation for ANSYS, ANSYS, Inc.

API (2000). Recommended Practice for Planning, Designing and Constructing Fixed Offshore Platforms—Working Stress Design, American Petroleum Institute. API RP 2A-WSD.

BAM (2009). IMO-WIND: Integrales Monitoring-und Bewertungssystem für Offshore-Windenergieanlagen. Final research report for InnoNet-Projects 16INO326 and 16INO327.

Basseville, M., et al. (2004). Statistical model-based damage detection and localization: subspace-based residuals and damage-to-noise sensitivity ratios. Journal of Sound and Vibration 275(3-5): 769-794.

Bathe, K. J. (1996). Finite Element Procedures, Prentice Hall.

Bekowich, R. S. (1968). Instrumentation in prestressed concrete containment structures. Nuclear Engineering and Design 8(4): 500-512.

Bich, W. (2008). How to revise the GUM? Accreditation and Quality Assurance: Journal for Quality, Comparability and Reliability in Chemical Measurement (13): 271–275.

Blockley, D. I. (1978). Analysis of subjective assessments of structural failures. International Journal of Man-Machine Studies 10(2): 185-195.

Bolotin, V. V. (1981). Wahrscheinlichkeitsmethoden zur Berechnung von Konstruktionen. Berlin, Germany, VEB Verlag für Bauwesen.

Bossanyi, E. A. (2006). GH Bladed Theory Manual. GH Bladed: 282/BR/009.

Box, G. E. P. and K. B. Wilson (1951). On the Experimental Attainment of Optimum Conditions. Journal of the Royal Statistical Society. Series B (Methodological) 13(1): 1-45.

BSH (2007). Konstruktive Ausführung von Offshore-Windenergieanlagen. Bundesamt für Seeschifffahrt und Hydrographie (BSH) Nr. 7005.

Bucher, C. (2009a). Asymptotic sampling for high-dimensional reliability analysis. Probabilistic Engineering Mechanics 24(4): 504-510.

Bucher, C. (2009b). Computational Analysis of Randomness in Structural Mechanics, CRC Press, Taylor and Francis Group.

Bucher, C. and U. Bourgund (1990). A fast and efficient response surface approach for strutural reliability problems. Structural Safety 7: 57-66.

Bucher, C. and T. Most (2008). A comparison of approximate response functions in structural reliability analysis. Probabilistic Engineering Mechanics 23(2-3): 154-163.

Bundesministerium für Wirtschaft und Technologie (BMWi) (2010). Energiekonzept für eine umweltschonende, zuverlässige und bezahlbare Energieversorgung.

Callendar, G. S. (1938). The Artificial Production of Carbon Dioxide and Its Influence on Climate. Quarterly J. Royal Meteorological Society 64: 223-240.

Clormann U. H. and Seeger T. (1986). Rainflow - HCM: Ein Zählverfahren für Betriebsfestigkeitsnachweise auf werkstoffmechanischer Grundlage. Stahlbau 3: 65-71.

Cornell, A. (1969). A Probability-Based Structural Code. ACI Journal: 974-985.

Cornell, C. A. (1967). Bounds on the reliability of structural systems. ASCE J. Struct. Div. 93(ST 1).

Das, P. K., et al. (2003). Buckling and ultimate strength criteria of stiffened shells under combined loading for reliability analysis. Thin-Walled Structures 41(1): 69-88.

De Sanctis, G. (2009). Zustandsbewertung von Windenergieanlagen durch Monitoringdaten. Masterarbeit. Lehrstuhl für Risiko und Sicherheit, Institut für Baustatik und Konstruktion. ETH Zürich.

DIBt (1993). Richtlinie für Windkraftanlagen. DIBt.

DIBt (2004). Richtlinie für Windenergieanlagen. DIBt.

DIN (2002). Eurocode: Basis of structural design. DIN EN 1990.

DIN (2005a). Eurocode 3: Bemessung und Konstruktion von Stahlbauten, Teil 1-9: Ermüdung. DIN EN 1993-1-9.

DIN (2005b). Warmgewalzte Erzeugnisse aus Baustählen Teil 2: Technische Lieferbedingungen für unlegierte Baustähle. DIN EN 10025.

DIN (2007). Eurocode 3: Bemessung und Konstruktion von Stahlbauten – Teil 1-6: Festigkeit und Stabilität von Schalen. DIN EN 1993-1-6.

DIN (2009). Wind turbines - Part 3: Design requirements for offshore wind turbines. DIN EN 61400-3.

Ditlevsen, O. (1973). Structural Reliability and the Invariance Problem. Solid Mechanics Division, University of Waterloo. Report No. 22.

Ditlevsen, O. (1979a). Narrow Reliability Bounds for Structural Systems. Journal of Structural Mechanics 7(4): 453-472.

Ditlevsen, O. and P. Bjerager (1986). Methods of Structural Systems Reliability. Structural Safety 3: 195-229.

Ditlevsen, O. and H. O. Madsen (2005). Structural Reliability Methods, Coastal, Maritime and Structural Engineering and Department of Mechanical Engineering, Technical University of Denmark.

Ditlevsen, O. D. (1979b). Generalized Second Moment Reliability Index. Journal of Structural Mechanics 7(4): 435-451.

DNV (2004). Design of Offshore Wind Turbine Structures, Det Norske Veritas. DNV-OS-J101.

Engelund, S. and R. Rackwitz (1993). A benchmark study on importance sampling techniques in structural reliability. Structural Safety 12(4): 255-276.

Enright, M. P., et al. (2006). Application of Probabilistic Fracture Mechanics to Prognosis of Aircraft Engine Components. AIAA JOURNAL 44(2): 311-316.

Ersdal, G. (2005). Assessment of existing offshore structures for life extension. PhD Thesis. Department of Mechanical and Structural Engineering and Material Science. University of Stavanger.

European Commision (2007a). An Energy Policy for Europe.

European Commision (2007b). Renewable Energy Road Map.

European Union (2010). The European Strategic Energy Technology Plan: SET-Plan.

European Wind Energy Association (EWEA) (2009a). Annual Report 2009.

European Wind Energy Association (EWEA) (2009b). The Economics of Wind Energy.

Faber, M. H. (2000). Reliability based assessment of existing structures. Progress in Structural Engineering and Materials 2(2): 247-253.

Faber, M. H. (2008a). Lecture Notes: Risk and Safety in Civil, Surveying and Environmental Engineering, ETH Zurich.

Faber, M. H. (2008b). Risk Assessment in Engineering - Principles, System Representation & Risk Criteria, JCSS Joint Committee on Structural Safety.

Faber, M. H., et al. (2000). Simplified and Generic Risk Based Inspection Planning. Proceedings OMAE2000, 19th Conference on Offshore Mechanics and Arctic Engineering, New Orleans, Louisiana, USA.

Faber, M. H., et al. (2007). Principles of Risk Assessment of Engineered Systems. 10th International Conference on Applications of Statistics and Probability in Civil Engineering, The University of Tokyo, Kashiwa Campus, JAPAN.

Faber, M. H., et al. (2005). Field Implementation of RBI for Jacket Structures. Journal of Offshore Mechanics and Arctic Engineering 127(3): 220-226.

Faber, M. H., et al. (2001). Unified Approach to Risk Based Inspection Planning for Offshore Production Facilities. Proceedings of OMAE, 20th Conference on Offshore Mechanics and Arctic Engineering, Rio de Janeiro, Brazil.

Faber, M. H., et al. (2000). Proof load testing for bridge assessment and upgrading. Engineering Structures 22(12): 1677-1689.

Folsø, R., et al. (2002). Reliability-based calibration of fatigue design guidelines for ship structures. Marine Structures 15(6): 627-651.

Frangopol, D. M., et al. (2008). Use of monitoring extreme data for the performance prediction of structures: General approach. Engineering Structures 30(12): 3644-3653.

Frank Busby, R. (1979). Underwater inspection/testing/ monitoring of offshore structures. Ocean Engineering 6(4): 355-491.

Freudenthal, A. M. (1947). The Safety of Structures. Transactions of American Society of Civil Engineering: Paper N. 2296.

Freudenthal, A. M. (1954). Alfred M. Freudenthal Safety and Probability of Structural Failure. Transactions of American Society of Civil Engineering Paper N. 2843: 1337-1397.

Freudenthal, A. M. (1956). Safety and the Probability of Structural Failure. Trans. ASCE 121.

Fritzen, C. P. and P. Kraemer (2009). Self-diagnosis of smart structures based on dynamical properties. Mechanical Systems and Signal Processing 23(6): 1830-1845.

Gasch, R. and J. Twele (2007). Windkraftanlagen - Grundlagen, Entwurf, Planung und Betrieb, B. G. Teubner Verlag.

GL Wind (2005). Guideline for the Certification of Offshore Wind Turbines, GL Wind. GL Wind IV - Part 2.

GL Wind (2007). Richtlinie für die Zertifizierung von Condition Monitoring Systemen für Windenergieanlagen, GL Wind. GL Wind IV - Teil 4.

Gollwitzer, S., et al. (2006). PERMAS-RA/STRUREL system of programs for probabilistic reliability analysis. Structural Safety 28(1-2): 108-129.

Goris, A. and K.-J. Schneider (2006). Bautabellen für Ingenieure, Werner-Verlag.

Haldar, A. and S. Mahadevan (2000). Reliability Assessment Using Stochastic Finite Element Analysis, John Wiley & Sons, Inc.

Hasofer, A. M. and N. C. Lind (1974). Exact and Invariant Second-Moment Code Format. Journal of Engineering Mechanics Division, Proceedings of the American Society of Civil Engineers 100: 111-121.

HBM (2008). Dokumentation Messverstärkersystem HBM MGCplus.

Hendriks, H. B. and M. Zaaijer (2004). DOWEC: Executive summary of the public research activities. ECN, TU Delft.

Hildebrandt, N. (2010). FACT-SHEET alpha ventus. from http://www.alpha-ventus.de/.

Hoffmann, K. (1987). Eine Einführung in die Technik des Messens mit Dehnungsmessstreifen, HBM Publications.

ISO (1998). General Principles on Reliability for Structures International Organisation for Standardization. ISO 2394.

ISO (2001). Bases for the design of structures - Assessment of existing structures. ISO 13822.

ISO (2007). Petroleum and natural gas industries - Fixed steel offshore structures. ISO 19902.

ISO (2008a). Part 3: Guide to the Expression of Uncertainty in Measurement (GUM:1995). ISO/IEC Guide 98-3.

ISO (2008b). Part 3: Guide to the Expression of Uncertainty in Measurement (GUM:1995): Supplement 1 - Propagation of distributions using a Monte Carlo method. ISO/IEC Guide 98-3/Suppl.1.

ISO/FDIS (2006). Petroleum and Natural Gas Industries - Fixed Steel Offshore Structures, ISO/FDIS. ISO/FDIS 19902.

JCGM (2009). Evaluation of measurement data - An introduction to the Guide to the expression of uncertainty in measurement" and related documents. JCGM 104:2009.

JCSS (2001). Probabilistic Assessment of Existing Structures. A publication of the Joint Committee on Structural Safety, RILEM Publications S.A.R.L.

JCSS (2006). Probabilistic Model Code, JCSS Joint Committee on Structural Safety.

Jovanovic, A., et al. (2010). 2nd iNTeg-Risk Conference: New Technologies & Emerging Risks. Dealing with multiple and interconnected emerging risks, Steinbeis-Edition.

Keil, S. (1995). Beanspruchungsermittlung mit Dehnungsmessstreifen, Cuneus.

Kühn, M. J. (2001). Dynamics and Design Optimisation of Offshore Wind Energy Conversion Systems. PhD. Thesis. Technical University of Delft.

Liu, M., et al. (2010). Fatigue reliability assessment of retrofitted steel bridges integrating monitored data. Structural Safety 32(1): 77-89.

MacGregor, C. W. (1944). The true stress-strain tension test--Its role in modern materials testing: Part I. Journal of the Franklin Institute 238(2): 111-135.

Madsen, H. O., et al. (1986). Methods of Structural Safety, Prentice Hall.

Madsen, H. O., et al. (1987). Probabilistic Fatigue Analysis of Offshore Structures - Reliability Updating Through Inspection Results. Proceedings from the Third International Symposium on Integrity of Offshore Structures, University of Glasgow.

Mayer, M. (1926). Die Sicherheit der Bauwerke. Berlin, Verlag von Julius Springer.

Moan, T. (2005). Reliability-based management of inspection, maintenance and repair of offshore structures. Structure and Infrastructure Engineering 1(1): 33 – 62.

Myers, R. H. and D. C. Montgomery (2002). Response Surface Methodology, John Wiley & Sons, Inc.

Naess, A., et al. (2009). System reliability analysis by enhanced Monte Carlo simulation. Structural Safety 31(5): 349-355.

Niemi, E., et al. (2006). Fatigue Analysis of Welded Components, Woodhead Publishing Limited.

Nishijima, K. and M. H. Faber (2007). Bayesian approach to proof loading of quasi-identical multi-components structural systems. Civil Engineering and Environmental Systems 24(2): 111-121.

Nishijima, K., et al. (2010). A scalable parametric approximation to multi-normal probability integrals. IFIP WG 7.5 Working Conference on Reliability and Optimization of Structural Systems. Munich, Germany.

OWT (2009). WEC Multibrid M5000, Load Calculation. IMO-WIND: Internal project report.

Pearson, C. and N. Delatte (2005). Ronan Point Apartment Tower Collapse and its Effect on Building Codes. Journal of Performance of Constructed Facilities 19(2): 172-177.

Pestke, S. F. (2010). Offshore-Windparks: Genehmigungs- und Vollzugspraxis. VGB-Fachtagung - Instandhaltung von Windenergieanlagen 2010, BSH Hamburg.

Raiffa, H. and R. Schlaifer (2000). Applied statistical decision theory. New York, Wiley.

Reh, S., et al. (2006). Probabilistic finite element analysis using ANSYS. Structural Safety 28: 17-43.

Rohrmann, R. G., et al. (2007). Integrated Monitoring Systems for Offshore Wind Turbines. Proceedings of the International Workshop on Structural Health Monitoring (IWSHM), Stanford University, Stanford, CA USA.

Rohrmann, R. G., et al. (2010). Integrated monitoring of offshore wind turbines – requirements, concepts and experiences. Structure and Infrastructure Engineering: Maintenance, Management, Life-Cycle Design and Performance 6(5): 575 - 591.

Rücker, W., et al. (2005). Guideline for the assessment of existing structures. 5th International Conference on Bridge Management, Inspection, Maintenance, Assessment and Repair, Guilford, UK, Thomas Telford Publishing.

Rücker, W., et al. (2006). Guideline for the assessment of existing structures. SAMCO F08a.

Schaumann, P., et al. (2007). Tragstrukturen für Windenergieanlagen. Stahlbaukalender 2007. Prof. Dr.-Ing. Ulrike Kuhlmann. Ernst & Sohn Verlag: 571-645.

Schneider, W. B. (1991). Wege in der Physikdidaktik: Zu den Grundsätzen des physikalischen Maßsystems. Erlangen, Verlag Palm & Enke.

Schumacher, A. and A. Nussbaumer (2006). Experimental study on the fatigue behaviour of welded tubular K-joints for bridges. Engineering Structures 28(5): 745-755.

Shan, L. T. and A. S. Nowak (1984). Proof loading and structural reliability. Reliability Engineering 8(2): 85-100.

Shinozuka, M. (1964). Probability of structural failure under random loading. Journal of the Eng. Mech. Div., ASCE 90: 147-170.

Shinozuka, M. (1983). Basic analysis of structural safety. ASCE J. of Struct. Eng.(109): 721-740.

Slater, W. A., et al. (1923). Test of a hollow tile and concrete floor slab reinforced in two directions. Journal of the Franklin Institute 195(1): 114-116.

Sommer, K.-D., et al. (2009). A Bayesian approach to information fusion for evaluating the measurement uncertainty. Robotics and Autonomous Systems 57(3): 339-344.

Sørensen, J. D. and N. J. Tarp-Johansen (2005). Optimal Structural Reliability of Offshore Wind Turbines. 9th International Conference on Structural Safety and Reliability (ICOSSAR), Rom.

Stein, P. K. (2006). 1936—A Banner Year for Strain Gages and Experimental Stress Analysis - an Historical Perspective. Experimental Techniques 30(1): 23-41.

Straub, D. (2004). Generic Approaches to Risk Based Inspection Planning for Steel Structures. PhD. thesis. Chair of Risk and Safety, Institue of Structural Engineering. ETH Zürich.

Straub, D. and A. Der Kiureghian (2008). Improved seismic fragility modeling from empirical data. Structural Safety 30(4): 320-336.

Tang, W. H. (1973). Probabilistic Updating of Flaw Information. Journal of Testing and Evaluation 1: 459-467.

Thöns, S., et al. (2010). On measurement uncertainties, monitoring data and structural reliability. Submitted to the journal Structural Safety.

Thöns, S., et al. (2009a). Fatigue and Serviceability limit state model basis for assessment of offshore wind energy converters. Accepted for publication in the Journal of Offshore Mechanis and Artic Engineering.

Thöns, S., et al. (2009b). Ultimate limit state model basis for assessment of offshore wind energy converters. Accepted for publication in the Journal of Offshore Mechanis and Artic Engineering.

Thöns, S., et al. (2010). Support Structure Reliability of Offshore Wind Turbines Utilizing an Adaptive Response Surface Method. 29th International Conference on Ocean, Offshore and Arctic Engineering (OMAE 2010).

Thöns, S., et al. (2008). Assessment and monitoring of reliability and robustness of offshore wind energy converters. ESREL 2008 and 17th SRA-Europe Conference. Valencia, Spain: 1567-1575.

Thöns, S., et al. (2008). Bewertung der Ermüdungsfestigkeit von Baustrukturen in Offshore-Windenergie-Anlagen. Stahlbau 77(9/2008): 630-638.

TML (2008). TML WFLA-6-17 strain gauge test data.

VCE (2009). IRIS Integrated European Industrial Risk Reduction System (CP-IP 213968-2), Description of Work.

VDI/VDE/GESA (2007). Experimental structure analysis, Metallic bonded resistance strain gages, Characteristics and test conditions. VDI/VDE/GESA 2635, Part 1.

Visser Consultancy Limited (2000). POD/POS curves for non-destructive examination. Offshore technology report. Offshore Technology Report 2000/018.

Wirsching, P. H. (1984). Fatigue Reliability for Offshore Structures. Journal of Structural Engineering 110(10): 2340-2356.

Yao, J. T. P. (1979). Damage assessment and reliability evaluation of existing structures. Engineering Structures 1(5): 245-251.

Yao, J. T. P. and H. G. Natke (1994). Damage detection and reliability evaluation of existing structures. Structural Safety 15(1-2): 3-16.

Zielke, W. and G. Haake (2007). Validierung bautechnischer Bemessungsmethoden für Offshore-Windenergieanlagen anhand der Messdaten der Messplattformen FINO 1 und FINO 2. GIGAWIND-Jahresbericht 2006.